POLITECNICO DI MILANO

Facoltà di Ingegneria
Dipartimento di Elettrotecnica

Power Transformer Modelling
Advanced Core Model

Relatore
Prof. Francesco CASTELLI DEZZA

Correlatore
Prof. Hans Kristian HØIDALEN

Tesi di laurea di:
Nicola CHIESA
matr. n. 643738

Anno Accademico 2004-2005

Acknowledgements

I would like to express my gratitude to my supervisor Professor H. K. Høidalen for motivateing and guiding me durig my thesis work. It has been a pleasure to collaborate with him and I hope to continue.

I also thank Professor F. Castelli Dezza.

I am also grateful to all my relatives and friends for being supportive and interested in my studies during these years.

Special thanks go to my cousin Luisa whom I deeply admire. She has been an example and a source of inspiration. Luisa, let's celebrate our doctoral graduation together, there is still a long way to go but...

Thanks to the one that don't want to be in this page. He is too similar to his father...

Thanks go to zia Bruna and zio Agostino for helping me during my stay in Milano. Without your help I would have given up before.

Finally I would like to express my best gratitude to my parents Mirella and Mario. Thanks for being confident in my capabilities, often more than I have dreamed of. Your guide free of coercive elements have given me the freedom necessary to take off in a ocean of undiscovered possibilities.

Trondheim, June 2005
Nicola Chiesa

Contents

List of Figures

List of Tables

Italian Abstract

Questo capitolo riassume i concetti e i risultati sostanziali della tesi. L'estratto è diviso in quattro sezioni che rispecchiano le parti principali del lavoro: introduzione, analisi del problema e modellizzazione, implementazione e test del modello, conclusioni. In ogni sezione vengono ripercorsi i relativi capitoli facendo riferimento a figure e tabelle contenute nel corpo della tesi.

0.1 Introduzione

Negli ultimi decenni la struttura degli impianti di produzione e distribuzione dell'energia ha subito importanti cambiamenti a causa della liberalizzazione del mercato dell'energia elettrica. Aumento di efficienza, taglio dei costi e riduzione degli investimenti sono necessari per poter essere competitivi in un mercato di libera concorrenza. D'altra parte, il numero di transitori nella rete è destinato ad aumentare in un sistema di generazione distribuito a causa dell'aumento di operazioni di commutazione.

Al tempo stesso la domanda di un'affidabile fonte di energia è aumentata considerevolmente. Questa richiesta è aggravata dal fatto che l'età media dei trasformatori in servizio sta entrando in una fase critica. Quei trasformatori che sono stati soggetti a condizioni gravose, quali sovraccarichi o invecchiamento precoce, potrebbero essere vicini ai loro limiti di funzionamento.

Attualmente l'energia eolica sta prendendo piede come fonte di energia alternativa. Negli impianti eolici le operazioni di commutazione e i transitori di messa in servizio sono molto più frequenti che nelle centrali termo e idroelettriche. Inoltre, questo tipo di impianti è maggiormente esposto a fulminazioni. L'alto numero di generatori e cavi di connessione può incrementare il rischio di risonanza del sistema.

Un accurato calcolo delle perdite e delle condizioni di lavoro gravose, come correnti di magnetizzazione e inrush currents, portano a maggiore efficienza, migliori schemi di protezione, riduzione dei costi e ottimizzazione degli impianti.

La modellizzazione dei trasformatori ha tradizionalmente occupato un ruolo importante negli anni a causa della peculiare importanza dei trasformatori nei sistemi di generazione e distribuzione, ma anche per la complessità del componente. In letteratura ci sono ancora divergenze su quali siano le ipotesi da considerare o meno per poter costruire un modello preciso. Considerando la corretta topologia del nucleo del trasformatore si ottengono risultati accurati, quindi questa sembra essere la scelta migliore per lo sviluppo di nuovi modelli. Importante è lo studio di modelli generali e completi che richiedano l'inserimento di un tipico set di dati.

Scopo del lavoro

La tesi fa parte di un progetto che studia gli effetti dalla saturazione su un trasformatore di potenza. L'obiettivo è lo sviluppo di un modello di trasformatore per EMTP-type software. Lo studio è focalizzato sulla bassa frequenza dove la saturazione è un rischio. Il modello sviluppato potrà essere usato per la simulazione di transitori nelle reti elettriche e sarà un utile strumento per lo studio di transitori di commutazione e inrush currents.

Per poter predire sollecitazioni elettromagnetiche sui trasformatori devono essere instaurati nuovi modelli. Gli attuali modelli di trasformatori trifase presenti nei programmi di simulazione sono basati su trasformatori monofasi. Questi non tengono conto delle differenze e degli accoppiamenti tra le fasi dovute alla struttura del nucleo magnetico. Anche la rappresentazione di isteresi, perdite anomale e magnetizzazione residua deve essere migliorata. Il maggior problema per la caratterizzazione di modelli avanzati è la mancanza di dati; essi, tipicamente contenuti nelle schede tecniche, risultano spesso insufficienti a descrivere un accurata curva di saturazione.

Aspetti innovativi presentati in questa tesi riguardano lo sviluppo e l'implementazione di un modello avanzato di trasformatore, basato sulla corretta rappresentazione topologica del nucleo magnetico. La parte più complessa riguarda appunto la modellizzazione del circuito magnetico che richiede molti calcoli matematici e procedure iterative.

Struttura della tesi

La tesi è costituita da tre parti principali: informazioni generali, implementazione e esame del modello. I capitoli 1-3 contengono informazioni generali e cenni teorici utili alla comprensione dei successivi capitoli. I capitoli 4-5 illustrano il modello e

la sua implementazione. I capitoli 6-8 contengono la verifica e i risultati.

Non considerando questo estratto gli altri capitoli trattano:

Il Capitolo 1 è introduttivo e descrive a grandi linee il contenuto della tesi.

Il Capitolo 2 presenta il software per cui il modello è stato implementato e da una rapida panoramica sui modelli di trasformatore attualmente implementati.

Il Capitolo 3 descrive lo sviluppo del modello avanzato. Mostra come il modello completo può essere diviso in quattro distinte sezioni: resistenza degli avvolgimenti, flussi di dispersione, effetti capacitivi e nucleo magnetico.

Il Capitolo 4 analizza in dettaglio la rappresentazione del nucleo magnetico. Si presenta l'elaborazione del modello, dalla struttura fisica del trasformatore alla sua modellizzazione. Viene poi illustrato come ottenere i parametri da inserire nel modello partendo da tre differenti fonti: relazioni tecniche, disegni tecnici e dati tipici (in caso di completa approssimazione).

Il Capitolo 5 tratta l'implementazione del modello usando un linguaggio di programmazione di basso livello.

Il Capitolo 6 mostra i risultati di alcuni test di laboratorio eseguiti su un piccolo trasformatore da distribuzione.

Il Capitolo 7 discute il confronto tra i risultati ottenuti in laboratorio e i risultati delle simulazioni.

Il Capitolo 8 contiene le conclusioni del lavoro e suggerimenti per futuri miglioramenti del modello.

0.2 Modello Avanzato di Trasformatore

Le Fig. 3.7 e 3.8 a pag. 25 illustrano l'idea generale alla base del modello avanzato del trasformatore. Le quattro distinte sezioni sono rappresentate con diversi colori: resistenza degli avvolgimenti in arancione, modello dei flussi di dispersione in blu, effetti capacitivi in rosso e modello del nucleo magnetico in verde. Di queste quattro sezioni quella relativa al nucleo è discussa in dettaglio e costituisce il punto centrale della tesi.

Il nucleo è stato modellizzato considerando la struttura fisica del trasformatore. Per questo si avranno modelli diversi a seconda che il trasformatore considerato sia a tre gambe, a cinque gambe, a mantello o composto da tre trasformatori monofasi. Solo i tipi a tre e cinque gambe sono stati attualmente implementati nel modello. Dalla struttura fisica si è ottenuto il circuito magnetico e quindi l'equivalente elettrico. Le varie trasformazioni e semplificazioni sono basate sul principio della

dualità tra reti magnetiche ed elettriche. Le figure da 4.5 a 4.13 (da pag. 34) riportano i passaggi fondamentali. La Fig. 4.13 è particolarmente importante in quanto rappresenta il circuito base, fondamento del restante studio. Un'importante ipotesi è stata introdotta a questo punto: è stato considerato possibile dividere il circuito di Fig. 4.13 in due sotto-circuiti. Il primo considera solamente le non-linearità causate dalla saturazione del nucleo magnetico e il secondo considera le sole perdite ferro. Si è dimostrato che gli errori introdotti da questa approssimazione sono trascurabili.

Il passo successivo è stato quello di calcolare i parametri circuitali da inserire nel modello avendo a disposizione dei set standard di valori. I dati circuitali possono essere ricavati basandosi su relazioni tecniche, disegni tecnici o valori tipici. La procedura è relativamente semplice nei casi in cui si abbiano a disposizione disegni tecnici o ci si basi su valori tipici. Risulta più interessante analizzare il caso in cui si abbiano a disposizione relazioni tecniche; esempi di queste sono riportati nell'Appendice A. I dati relativi alla prova a vuoto riportano come minimo il valore della corrente di eccitazione alla tensione nominale. È sempre più frequente trovare rapporti che includono prove a vuoto a tensioni diverse da quella nominale, i valori più comuni sono 90% e 110%. Se si ha a disposizione un opportuno set di dati (come minimo i risultati di due prove a vuoto a diversa tensione) la curva di magnetizzazione può essere caratterizzata. Per descrivere analiticamente la curva di magnetizzazione si è scelto di usare l'equazione di Frolich. La forma base nelle variabili $\lambda - i$ è:

$$\lambda = \frac{i}{a + b \cdot |i|}$$

Si è osservato che l'andamento di questa curva non si adatta bene nella zona del ginocchio alla curva di magnetizzazione. Per questo motivo è stata proposta una versione modificata a tre parametri dell'equazione di Frolich:

$$\lambda = \frac{i}{a + b \cdot |i| + c \cdot \sqrt{|i|}}$$

Fig. 4.17 a pag. 47 mostra il miglioramento apportato da questa nuova versione. Entrambe le curve sono invertibili. Per maggiori dettagli riferirsi al Paragrafo 4.6.1 e all'Appendice B.

Una procedura iterativa permette di calcolare i parametri a, b ed eventualmente c. Per maggiori dettagli riferirsi al Capitolo 4.

0.3 Implementazione e Verifica del Modello

Il modello presentato in dettaglio nel Capitolo 4 è stato implementato nella routine *BuildCore* usando *Borland Delphi 6*. Questa routine fa parte del modello completo XFMR e gestisce la modellizzazione del circuito magnetico del trasformatore. La Fig. 5.1 a pag. 68 mostra lo schema a blocchi della routine, mentre le subroutine principali e le loro dipendenze sono rappresentate nel diagramma di Fig. 5.3 a pag. 70.

Per la routine *BuildCore* sono state scritte 1400 righe di codice, di cui più di 1000 solamente per la subroutine *CoreTestReport*. Quest'ultima routine gestisce la procedura iterativa che permette di calcolare i parametri a, b e c dell'equazione di Frolich basandosi sui dati delle prove a vuoto. La ricerca dei tre parametri è un problema di ottimizzazione non lineare e multidimensionale. Per la ricerca dei parametri è stato utilizzato il metodo *"Golden Section Search"* esteso a tre dimensioni. Lo schema a blocchi che schematizza il funzionamento di questa subroutine è riportato in Fig. 5.4 a pag. 72.

Alcune prove di laboratorio sono state eseguite su un piccolo trasformatore da distribuzione, vedi Fig. 6.2 e Fig. 6.3 a pag. 76. Sono stati confrontati i dati ottenuti utilizzando strumenti analogici da laboratorio con quelli ottenuti utilizzando un oscilloscopio digitale, riferirsi alle figure riportate nel Capitolo 6. Il problema principale che si è avuto durante le prove di laboratorio è stato la presenza di una sorgente di tensione non simmetrica in uscita dal variac trifase; questo problema ha comportato la nascita di correnti omopolari e tensioni distorte.

Anche se non totalmente corretti, i valori misurati in laboratorio sono stati utilizzati per la verifica del modello. Le Fig. 7.2, 7.3, 7.4 e 7.5 a pag. 95 e seguenti mostrano il confronto tra le curve delle correnti di magnetizzazione misurate e quelle simulate dal modello. La corrispondenza è buona considerando che ci si è riferiti a tensioni distorte. In molti casi anche i picchi secondari sono rilevati dal modello.

Una seconda verifica è stata fatta confrontando le curve di magnetizzazione. Queste ultime sono ricavate usando dati contenuti nella relazione tecnica di un trasformatore e i relativi disegni tecnici. Il risultato è riportato in Fig. 7.7 a pag. 103. Anche in questo caso si è ottenuto un buon risultato: le curve, ottenute utilizzando due metodi differenti, corrispondono in modo soddisfacente.

0.4 Conclusioni

Il principale intento di questa tesi è di suggerire e testare un modello del nucleo del trasformatore topologicamente corretto. Il modello presentato è innovativo sia per i set di dati che possono essere specificati, che per la sua validità e applicabilità ad un ampio gruppo di trasformatori. Le principali conclusioni sono:

- Un modello avanzato di trasformatore (XFMR) è stato sviluppato per ATP-Draw. Questo componente è completo ed intuitivo. Le caratteristiche avanzate e la semplice interfaccia rendono XFMR un utile integrazione per le simulazioni di reti elettriche.

- La parte più innovativa di XFMR è la modellizzazione del nucleo magnetico. L'uso di un modello topologicamente corretto rende possibile un accurata rappresentazione della caratteristica non lineare del trasformatore. Questo tipo di modello diventa perciò indispensabile se si vuole esaminare con dettaglio fenomeni quali i transitori di commutazione o tenere in considerazione la saturazione del circuito magnetico del trasformatore.

- Un aspetto innovativo di questo lavoro è l'elaborazione dell'equazione di Frolich nella sua forma modificata. Questa nuova versione permette una più accurata corrispondenza con la curva di magnetizzazione.

- La routine SATURA incorporata in ATP è stata rivista e migliorata. La nuova routine è stata chiamata *rms2peak* che a differenza di SATURA tiene in considerazione il tipo di connessione (stella o triangolo).

- Gli esperimenti svolti in laboratorio sono stati di grande aiuto nella comprensione del problema. Non sono però risultati completamente adeguati per la verifica del modello e dovrebbero essere ripetuti a causa di problemi legati alla dissimmetria della sorgente di tensione.

- Suggerimenti per futuri sviluppi sono riportati nel Paragrafo 8.1

Chapter 1

Introduction

During the last decades there has been a great change in the general terms and conditions for power system utilities. Opening up for free competition has led to major restrictions regarding the development of one of the major utility: electricity. Efficiency improvements, cutting cost and reducing investments are necessary to be more competitive. Moreover, the number of transient situations is believed to increase in a distributed power generation regime due to more switching operations.

At the same time, the demand for a reliable supply of energy has increased considerably requiring nearly a no-fault operation of power systems. The age distribution of transformer population is entering in a critical era. Transformers subjected to overload condition and/or accelerating ageing might be near at the end-of-life.

At present, wind farm are gradually increasing as alternative source of energy. In this plants frequent switching operations and energization transients occur more than in thermo- and hydro-electric systems. Moreover, windmill plants are extensively exposed to lightning over-stresses. The large number of generators and connecting cables in such plant can also increase the risk of resonance.

Accurate estimation of losses and heavy working conditions, reads no-load losses and inrush currents, helps efficiency improvements, better protection scheme, costs reduction and plants optimization. In generally the integration of power transformers in the network is better taken care of.

Transformer modelling has traditionally occupied a lot of attention during the years due to its importance in power systems and also to the complexity of the component. There is still disagreement in literature on which assumptions should be allowed or not in order to make a good model. Topologically correct core models give high accurate results and seems to be the preferred choice for developing new

model. Establishing general and comprehensive models, when only standard set of data are available is also a challenge.

1.1 Scope of Work

The thesis is part of the project that studies saturation effects in power transformers. The goal is to develop better models of transformers in EMTP-type software. The focus is on the low frequency region where saturation is a challenge. Such models can be used in transient simulations to predict switching transients and inrush currents. Inrush currents are caused by saturation effects in the iron core when a transformer is energized. High inrush current can result in voltage dips and tripping of differential current relays, both leading to reduce power quality. Some providers have installed synchronized breakers to migrate high inrush currents, but this practice generally results in higher overvoltages and increases the risk of resonances. The trends of increased short circuit capacity and reduced losses in power systems increase the inrush currents and make proper setting of relays more difficult.

To predict the electromagnetic stresses on transformers calculation models must be established. The single-phase based equivalent models used in present simulation packages does not sufficiently represent differences and coupling between phases due to the iron core geometry. The representation of hysteresis, anomalous losses and remanence should also be improved. Lack of input data is the main problem as the typical test report procedure is insufficient to establish an accurate saturation curve.

Novel aspects presented in this thesis concern the development of a transformer model based on a topologically correct core model. The implementation is based on the reports of Prof. Bruce Mork and his team, but the model has been revised and refined in order to obtain a more generalize representation. The most complex part regards the implementation of the core model. It requires extensive mathematical calculation and iterative procedures. The speed and capacity of modern computers now allow for this kind of calculations that earlier were considered impracticably.

1.2 Thesis Outline

The thesis has three main parts: background information, implementation and test of the model. Chapter 1-3 contains background material, state of the art, and all

necessary information for the comprehension of this work. Chapter 4-5 contains the implementation. Chapter 6-8 contains the validation and the results.

In addition of the outline of the work in this chapter, the other chapters include:

Chapter 2 presents the program where the model has been implemented and the present transformer models offered.

Chapter 3 describes the stage of the development of an advanced model. It show how the behaviour of a transformer can be split in four independent sections: coil resistance, leakage representation, capacitive effects and core representation.

Chapter 4 analyses in detail the core representation. The development of the model from the physical structure to the core model is presented here. The parameter estimation technique is discussed, and three methods to obtain the data are presented: from factory test report, from design information, and based on a complete approximation.

Chapter 5 discusses the implementation of the model using a low-level programming language.

Chapter 6 shows the results of some tests done in laboratory on a small distribution transformer.

Chapter 7 discusses the comparison between the laboratory tests and the results obtain from simulations. Optional solutions for improve the iron core representation are analysed.

Chapter 8 contains the main conclusions from this work and suggests topic for further development.

Chapter 2

EMTP-ATP and ATPDraw

This chapter gives a brief presentation of the EMTP-ATP program and its graphic interface. The major characteristics and possible applications of this powerful tool are discussed. More detailed information is given on the transformer models. Starting from simplest transformer topology, to more advanced transformer representation. The chapter ends with a remark on the absence of a valid frequency dependent model.

2.1 Alternative Transient Program

This section provide a short historical introduction and present the main peculiarity of the EMTP-ATP program. The information is obtained from the official EMTP web-site, [1].

The Alternative Transient Program (ATP) is considered to be one of the most widely used universal program system for digital simulation of transient phenomena of electromagnetic as well as electromechanical nature. With this program, complex network and control system of arbitrary structure can be simulated. ATP has extensive modelling capabilities and additional important features besides the computation of transients.

The Electromagnetic Transient Program (EMTP) was developed in the public domain at the Bonneville Power Administration (BPA) of Portland, Oregon prior to the commercial initiative in 1984 by EMTP Development Coordination Group and the Electric Power Research Institute (EPRI) of Palo Alto, California. The birth of ATP dates to early in 1984, when Dr. Meyer and Dr. Liu did not approve the proposed commercialization of BPA's EMTP. They started a new program from

Element	Limit
Buses	6000
Branches	10000
Switches	1200
Sources	900
Non-linear elements	2250
Synchronous machines	90

Table 2.1: Limits for standard distribution.

a copy of BPA's public-domain EMTP. Since then ATP has been continuously developed through international contributions of several experts.

Whereas EMTP remains in the public domain by U.S. law, ATP is not in the public domain. Licensing is, however, available free of charge to anyone in the world.

The ATP program predicts variables of interest within electric power network as function of time, typically initiated by some disturbance. Basically, trapezoidal rule of integration is used to solve the differential equations of system components in the time domain. Non-zero initial conditions can be determined either automatically by a steady state phasor, or they can be entered by the user for simpler components.

ATP has many modules including rotating machines, transformers, surge arrester, transmission lines, and cables. Interfacing capabilities to the program modules TACS [1] and MODELS [2] enables modelling of control system and components with nonlinear characteristics such as arcs and corona. Dynamic systems without any electrical network can also be simulated using TACS and MODELS control system modelling.

Symmetrical or unsymmetrical disturbances are allowed, such as faults, lighting surges, and several kind of switching operations including computations of valves. Frequency-domain harmonic analysis using harmonic current injection method and calculation of the frequency response of phasor networks are also supported.

ATP-EMTP tables are dimensioned dynamically at the start of execution to satisfy the needs of users and their hardware. No absolute limits have ever been observed. The standard version has limits that average more than twenty times default table sizes. The standard limits for the standard program distribution are reported in Tab. 2.1.

[1] Transient Analysis of Control System
[2] a simulation language

ATP-EMTP is used world-wide for switching and lighting surge analysis, insulation coordination and shaft torsional oscillation studies, protective relay modelling, harmonic and power quality studies, HVDC and FACTS modelling. Typical EMTP studies are:

- Lighting overvoltage studies
- Switching transients and faults
- Statical and systematic overvoltage studies
- Very fast transient in GIS and grounding
- Machine modelling
- Transient stability, motor startup
- Shaft torsional oscillations
- Transformer and shunt reactor/capacitor switching
- Ferroresonance
- Power electronic application
- Circuit breaker duty (electric arc), current chopping
- FACTS devices: STATCOM, SVC, UPFC, TCSC modelling
- Harmonic analysis, network resonances
- Protection device testing

2.2 ATPDraw

ATPDraw for Windows [2] is a graphical, mouse-driven preprocessor to the ATP version of the Electromagnetic Transients Program (EMTP). In ATPDraw the user can construct the digital model of the circuit to be simulated using the mouse and selecting predefined component from an extensive palette, interactively. Fig. 2.1 shows the layout of the ATPDraw program with a circuit window showing most of the predefined objects. The ATPDraw generates the input file for the ATP simulation in the appropriate form based on “what you see is what you get”. Circuit

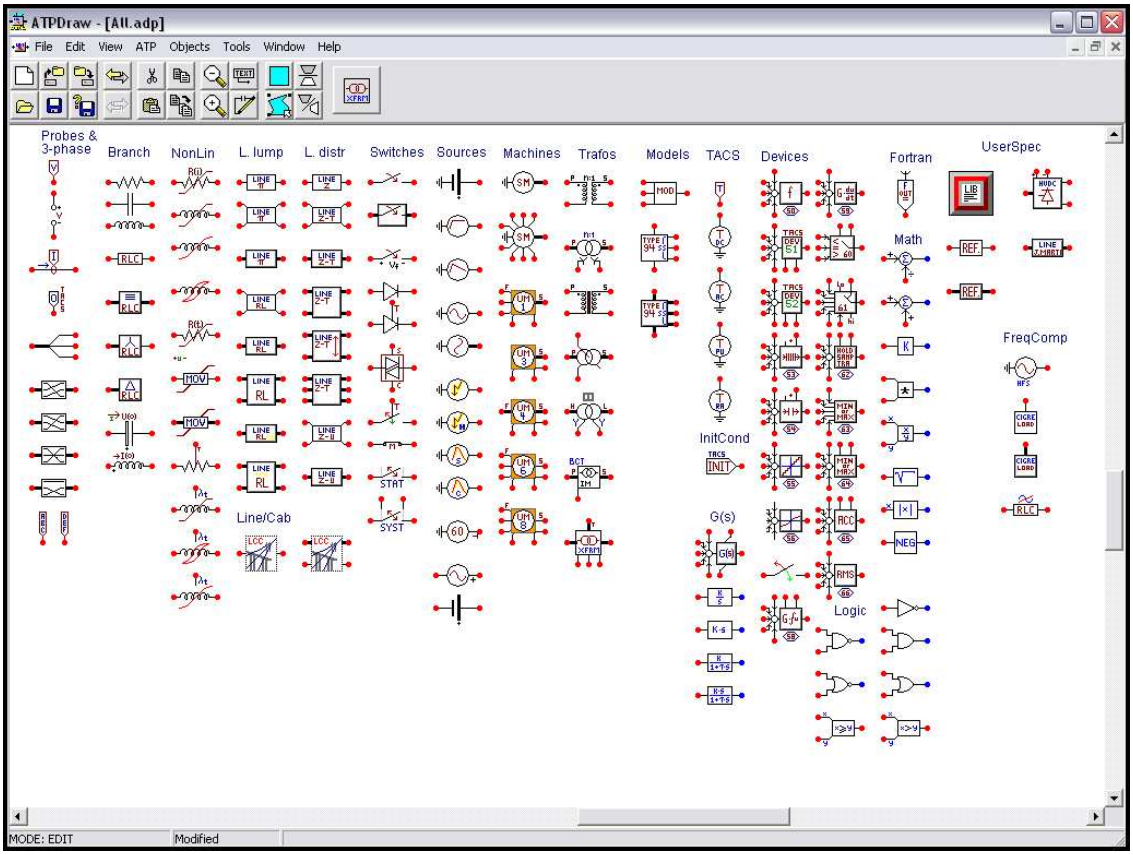

Figure 2.1: ATPDraw main windows showing most of the predefined components.

node naming is administrated by ATPDraw, thus the user needs to give name only to nodes having special interest.

Most of the standard component in ATP, as well as TACS, are supported. In addition the user can create new objects based on MODELS and $INCLUDE[3]. Both single and 3-phase circuits can be constructed. Line and cable modelling[4] is also included in ATPDraw where the user specify the geometry and material data; user has the option to view the cross section graphically and verify the model in the frequency domain. Object for Harmonic Frequency Scan (HFS) have also been added. Special objects help user in machine and transformer modelling, including the powerful UNIVERSAL MACHINE and BCTRAN[5] features of ATP.

ATPDraw, thanks to its intuitive interface, is more valuable to the new user of ATP-EMTP and it is an excellent tool for educational purposes. However, the possibility of multilayer modelling makes ATPDraw a powerful front-end processor

[3]Data Base Module
[4]KCLee, PI-equivalent, Semlyen, JMarti and Noda
[5]Soon replaced with the more general transformer model XFMR

for professional in analysis of electric power system transients, as well [3].

ATPDraw is the propriety of SINTEF Energy Research, Norway, and Bonnerville Power Administration, BPA, Portland, USA. The development is founded by BPA. Program developer is Dr. Hans Kristian Høidalen at SINTEF Energy Research in Trondheim, Norway. The ATPDraw program is royalty free and can be downloaded free of charge from several Internet sites. The on-line help and the program documentation includes third-party proprietary information, thus ATP licensing is mandatory prior to get permission to download the program and documentation from the Internet, or receive ATP related material from the others.

2.3 Transformer Model in ATP-EMTP

The first representation of transformer in EMTP was in the form of branch resistance and inductance matrices [R] and [L]. The support routine XFORMER was written to produce these matrices from the test data of single-phase two and three-winding transformers. Stray capacitances are ignored in these representations, and they are therefore only valid up to few kHz. A star circuit representation for N-winding transformers (called "saturable transformer component") was added later, which uses matrices $[R]$ and $[L]^{-1}$ with the alternate equation

$$[L]^{-1} \cdot [v] = [L]^{-1} \cdot [R] \cdot [i] + [di/dt] \tag{2.1}$$

in the transient solution. This formulation also became useful when support routines BCTRAN and TRELEG were developed for inductance and inverse inductance matrix representations of three-phase units. An attempt was made to extend the star circuit to three-phase units as well, through the addition of a zero-sequence air return path reluctance. This model has seldom been used, however, because the zero sequence reluctance value is difficult to obtain.

Saturation effect have been modelled by adding extra nonlinear inductance and resistance branches to the inductance or inverse matrix representations, or in the case of star circuit, with the built-in nonlinear magnetizing inductance and iron core resistance. A nonlinear inductance with hysteresis effect has been developed as well. An accurate representation of hysteresis and eddy current effect, of skin effect in the coils, and of stray capacitance effects is still difficult at this time; progress in modelling these effects is expected from this and following projects. The simplest transformer representation in the form of an "ideal" transformer was the last model

to be added. See [3], [4], [5], and [6].

2.3.1 Transformer Support Routine in ATP-EMTP

The "Saturable Transformer Component" uses an input option specific to the transformer topology. All other transformer representations use the general branch input option for π-circuits (with C = 0). It is possible to add linear or nonlinear uncoupled resistance and inductance branches for the representation of exiting current. There are three support routine XFORMER, TRELEG, and BCTRAN which convert the transformer data into impedance or admittance matrices, as well as a support routine CONVERT for the conversion of saturation curves $V_{rms} = f(I_{rms})$ into $\lambda = f(i)$. These support routines, as well as saturable transformer component, are briefly described in the following pages, for more details see [5].

Support Routine XFORMER

XFORMER is a support routine for single phase transformer. It is somewhat obsolete, and it recently has been replaced by BCTRAN. XFORMER can be used for two- and three-winding transformers.

Except for error at extremely low frequencies the model produces by XFORMER is useful if one takes precautions for ill-conditioned matrices.

Support Routine BCTRAN

BCTRAN works for any number of windings, and for single-phase as well as for three-phase units. It uses the approach to produce the $[R]$ and $[L]^{-1}$ matrices of coupled branches. BCTRAN has also an option for inductance matrices $[L]$, in case of non zero exiting current. If this option is used, the ill-conditioning problem has to be carefully taken into account.

A circuit can be added externally to BCTRAN if the user wants to consider a nonlinear core.

Impedance matrices produced by BCTRAN and XFORMER differ mainly in the existence of off-diagonal resistance values produced by XFORMER routine. For this reason the model obtained from BCTRAN routine is more accurate than that from XFORMER at very low frequencies ($\ll 50Hz$).

Support Routine TRELEG

TRELEG was developed concurrently with the development of BCTRAN. It builds impedance matrix of N-winding single- or three-phase transformers directly from short-circuit and excitation test data. The excitation current must be always nonzero, and for very small values of exiting current, the matrices are subjected to the ill-conditioning problem.

Since the ill-conditioning problems do not exist with $[L]^{-1}$, support routine BCTRAN makes TRELEG unnecessary.

Support Routine CONVERT

Saturation curves supplied by manufactures often give rms voltage as a function of rms currents. The support routine CONVERT changes V_{rms}/I_{rms}-curves into flux/current-curves $\lambda = f(i)$ with the following simplifying assumptions:

1. hysteresis and eddy current losses in the iron-core are ignored;
2. resistance in the winding is ignored;
3. the λ/i-curve is to be generated point by point at such distances that linear interpolation is acceptable in between points.

Very often, the V_{rms}/I_{rms}-curve is only given around the knee-point, and not for high values of saturation. In such cases, it is best to do the conversion first for the given points, and then to extrapolate on the λ/i-curve with the air-core inductance.

Saturable Transformer Component

This built-in model was originally developed for single-phase N-winding transformers. It is based on a star-circuit representation. The primary winding is handled as an uncoupled $R - L$ brunch and a magnetizing brunch that outlined the saturable characteristic of the transformer. Each of the other winding is treated as two-winding transformer. Each of this two-winding transformer are derived from the cascade connection of an ideal transformer with an $R - L$ brunch.

This model can also be used to construct three phase transformers. Three-phase transformer are presented in EMTP Rule Book [4] as composed of three single-phase transformers. In this way phase-to-phase magnetic coupling, in the case of multi-limbed three-phase cores, is not properly represent in the model.

The input data consist of the R, L-values of each star branch, and the turn ratio, as well as information for the magnetizing branch.

The saturable transformer component has some limitations, which user should be aware of:

1. It cannot be used for more than three winding, because the star circuit used is not valid for model with $N > 3$.

2. The linear or nonlinear magnetising inductance, with R_m in parallel, is connected to the star point that is not always the best connecting point.

3. Numerical instability has occasionally been observed for the three-winding case due to a negative inductance in the star circuit.

4. While the saturable transformer component has been extended from single- to three-phase units through the addition of a zero-sequence reluctance parameter, its usefulness for three-phase units is limited. Three-phase units are better modelled with inductance or inverse inductance matrices obtained from support routines BCTRAN or TRELEG.

2.3.2 Frequency-Dependent Transformer Models

At this time, no frequency-dependant effects have yet been included in the transformer model. There are basically three such effects:

- Frequency-dependent damping in the short-circuit impedances;
- Frequency-dependence in exiting current;
- Influence of stray capacitances at frequencies above 1 to 10 kHz.

The next chapter will present how it is possible to include such effects in a transformer model. In addition to frequency dependent effect of the winding resistance and capacitances, also a topologically correct core model will be introduced.

Chapter 3

Advanced Transformer Model

This chapter discusses the development of more advanced transformer models. The BCTRAN routine is improved and a self contain hybrid model is obtained. This hybrid model is developed to become an ATPDraw component and takes the name of XFMR. This component takes into account frequency dependency, capacitive effects, leakage representation and use a topologically correct core model. Each of these parts is briefly analysed and commented.

3.1 Need for Advanced Model

The transformer is an essential component in power systems, but the models used for these component in transient calculations suffer from low accuracy. Transient simulations of special concern are inrush currents, resonances, and switching impulse stresses. Internal resonances and lighting impulse stresses would require even more sophisticated models not discussed here. The number of transient situations is believed to increased in a distributed power generation regime due to more switching operations. A main problem is the lack of measurement and data; quite often typical value must be used instead.

The development of a low- and mid-frequency model is essential to investigate excitation and inrush current, ferroresonance, DC offset and harmonics, and switching transients. Lumped parameter model can be sufficient for frequencies up to 3-5 kHz[1]. The model must use the proper core topology and include capacitive effects, as well as frequency-dependent coil resistance.

The implementation of an advanced model in ATPDraw is mostly based on the

[1]or higher, up to the first resonance peak.

work made by Bruce Mork and his group at MTU as reported in [7], [8], and [9].

3.2 BCTRAN-Based Model

A linear representation of single and three-phase transformers can be made in the form of branch impedance or admittance using BCTRAN [4], [5]. However, this approach cannot include nonlinear effects of iron cores, capacitance, and other effects. Detailed model incorporating core nonlinearities can be derived using the principle of duality, [10], [11].

A hybrid model is developed using the strengths of BCTRAN and duality. This allows to build BCTRAN-based transformer models. The hybrid model also incorporate the frequency-dependency of resistances and capacitive effects. This model is valid for low and mid-frequency ranges. Care has been taken to develop a general unified model that is implementable for various core and coil topologies. A unified model is more reliable then a large library of specific transformer models.

3.2.1 Duality

Detailed models incorporating core nonlinearities, valid for low frequency transient simulations, can be derived using the principle of duality. These models are based on the development of a magnetic circuit representing the flux paths in the core of a three-phase transformer and sequent conversion of this magnetic circuit to an equivalent electric circuit using duality transformation.

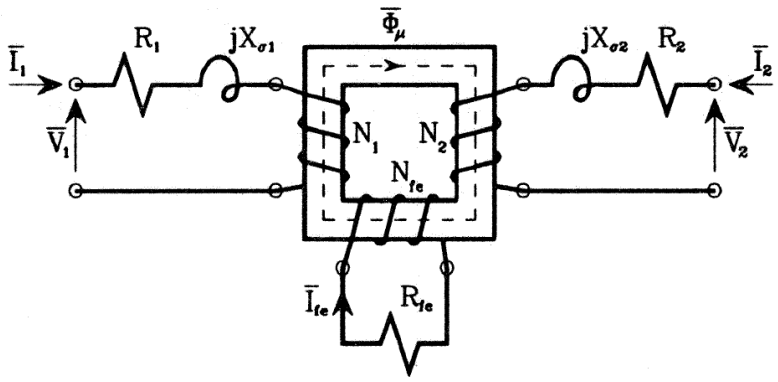

Figure 3.1: Fictitious third coil [14].

Fictitious N+1th Coil

The process used to convert a magnetic circuit into the dual electric one shows that the core losses can be removed from the iron core. The losses are then taken into account connecting the core equivalent to a fictitious winding. Fig. 3.1 shows this concept for the case of a fictitious winding used to take into consideration the rate of the eddy current.

Using the method of the fictitious winding it is also possible to consider the leakage flux linked by the low voltage winding but not flowing in the core. This can be conceptually dealt by assuming the fictitious coil infinitely thin and attached at the surface of the core leg. Conceptual representation is shown in Fig. 3.2.

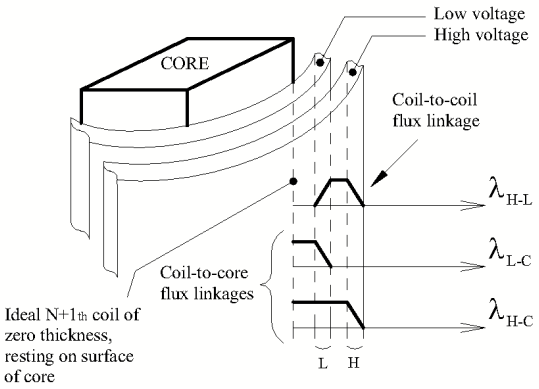

Figure 3.2: Conceptual implementation of N+1th winding flux leakage model [8].

The fictitious winding will be used for the complete leakage representation and as attachment point for the core equivalent, as show in Fig. 3.3.

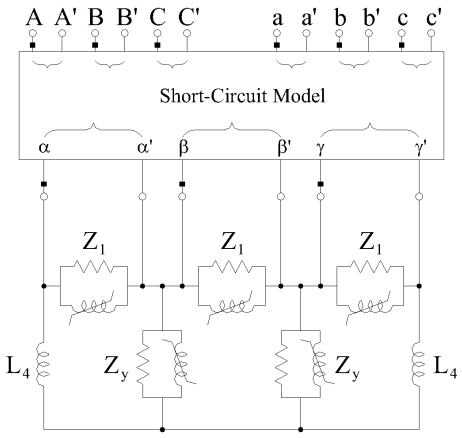

Figure 3.3: Three-legged stacked core transformer; N+1th winding attached core [7].

3.2.2 BCTRAN

ATPDraw provides an interface for the BCTRAN transformer matrix modelling to represent single and three-phase, two and three windings transformer [3]. After the user has entered data for the structure of the transformer, the rating, and the open and short circuit factory test, ATPDraw calls ATP to create the punch file that will finally be inserted into the main ATP file.

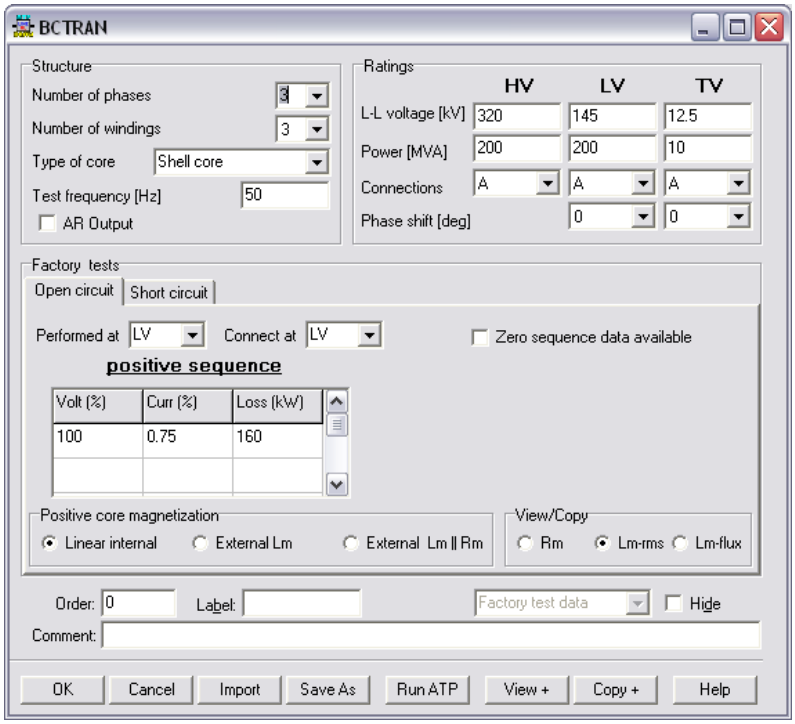

Figure 3.4: BCTRAN transformer modelling, input data in ATPDraw.

Fig. 3.4 shows the dialog box used for entering the data. In the part related to the structure of the transformer the information to be specified are: number of phases, number of windings, and test frequency. The type of core is not supported. The user can also request the inverse L matrix as output by checking the option "AR output"[2] An "Auto-add nonlinearities" button appears when an external magnetising branch is requested.

The information to be specified under the ratings tab are the line-to-line voltage levels, the power, the connection, and the phase shift for each winding.

Under factory tests, the user can choose either the open or the short circuit test. In the open circuit tab the user can specify the test winding and at which the

[2]L can have singularity problem if the excitation branch is neglected.

excitation branch should be connected. Up to six points on the magnetising curve can be specified. The value for other voltages then 100% can be used to define a nonlinear magnetising inductance/resistance, choosing: *"linear internal"*, it will result in a linear core representation; *"external Lm"*, will result in the calculation of a nonlinear magnetising inductance as $I_{rms} - U_{rms}$; *"external Lm/Rm"*, the nonlinearities are handle as external objects to the model. Short circuit data are specified as binary short circuit impedance in %, losses in kW, and base power used for the test in MVA. If available, also zero sequence data can be specify.

3.2.3 Hybrid Model

Using BCTRAN, a linear representation of single and three phase transformers can be made in the form of branch impedance or admittance matrices. A simple nonlinear core model can be added externally.

Detailed models incorporating core nonlinearities, and valid for low frequency transient simulations, can be derived by using the principle of duality. However, the most important disadvantage for the model based on duality is the lack of a complete leakage representation present in the model obtained using BCTRAN.

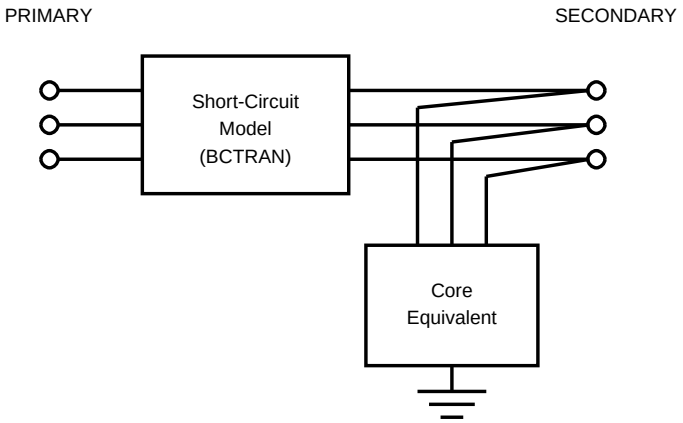

Figure 3.5: Basic concept of BCTRAN-duality model for two-winding transformer.

A hybrid model can achieve the advantages of the two approaches. The idea is to use BCTRAN for the short circuit model and to use duality to take into account nonlinearities and couplings. Fig. 3.5 show the basic concept applied to a two winding transformer.

A further step in the development of a hybrid model has been achieved with the introduction of XFMR. This component in fact does not require the execution

of ATP's BCTRAN support routine (Sec:3.2.2) to create the $[A]$ matrix. This allows faster calculation and more simpler implementation. The following sections examines in detail the main components and functions of the hybrid model.

3.3 XFMR

The model includes advanced core models and automatic calculation of the A-matrix[3]. Leakage inductance and capacitance matrix, nonlinear core equivalent, and frequency dependency coil resistance are all aspect included in this model. For these reasons, this component is believed to replace the BCTRAN, module that requires ATP execution.

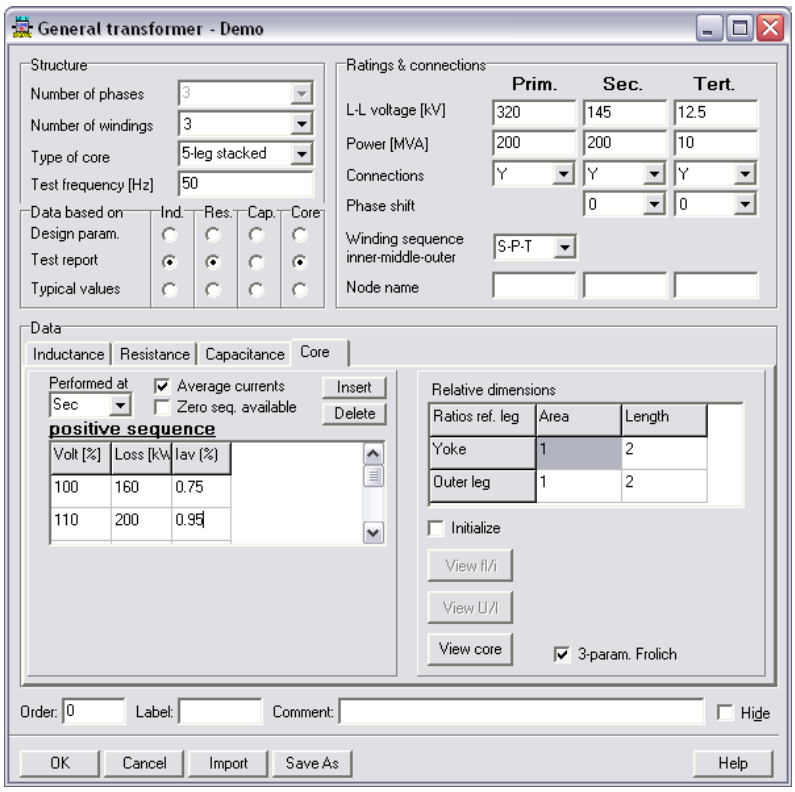

Figure 3.6: Input dialog of the XFMR advanced transformer object.

A transformer equivalent circuit that takes leakage, capacitive, and frequency effects in to account, can be divided in four main parts that when combined provide the complete transformer model. In Fig. 3.7 and 3.8 the green traits represent the

[3]inverse of L

core, the orange the winding resistance, the blue the leakage, and the red the capacitive effect. Each of these sections are now examined more in detail.

3.3.1 Frequency Dependent Coil Resistance

Resistances are in orange in Fig. 3.7 and 3.8. Coil resistance vary widely depending on the frequency of the current flowing. The variation is due to the skin effect and proximity effect. Skin effect is caused by the non uniform distribution of current in the conductor; as the frequency increases, more current flows near the surface of the conductor, therefore, the effective resistance increases. Proximity effect is due to the external magnetic field generated from current in the other conductors; in a transformer, a high number of layers in the coil lead to a great resistance variation due to this effect. Skin effect dominates the losses up to a certain frequency, then proximity effect becomes predominant. Eddy current within the conductor can also be considered.

The frequency-dependency of the winding resistances is implemented in the model using a Foster equivalent circuit. This method does not work properly with one cell, since a single order frequency dependent representation is not as good as desired. To obtain a robust frequency dependent representation it is necessary to use a two cell Foster equivalent circuit, shown in Fig. 3.9.

In the circuit, Rs represent the DC resistance, measurable with a simple volt-amperometer test. From test data performed at different frequency, the value of the other element can be obtained from Eq. (3.1) and Eq. (3.2) with the least square curve fitting. If there are no test data for frequency higher then 50 Hz, than the value of the effective resistance can be obtained from tabulated values, see [8].

$$R_{eff} = R_S + \frac{R_1 \cdot (\omega L_1)^2}{R_1^2 + (\omega L_1)^2} + \frac{R_2 \cdot (\omega L_2)^2}{R_2^2 + (\omega L_2)^2} \tag{3.1}$$

$$F(R_1, L_1, R_2, L_2) = \sum_{i=1}^{N} [R_{given_i} - R_{eff}]^2 \tag{3.2}$$

The inductance L_1 and L_2 are required to provide a frequency dependent behaviour. To obtain the pure resistive behaviour, the equivalent inductance is compensated by adding a negative inductance, $-L_{ART}$, in series with the Foster circuit.

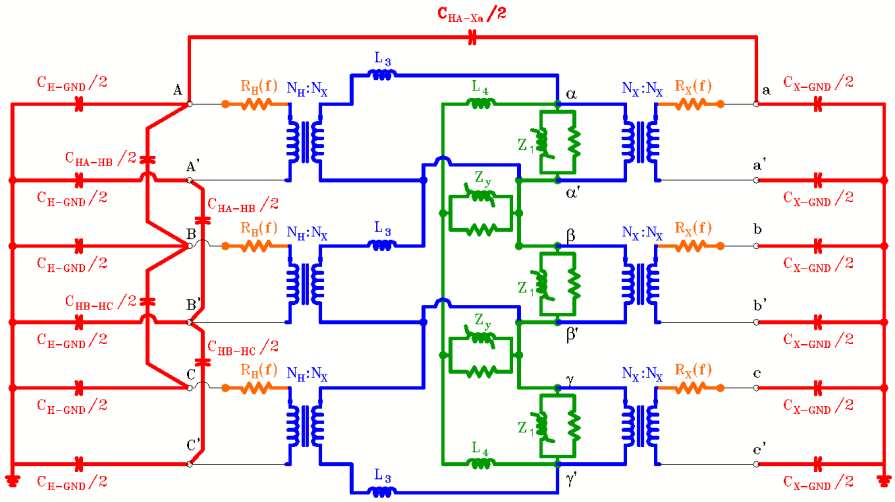

Figure 3.7: Three-phase, three-leg transformer. Equivalent Circuit [8].

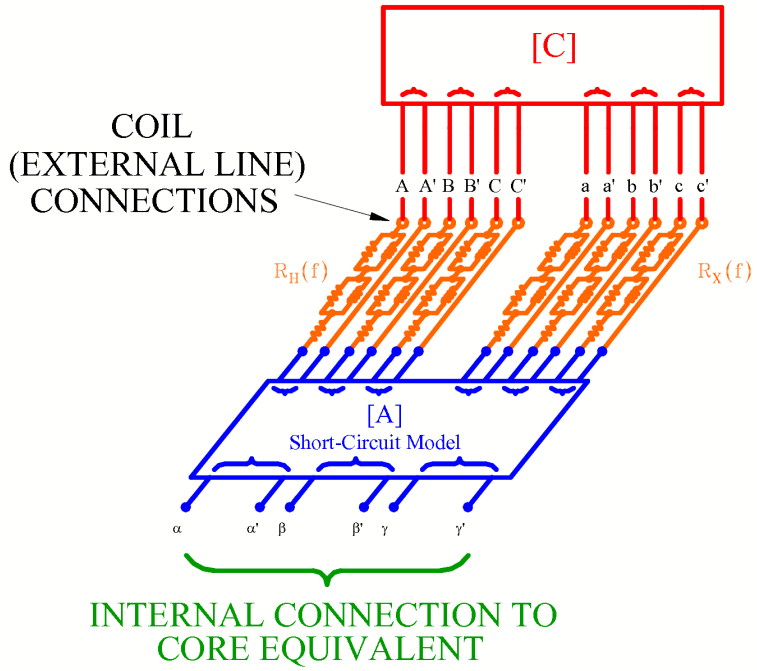

Figure 3.8: Hybrid Model [7].

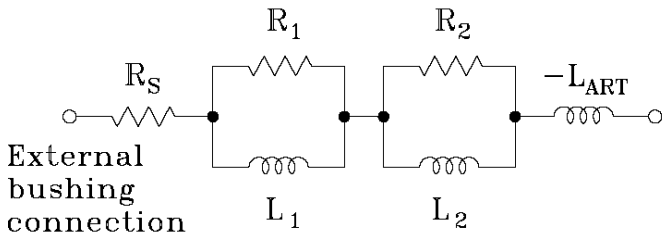

Figure 3.9: Foster circuit with two cells.

3.3.2 Leakage Representation

Leakage representation is in blue in Fig. 3.7 and 3.8. The leakage representation correspond to the $[A]$ matrix (inverse of the inductance matrix). The elements that form this matrix include the effect of the respective turns ratios between coils. The leakage reactances are determined from binary short circuit tests. In general, $[A]$ represents the topology of a N-node network having connecting branches between all possible node pairs, and can be topologically constructed. The fictitious core winding is added as $N + 1$.

The matrix $[A]$ represent the short circuit behaviour of the transformer. This can be calculated from the short-circuit reactance that can be obtained in three different way:

- from factory test report, where available data are short circuit impedances and losses;
- from transformer design, where available data are the shape of windings, core material, and core and coil dimensions;
- from a complete estimation, where only basic ratings of the transformer are known.

More information related to these aspects can be found in [9].

3.3.3 Capacitive Effects

Capacitive effects are in red in Fig. 3.7 and 3.8. Capacitive effect may be significant and need to be included in the model. The mayor coupling capacitances are capacitances between high and low voltage windings and core, and capacitance between high voltage phases, outer legs, and grounded elements. All these are shown in

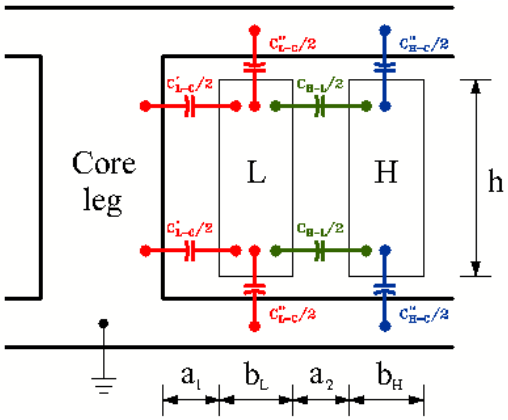

Figure 3.10: Capacitances between winding and core [9].

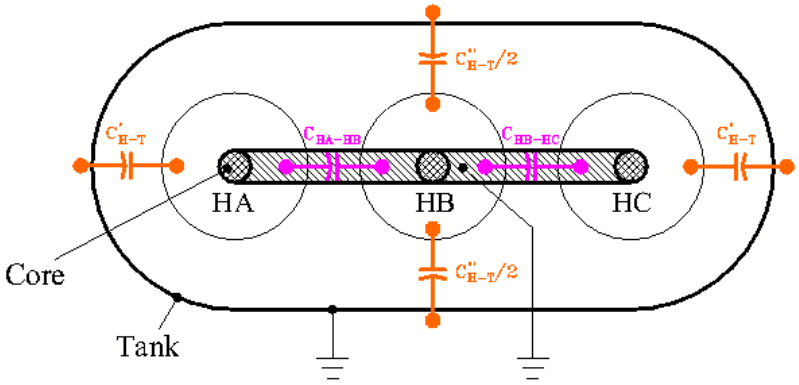

Figure 3.11: Three-legged transformer. Capacitances between phases [9].

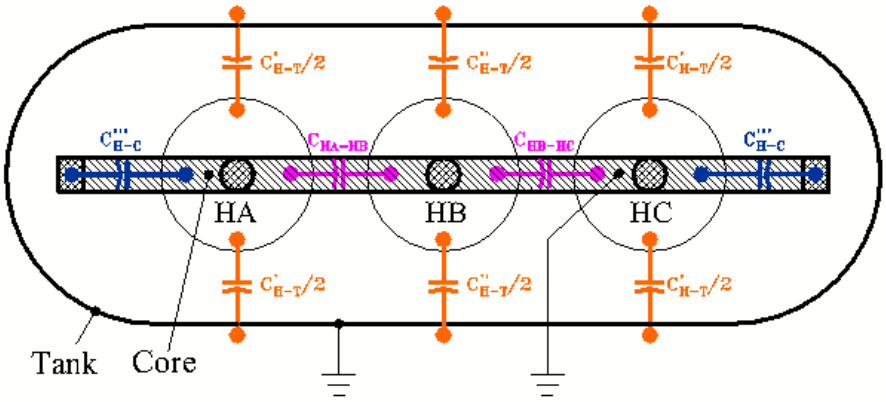

Figure 3.12: Five-legged transformer. Capacitances between phases [9].

Fig. 3.10, 3.11, and 3.12. For a better distribution of the capacitive effects, all capacitances are divided in two equal parts and added to each side of the N windings[4]. The capacitances outlined here compose the $[C]$ matrix.

Necessary data (coil-to-coil capacitances)for the matrix $[C]$ can be calculated in three different way:

- from factory test report, where available data are winding-to-ground and winding-to-winding capacitances;
- from transformer design, where available data are winding surfaces, winding heights, winding radiuses, and relative permeability;
- from a complete estimation, where only basic rating of the transformer are known.

More information related to these aspects can be found in [9].

As a future development, the size of both $[A]$ and $[C]$ matrices can be increased for higher frequency models. It would be possible to add more levels of detail for the capacitive effects, such as layer-to-layer or turn-to-turn capacitances.

3.3.4 Core Representation

Core representation is in green in Fig. 3.7 and 3.8. It corresponds to the nonlinear core representation attached to the fictitious $N + 1th$ winding. This section is the central part of this project and is fully explained in the next chapter.

[4]Lumped parameter model.

Chapter 4

Magnetization Characteristics in a Topologically Correct Transformer Core Model

This chapter can be considered as the core of my thesis work. It goes deeply in the analysis of the core representation. The procedure to obtain a four sections model starting for the physical structure is presented. This step is very important and validate the correctness of the model.

The magnetizing curve are described with the Frolich equation [23]. A modified version of this equation is suggested. The new version, when applicable, is shown to give more accurate results.

A good model is totally unusable if it is impossible to obtain the required input data. The parameter estimation technique is discussed in detail. It is shown how to obtain valid data starting from test report and detailed design information. In case of total lack of information, a complete approximation method is used.

4.1 Core Structure

There are two basic types of transformers characterized by the winding/core configuration: Shell Type and Core Type. Fig. 4.1 shows examples of different structures available for three phase transformers.

In a shell-type transformer the flux-return-paths of the core are external to and enclose the windings. Because of the intrinsically better magnetic shield provided by this structure, this is particularly suitable for supplying power at low voltage and

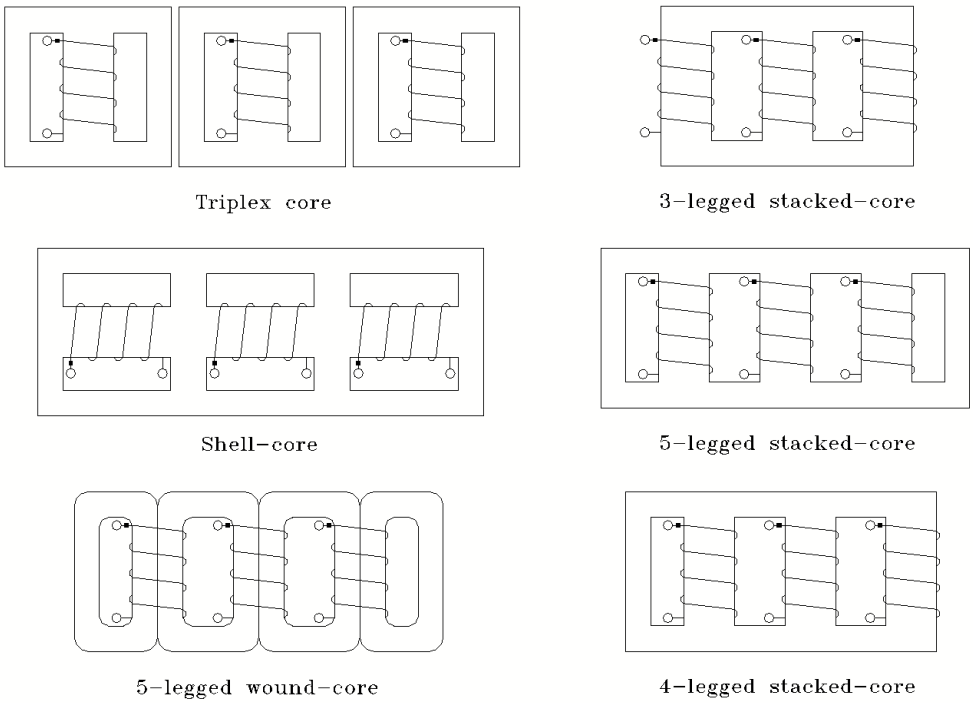

Figure 4.1: Three phase core designs [7].

large current. Core-type transformers have their limbs surrounded concentrically by the main windings. With this configuration, having top and bottom yokes equal in cross section to the wound limbs, no separate flux-return path is necessary.

A three-phase transformer has considerable economic advantage over three single phase units used to provide the same function. For this reason the great majority of power transformers are of three-phase construction. The only advantage of three single-phase transformers is that only one single-phase unit is required as spare part. The triplex core design allows cost saving due to the use of one single tank for all three phases.

An important distinction should be made between low and high reluctance transformers. Low reluctance transformer are composed from: bank of single-phase transformers, three-phase shell-type transformers, and three-phase four or five-leg transformers. For this category, the homopolar or zero-sequence flux flows in the core material, thus following a low reluctance path. The zero sequence excitation current will be small, and also the resulting excitation losses. Three-phase three-leg core-type transformers are included in the high reluctance group. The homopolar flux flows through the air and the tank of the transformer. That is a high reluc-

Magnetic Circuit		Dual Electric Circuit
MMF $m(t) = N\xi(t)$	$\Leftrightarrow$	Current $a = i(t)$
Reluctance ϑ	$\Leftrightarrow$	Susceptance $1/Lp = \vartheta/N^2$
Meshes	$\Leftrightarrow$	Nodes
Nodes	$\Leftrightarrow$	Meshes

Table 4.1: Duality transformation.

tance path. In this case the the zero sequence excitation current is important and the excitation losses cannot be neglected. Saturation effects will even occur in the transformer tank.

4.2 Duality Principle

In this chapter the core model will be analysed deeply in all its aspects. First of all is it important to analyse the theoretical principle on which the model is based: the duality principle. The duality principle is a method that allows the investigation and analysis of magnetic network with an electric network analogy. An electric network can be constructed from a magnetic circuit based on the topologic method due to Colin Cherry, dated back to 1949. The principle is mainly based on three points [14]:

- first it is necessary to draw physical structure of the magnetic circuit, so it is possible to recognize the leakage and common flux, and the magneto motive force (MMF);
- it is then possible to represent the magnetic network;
- finally, the transformer electric equivalent circuit is obtained applying the base rules of duality of interlinked electric and magnetic network reported in Tab. 4.1.

Briefly, meshes are substituted with nodes and vice versa; MMF sources in magnetic circuit become current sources in electric circuit, likewise reluctances become susceptances.

At this point the circuit can be simplified, but it is still not complete. Dissipative and reactive elements are introduced to consider winding resistance, core losses and coupling capacitances. Further in the chapter will be reported the complete duality circuits for three and five-leg transformers.

4.3 Core Nonlinearities and Losses Representation

The duality principle introduced in the previous section ensures a proper representation of the core circuit. The conjecture of the fictitious n+1th coil presented in Section 3.2.1 gives a valid attaching point for the core representation. Now the most important element to consider for obtaining a valid model is the nonlinear behaviour due to the magnetic saturation of the core, [8], [24]. The representation of the core is also depend on frequency and level of excitation.

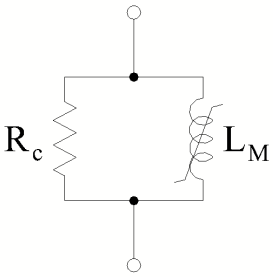

Figure 4.2: Traditional core representation.

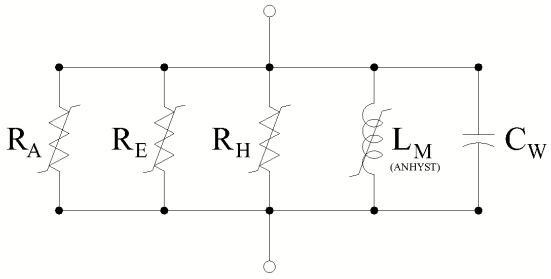

Figure 4.3: Advanced core representation.

Fig. 4.2 show the traditional and simple representation of the core. The resistance R_C represent the power losses, and the nonlinear inductance L_M represent the magnetic saturation.

The magnetic saturation is traditionally described using the virgin magnetisation curve. Saturation is more correctly modelled if it is considered separately from hysteresis. For this reason an improved model for L_M is based on the anhysteretic saturation curve, see Fig. 4.4.

With the anhysteretic approach a more advanced model can be built. The model shown in Fig. 4.3 has nonlinear resistances that represent various loss characteristics present in the transformer: hysteresis losses, R_H; eddy current losses, R_E; and anomalous losses, R_A.

Hysteresis is the loss in a transformer core due to domain wall movement when it is excited. Non linearities and sensitivities at high excitation level make it difficult

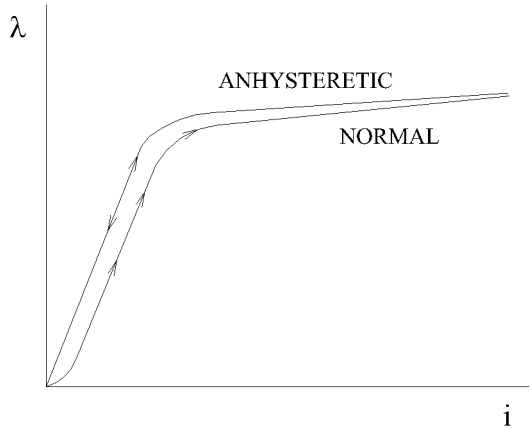

Figure 4.4: Anhysteretic and virgin saturation curves.

to model accurately. Hysteresis losses can be added directly to the saturation curve. This can be implemented either by modifying the equation of the saturation curve, or by adding a non-linear resistance element in parallel with the saturation curve. The resistance adds area to the $\lambda - i$ anhysteretic loop. This area represents the losses at a certain level of excitation. The hysteresis losses can be found by taking a family of DC magnetisation loops and subtracting the anhysteretic curve from them. Hysteresis losses should be defined as $\lambda - i$ function, since they are dependant on excitation level or flux level.

Eddy current losses are due to induced currents in the transformer core, windings and tank. The loss characteristics are dependant on frequency and voltage level. Steady state losses can be generated fairly easily. Transient responses are more difficult to model, since the frequency and maximum voltage level are unknown. The only way this can be solved in time domain is by using either parallel or series combinations of resistances and inductances, in a way similar to how frequency-dependent winding resistance is modelled.

Anomalous losses are core losses that cannot be explained by the other loss mechanisms. In standard transformers these losses are fairly small compared to hysteresis and eddy current losses, but in the new low-loss transformers these can be more significant. Some of the possible reasons for these anomalous losses are: the lack of uniform domain movements, non-sinusoidal domain movements, and non-sinusoidal flux densities. These increase the total losses of the transformer, and are added to the area of the $\lambda - i$ pattern. A characteristic for anomalous plus eddy current losses can be found by subtracting a family of DC magnetization loops from

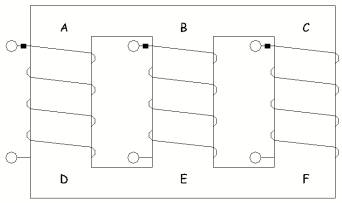

Figure 4.5: Three-leg stacked core transformer. Physical structure.

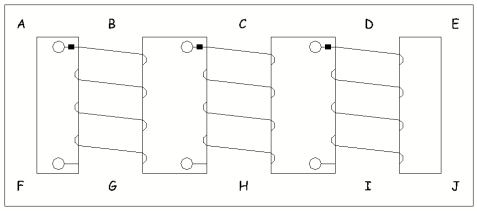

Figure 4.6: Five-leg stacked core transformer. Physical structure.

a corresponding family of 50 Hz open circuit $\lambda - i$ loops. Different test for different frequencies on the same level of excitation can help to describe the eddy currents behaviour.

Loss representation described above can be used to create the $\lambda - i$ loops around the anhysteretic curve. The area inside the $\lambda - i$ loop is the energy loss for one period of operation at a given level of excitation. All these losses can be modelled with a nonlinear resistances and represented on a $v - i$ curve.

4.4 Topologically Correct Transformer Core Model

Based on the consideration of the previous sections it is now possible to show how to obtain a topologically correct transformer core model. Three and five leg transformer are presented. Starting from the physical structure of the transformer, following succeeding steps, it will be shown how it is possible to split the model in four different parts. This provide the possibility of investigating only one of these sections at time. What is relevant to this project is the part related to the core. Once it is isolated, the core can be analysed and can be assessed the operational implementation of the model.

Physical Structure

The Fig. 4.5 and 4.6 represent the physical structure of the three and five leg staked transformers. These are the two main structure that will be studied in this thesis. The main parts that can be identified are the windings, the legs, the yokes, and for the 5-leg design the outer legs.

Magnetic Circuit

The magnetic circuit for the three-leg stacked core transformer is shown in Fig. 4.7. The current through the windings creates the magnetomotive force, forcing flux trough the iron core and the air. The reluctance of the iron core and the air relates the magnetomotive force to the flux. The reluctance for the leg (R_1) represent the paths A-D, B-E, and C-F, see Fig. 4.5. The reluctances for the yokes (R_y) represent the paths A-B, B-C, D-E, and E-F. The reluctance in the iron is represented by nonlinear inductances. Leakage paths are represented by:

- R_2, the leakage path between the legs and the innermost windings;
- R_3, the leakage path between the legs and the space between the two windings;
- R_4, the leakage path between the legs and outside the windings, also known

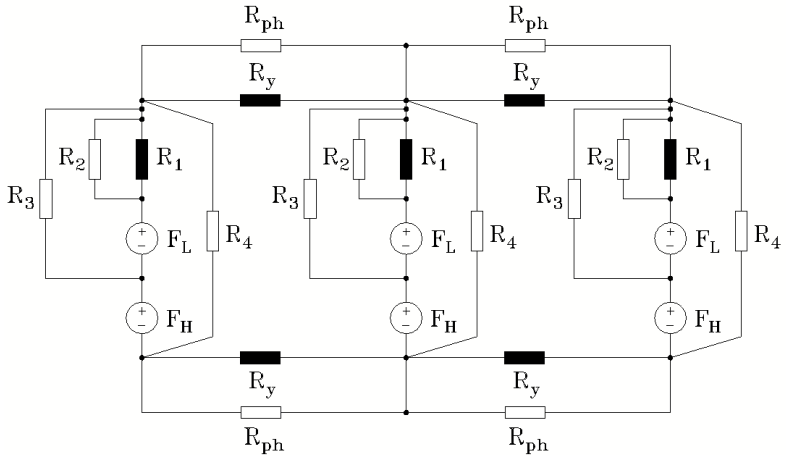

Figure 4.7: Three-leg stacked core transformer. Magnetic circuit [7].

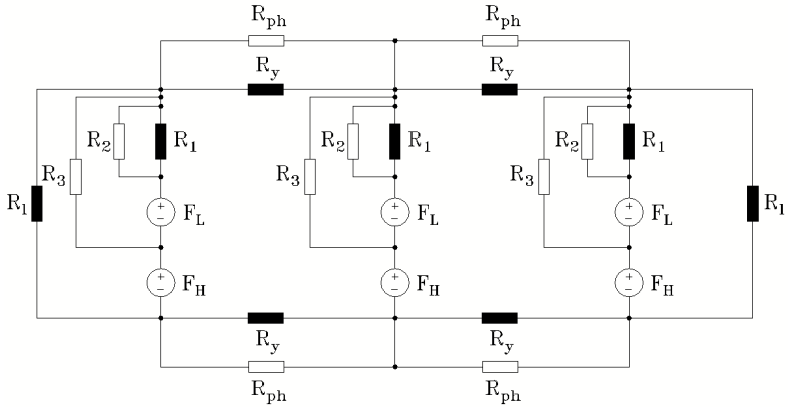

Figure 4.8: Five-leg stacked core transformer. Magnetic circuit [7].

as zero sequence path;

- R_{ph}, the leakage path through the air in parallel with the yokes.

These last paths lie outside the ferromagnetic core, so the resulting inductances for R_{ph}, R_2, R_3, and R_4 are linear.

The magnetic circuit for the five-leg stacked transformer is reported in Fig. 4.8. The only difference with the three-leg is the introduction of the two outer leg reluctances[1] (R_l).

Electrical Dual

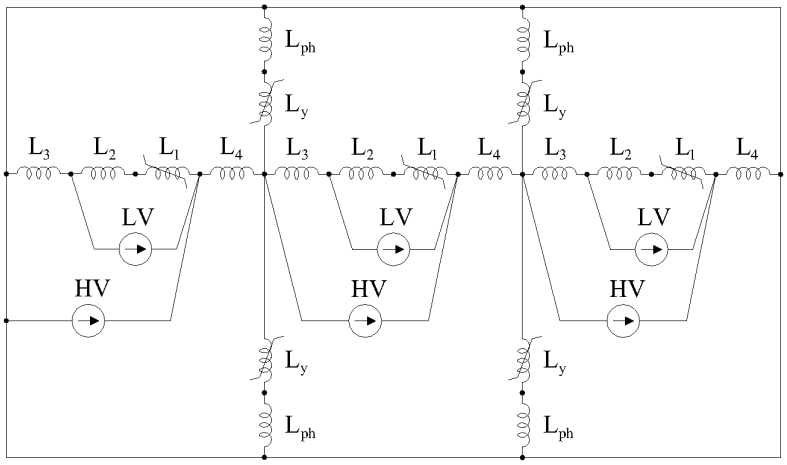

Figure 4.9: Three-leg stacked core transformer. Electric dual [7].

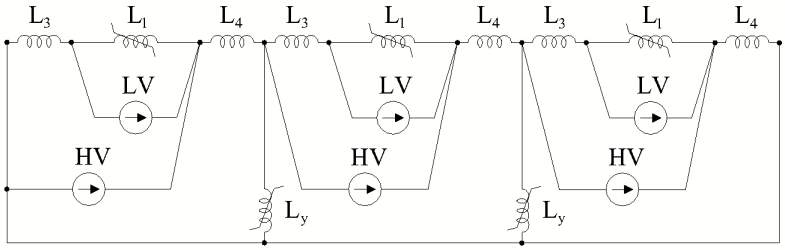

Figure 4.10: Three-leg stacked core transformer. Electric dual. Simplification [7].

The magnetic circuit is transformed into the electrical circuit model of Fig. 4.9, using the duality principle. The leakage flux between the core legs and the inner windings, L_2, can be neglected because it is small. L_{ph} can be also neglected

[1] outer limbs plus yokes

because it is quite small compared to L_y. Since the top and bottom yoke sections carry the same flux, the combination of these two section is lumped into only one L_y representation. Due to the previous reasons the electric dual circuit can be simplified in the one of Fig. 4.10.

These hypothesis are fully valid for the five-leg transformer. The only difference is the presence of the nonlinear inductance L_l in parallel to L_4. Furthermore L_4 can be neglected because it is quite small compared to L_l. The five-leg electric-dual circuit corresponds to the one shown in Fig. 4.9 and 4.10, but replacing the linear inductances L_4 with the nonlinear inductances L_l. This circuit is similar to the one for the three-leg core and therefore not reported here.

Equivalent Circuit

The following step is the creation of the equivalent electrical circuit. The two final circuit for three and five-leg transformers are represented in Fig. 4.11 and 4.12. Resistances and ideal transformers have been added. R_H and R_X represent the winding resistances[2] of the high and low voltage windings respectively. The parallel combination of the resistance R_1 and nonlinear inductance L_1 in each phase represents the saturable core of the corresponding limb. In the same way, the combination of $R_y - L_y$ and $R_l - L_l$ constitutes the saturable core for yokes and outer-leg[3] respectively.

The passage from electric dual to the equivalent circuit has to be handled very carefully. It is very important to obtain a proper representation that identify the correct attachment for the different components. The main problem is that the N+1th winding model needs to have the core and the leakage parts completely separated, see Fig. 3.7 and 3.8 at pag. 25.

Core nonlinearities and losses separation

What concerns this thesis is only the core and now it can be examined simply referring to the circuits of Fig. 4.13(a) and 4.13(b). The nonlinear core representation is here attached to the fictitious N+1th winding. These are the two most important figures and the following chapter are based on them.

The method for the practical implementation of the core nonlinearities and losses is based on the assumption that the resistive and the inductive parts of the

[2]here represented as simple resistances, but modelled with a second order foster-cell to add the frequency dependence.

[3]the second one only for five-leg transformer, in substitution to L_4.

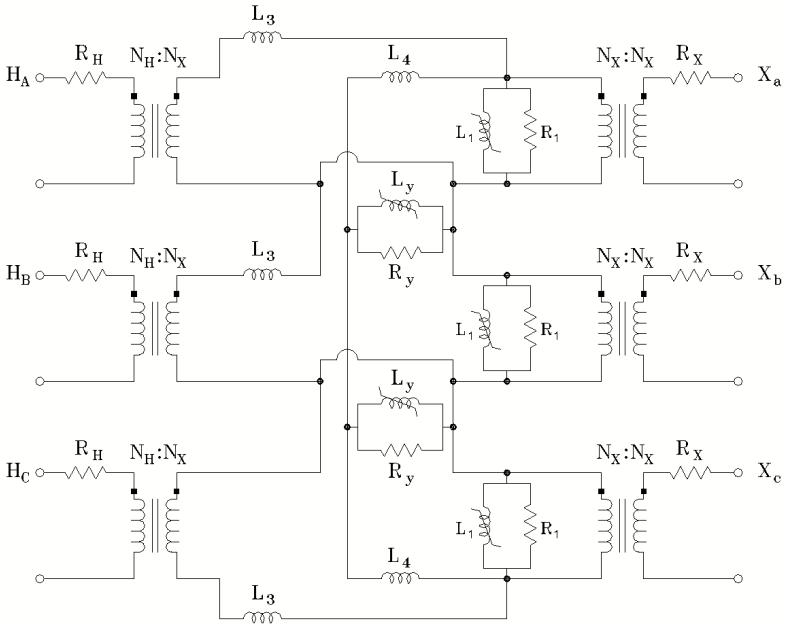

Figure 4.11: Three-leg stacked core transformer. Duality-equivalent circuit [7].

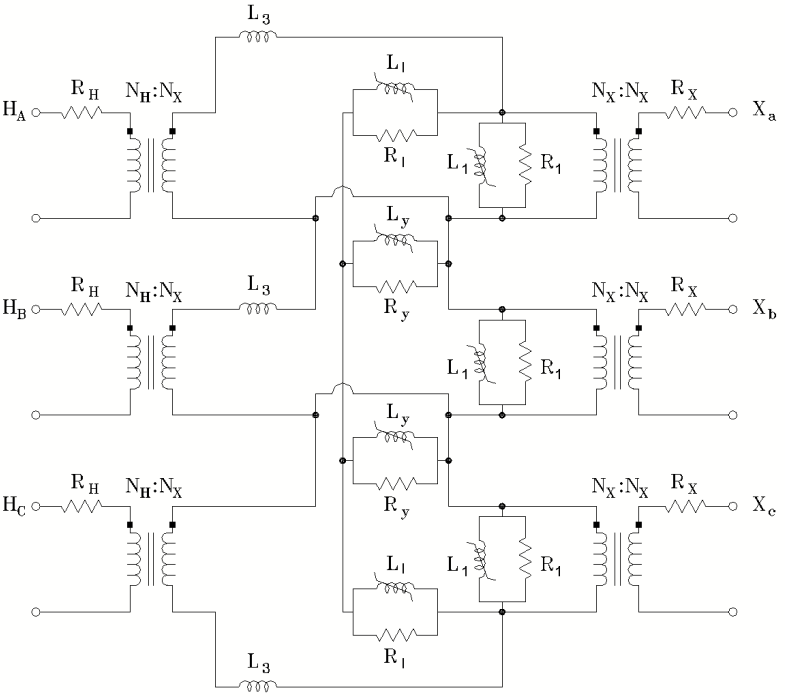

Figure 4.12: Five-leg stacked core transformer. Duality-equivalent circuit [7].

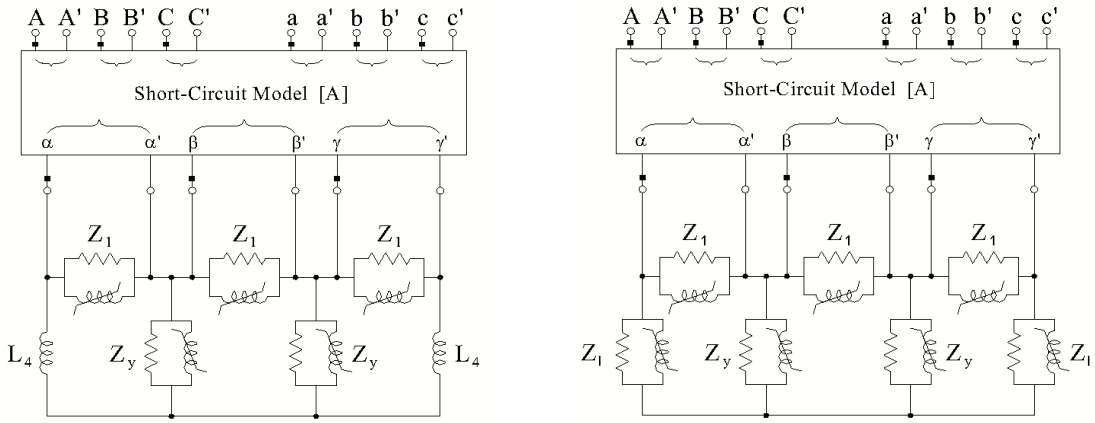

(a) Three-leg stacked core transformer. (b) Five-leg stacked core transformer.

Figure 4.13: N+1th winding attached core.

core equivalent circuit can be separated and solved independently. In reality, this might not be exactly correct, since some nonlinear voltages can appear between the resistances and the inductances in the combined circuit. To consider the two circuits separately one has to disconnect the blue wire shown in Fig. 4.14. However, for the inductive part of the circuit one can neglect the resistive current because it is much lower than the inductive current. Concerning the resistive part, a series of studies have demonstrated that the inductive current can be neglected for the calculation of the core losses, see Section 4.10.

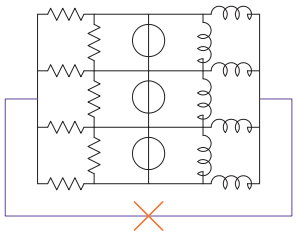

Figure 4.14: Core nonlinearities and losses separation.

4.5 Parameter Estimation Techniques

After validating the core model, the most important issue is to provide a procedure to obtain the operative parameters to insert in the model. The data obtained from manufacturer or from test report can not directly be used as operative parameters. The value of all the elements are deduced from:

- Factory test report, based on open-circuit test;
- Detailed factory design information;
- Complete estimation.

In addition the results have to be produced in the correct form that ATP can understand.

The operative parameters for the core representation are the nonlinear characteristics of the magnetising inductances, and of the core losses resistances, as explained in Section 4.3.

4.6 Factory Test Report

From the available open circuit test, it is usually possible to obtain: exciting current in % at 100% rated voltage, and core losses in W at 100% rated voltage. In some cases it is also possible to find these data at different levels of rated voltage, 90% and 110% being the most common. It is very desirable to have as many different available levels as possible from test reports to be able to build an accurate magnetising curve. The value other then 100% can be used to define a nonlinear magnetising inductance. In these available measurements, excitation current can be an average for the three phases, or measured for each individual phase.

A linear representation of the core can be obtained if only data at 100% of the excitation voltage are available. However, it is possible to use an assumed $B - H$ curve and some assumptions to scale this curve, and obtain the $\lambda - i$ curve for each section of the core.

Core dimension, if available, can be used to calculate the saturation model to each core section, as explained in Section 4.7. However the dimensions of legs and yokes are typically unknown, and in this case normalized ratios of core dimension can be used. If core dimension ratios are unknown, they must be assumed. Typical ratios can be used without great error, since the core dimension ratios vary within a small range.

The magnetic circuit for a five-leg core transformer is shown in Fig. 4.15. All the reluctances of the circuit are saturable. For non-load excitation only one set of MMFs is included. Fluxes in the three center leg are defined as ϕ_1, ϕ_2, and ϕ_3. The following expression can be written, based on the Ampere's circuital low for

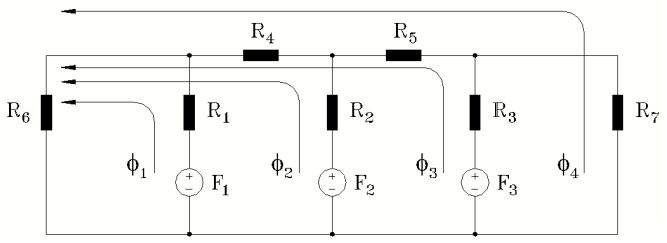

Figure 4.15: Magnetic circuit for five-leg core transformer [9].

magnetic circuits and on a normalized number of turns [9]:

$$i_1 = \frac{F_1}{N_1} = \phi_1 \cdot R_1 + R_6 \cdot (\phi_1 + \phi_2 + \phi_3 + \phi_4) \tag{4.1}$$

$$i_2 = \frac{F_1}{N_1} = \phi_2 \cdot R_2 + R_4 \cdot (\phi_2 + \phi_3 + \phi_4) + R_6 \cdot (\phi_1 + \phi_2 + \phi_3 + \phi_4) \tag{4.2}$$

$$\begin{aligned} i_3 = \frac{F_1}{N_1} = {} & \phi_3 \cdot R_3 + R_5 \cdot (\phi_3 + \phi_4) + R_4 \cdot (\phi_2 + \phi_3 + \phi_4) + \\ & + R_6 \cdot (\phi_1 + \phi_2 + \phi_3 + \phi_4) \end{aligned} \tag{4.3}$$

$$\begin{aligned} i_4 = \frac{F_1}{N_1} = 0 = {} & \phi_4 \cdot R_7 + R_5 \cdot (\phi_3 + \phi_4) + R_4 \cdot (\phi_2 + \phi_3 + \phi_4) + \\ & + R_6 \cdot (\phi_1 + \phi_2 + \phi_3 + \phi_4) \end{aligned} \tag{4.4}$$

where $R_i = l_i/(\mu \cdot A_i)$ is the reluctance of each section, being in function of the length l_i and the area A_i of each section, and the magnetic permeability of the material μ. Known values for Eq. (4.1) to (4.4) are the magnetizing current and the fluxes[4] for each leg. Unknown values are the flux through the leg (ϕ_4), and the magnetic permeability of the core material ($\mu = B/H$).

If the exact core dimension, saturation curve $B - H$, and windings turns are known, it is possible to calculate ϕ_4 from Eq. (4.1) to (4.4) by an iterative method. From the $B - H$ curve and core dimensions, the saturation curve $\lambda - i$ for each core section can be derived.

Most typically the solution is not so easy, because the saturation curve $B - H$ is not known. Many different mathematical functions can be used to describe the magnetisation curve, for example exponential, spline functions, and piece-wise linear. In this case, the Frolich equation [23] can be used to represent the core

[4]calculated from the peak voltage for each phase and the number of turns.

magnetisation curve.

$$B = \frac{H}{a + b \cdot |H|} \qquad ; \qquad \mu = \frac{B}{H} = \frac{1 - b \cdot |B|}{a} \tag{4.5}$$

One advantage of the Frolich equation is that only two data points on the curve are needed to fit this equation; these two points can be the average of the three rms magnetising currents at 100% and 110% voltages. The core dimension ratios are known or assumed. With this minimum set of data, and with an optimization technique, it is possible to estimate the "a" and "b" coefficients for the $B-H$ Frolich equation and ϕ_4 from Eq. (4.1) to (4.4).

For three-leg transformer, core data is assumed to be the same as those for the legs in a five-leg transformer. However, the two outer legs don't exist with this type of core. The procedure is similar to that explained for the five-leg transformer.

4.6.1 Frolich Equation

Core saturation curve can be represented with the empirical Frolich equation (4.5). This equation gives a smooth single-valued anhysteretic curve relating the flux density B to the magnetizing force H.

For ATP implementation of the magnetic core parameters, nonlinear current-dependent type-98[5] inductor is used. For this element the magnetization curve is specified in term of flux-linkage/current characteristic. In the case when $B - H$ curve of the core material and design data are available, the B-H parameters can be converted to $\lambda - i$ equivalent using the following scaling relations:

$$\lambda = B \cdot A \cdot N \tag{4.6}$$

$$i = \frac{H \cdot l}{N} \tag{4.7}$$

where A is the cross sectional area, l is the length of magnetic path, and N is the number of turns.

Using the relation Eq. (4.6) and (4.7) the Frolich equation of Eq. (4.5) can be

[5]it is a basic component of ATP. For more information refers to [3], [4], or [5].

reformulated as:

$$\lambda = \frac{i}{a' + b' \cdot |i|} \tag{4.8}$$

$$L_m = \frac{\lambda}{i} = \frac{1 - b' \cdot |\lambda|}{a'} \tag{4.9}$$

with

$$a' = a \cdot \frac{l}{A \cdot N^2} \qquad ; \qquad b' = \frac{b}{A \cdot l} \tag{4.10}$$

The passage to the $\lambda - i$ form of the Frolich equation consist only in a rescaling of the $B - H$ curve, so the shape of the curve is not chanced. This form of the Frolich equation is more suitable for the required use; in fact working with flux linkage, λ, has the advantage of avoiding the number of turns, which is usually an unknown value. Moreover, the relative core dimension, rather than the absolute dimension, are enough to rescale the excitation curve for each section of the core.

From this point only the Eq. (4.8) version of Frolich equation will be used; for convenience apex on a' and b' will be no longer considered refering to (4.8) and related.

The coefficient a and b are more than a numeric value, they are linked to the form of the magnetizing curve. From Eq. (4.8) and (4.9) the following relations follow:

$$\lambda|_{i=\infty} = \lim_{i \to \infty} \frac{i}{a + b|i|} = \frac{1}{b} \tag{4.11}$$

$$\left.\frac{\lambda}{i}\right|_{\lambda=0} = \lim_{\lambda \to 0} \frac{1 - b \cdot \lambda}{a} = \frac{1}{a} \tag{4.12}$$

$$\left.\frac{\partial \lambda}{\partial i}\right|_{i=\infty} = \lim_{i \to \infty} -\frac{b}{(a + b \cdot i)^2} = 0 \tag{4.13}$$

The inverse of a match the slope of the first part of the excitation curve, so it is equal to the inductance for very low excitation level. The inverse of b correspond to the saturation level of the linked flux, λ_{sat}. Eq. (4.13) shows the presence of a horizontal asymptote: after a certain point increasing the value of the current i, the value of λ no longer increases more than λ_{sat}.

As reported in [23], once defined the correct coefficient, the Frolich equation define the $\lambda - i$ curve between $\lambda = 0$ and $\lambda = \lambda_{sat}$. For flux densities greater then λ_{sat} the model is no more usable, and the inductance has to be set to the value of

empty-space inductance L_∞.

The model is based on two main assumptions:

- The $\lambda - i$ curve is assumed to be single valued. This is the same as assuming that the $\lambda - i$ curve has no area.
- The maximum inductance of the core occurs at $\lambda = 0$. For most magnetic material the inductance is low at low values of i, rises quickly to a maximum as i increases, and then gradually decreases for large value of i, approaching that of the empty-space at extreme value of i.

Due to extremely large excursions of the core flux, it turn out that these assumption have negligible effect on the accuracy of the results. On the other side, these assumptions limit the application of this model to large flux excursions caused by high currents. The results may not be very accurate for low currents. In standard condition, a transformer works just below the saturation level to optimize the core usage. Moreover, with an AC source the voltage excursion at any cycle is quite high, so the Frolich equation results are fully usable for our purpose.

A way for including the behaviour of the excitation curve for high level of excitation is to add the term "$L_\infty \cdot i$" to the Frolich equation (4.8). L_∞ represent the inductance of the empty-space and it is linked to the empty-space permeability $\mu_0 = 4 \cdot \pi \cdot e^-7$.

The Frolich equation turn into:

$$\lambda = \frac{i}{a + b \cdot |i|} + L_\infty \cdot i \tag{4.14}$$

This is a second grade equation, thus it can be inverted analytically. The inverse of this function is[6]:

$$i = \frac{-B(\lambda) + \sqrt{B^2(\lambda) - 4 \cdot A \cdot C(\lambda)}}{2 \cdot A} \tag{4.15}$$

with

$$\begin{aligned} A &= L_\infty \cdot b^2 \\ B(\lambda) &= L_\infty \cdot a \cdot b + b - \lambda \cdot b^2 \\ C(\lambda) &= -\lambda \cdot a \cdot b \end{aligned}$$

[6]The complete procedure is explained in Appendix B.

This version of the Frolich equation enclose the standard version, in fact for $L_\infty = 0$ Eq. (4.14) is identical to Eq. (4.8). For $L_\infty = 0$ the $A = 0$, so the denominator of the Eq. (4.15). In this case the inverse of the original Frolich equation has to be used:

$$i = \frac{\lambda \cdot a}{1 - \lambda \cdot b} \tag{4.16}$$

$$\left.\frac{\partial \lambda}{\partial i}\right|_{i=\infty} = \lim_{i \to \infty} -\frac{b}{(a + b \cdot i)^2} + L_\infty = L_\infty \tag{4.17}$$

Eq. (4.17) demonstrate that now, for high level of excitation, the slope of the magnetising curve satisfies the empty-space inductance.

Modified Frolich Equation

The Frolich equation is observed not to fit well the excitation curve in the knee area: the linked flux are usually overestimated. The proposed way to control the shape of the curve is to change Frolich equation in a three-parameter equation:

$$\lambda = \frac{i}{a + b \cdot |i| + c \cdot \sqrt{|i|}} \tag{4.18}$$

$$\lambda = \frac{i}{a + b \cdot |i| + c \cdot \sqrt{|i|}} + L_\infty \cdot i \tag{4.19}$$

The new added term is proportional to the square root of the current, and its influence is weak for low and high value of current. The three-parameter version of the Frolich equation is applicable only if three or more levels of excitation are known. With only two levels of excitation, only two parameter can be found, so the original version of the Frolich equation has to be used.

Eq. (4.18) and (4.19) are the two version of the modified Frolich equation, without and with the inclusion of empty-space inductance effect. The two equations are a third and a fourth equation grade, respectively, thus they are both analytically invertible. The complete procedure is reported in Appendix B.

- The inversion of Eq. (4.18) require the solution of a cubic equation and give:

$$i = \frac{4 \cdot a^2 \cdot \lambda}{(c \cdot \sqrt{\lambda} - \sqrt{c^2 \cdot \lambda + 4 \cdot a - 4 \cdot a \cdot b \cdot \lambda})^2} \tag{4.20}$$

- The inversion of Eq. (4.19) require the solution of a quartic equation and give:

$$i = \left(\mp \frac{H}{2} \pm \sqrt{\frac{H^2}{4} - \left(\alpha + w + \frac{H \cdot \beta}{4 \cdot w} \right)} - \frac{B}{4 \cdot A} \right)^2 \tag{4.21}$$

  Refer to Appendix B for the explanation of the parameter used in this equation.

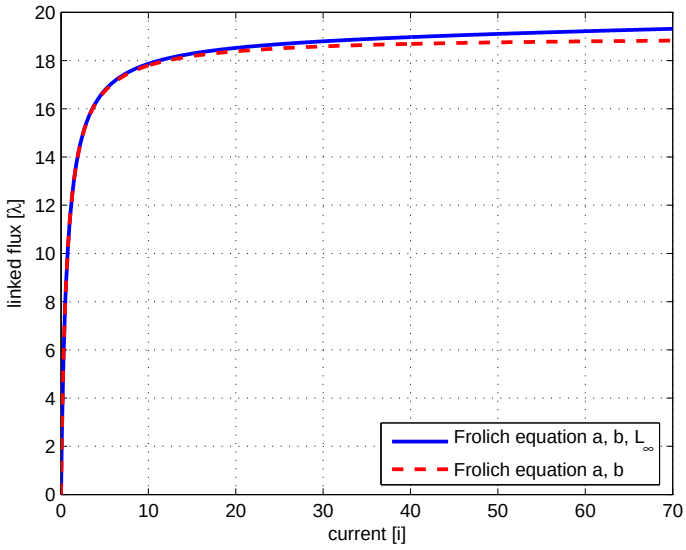

Figure 4.16: Effect of the empty-space inductance.

It is important to show that for $c = 0$ Eq. (4.18) and (4.20) are identical to Eq. (4.8) and (4.16), respectively. Thus, the two-parameter Frolich equation can be considered a sub case of the three-parameter version.

Fig. 4.16 and 4.17 show an example of anhysteretic-magnetizing curve fitting. The curve refer to the "A/S PerKure" transformer, see the test report in Fig. A.1. Fig. 4.16 has obtained from a two-parameter Frolich equation fitting. It is possible to observe the effect of L_∞[7] on the curve. Fig. 4.17(a) has obtained from seven points two and three-parameter Frolich equation fitting. The circles indicates the first estimation[8] of the $i_{peak} - \lambda_{peak}$ values. Fig. 4.17(b) outline the percent relative error of calculated exciting currents against measured currents for any excitation level. From these two figures, it is visible a general improvement with the three-parameter curves.

[7] to emphasise the effect the value of L_∞ used to produce this curve is higher than the real one.
[8] obtained with the *rms2peak* routine, see Chapter 5.

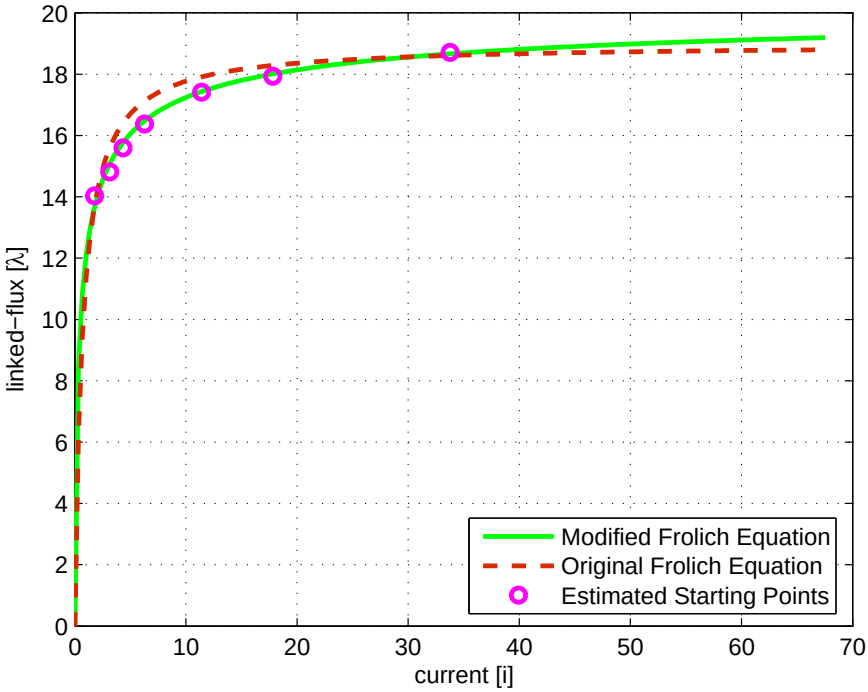

(a) Seven points fitting.

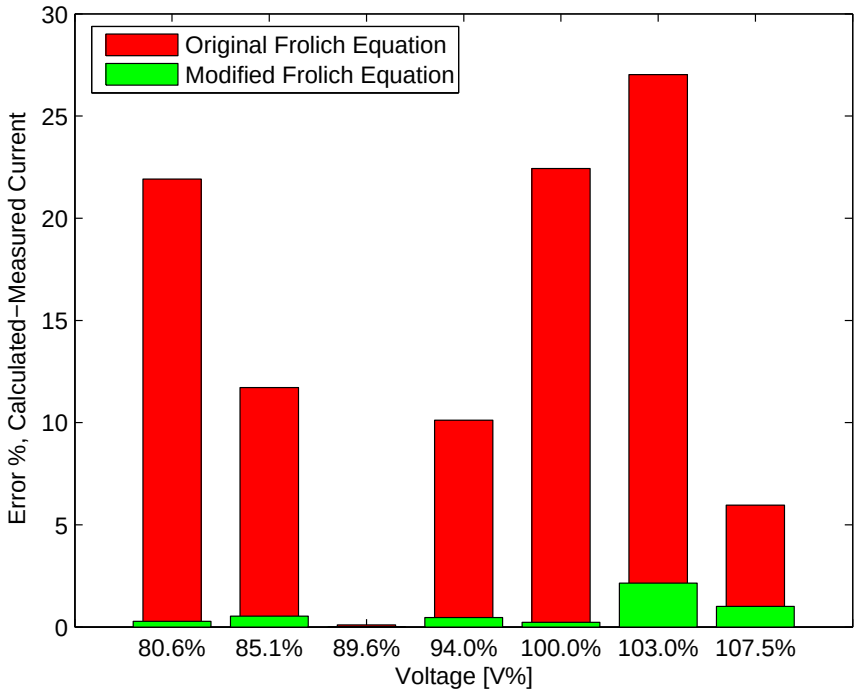

(b) Error-rate.

Figure 4.17: Comparison between two and three parameters Frolich curves. No L_∞ effect.

4.6.2 Two Level of Excitation Average Value of Excitation Current

In this section two different kinds of transformer (five and three-leg staked core transformers) are addressed, and the method to fit the parameters of the Frolich equation is presented.

The optimum values of a and b are obtained with an iterative process by minimizing the following cost function:

$$MinimizeF(a,b) = \left(\frac{I_{rms,meas}@100\%V - I_{rms,calc}@100\%V}{I_{rms,meas}@100\%V}\right)^2 + \\ + \left(\frac{I_{rms,meas}@110\%V - I_{rms,calc}@110\%V}{I_{rms,meas}@110\%V}\right)^2 \quad (4.22)$$

Relative difference is used in order to get the best overall fit for all points in term of % current error for each level of excitation. Given the nonlinear nature of the saturation curve, there would otherwise be relatively large differences at knee and below if this type of normalization is not used.

If only two excitation levels are known, usually they are at 100% and 110% V_n, but the procedure works for any couple of excitation levels. The value for $100\%V_n$ is usually know; as a second point it is better to have a value higher then $100\%V_n$. If over-excitation value are missed, it becomes very hard to get a good estimation of the saturation. With two levels of excitation only two-parameters version of Frolich equation can be used, if not the mismatch between equations and unknown variables (equation $<$ unknown variable) give an arbitrary degree of freedom.

Optimization can be implemented in different ways, but using a low-level programming language, a Golden-Search method result the more effective, see Chapter 5. The implementation technique needs initial condition and boundaries for parameters a and b. They are founded by approximating the simplistic magnetising curve calculated with two points, the two values of excitation current given as data. These two values need first to be converted from $v - i$ rms values to $\lambda - i$ peak values[9]. Once the two $\lambda - i$ peak values are known, a_0 and b_0[10] are obtained form a system of two equations (4.8) evaluated for the two $\lambda - i$ known values. Solving

[9] *rms2peak* routine is used for this aim, see Chapter 5.

[10] initial values of a and b

the system results in the initial values a_0 and b_0:

$$a_0 = \frac{1/Y_{peak}[1] - 1/Y_{peak}[n]}{1/I_{0-max}[1] - 1/I_{0-max}[n]} \tag{4.23}$$

$$b_0 = \frac{(I_{0-max}[1]/Y_{peak}[1]) - (I_{0-max}[n]/Y_{peak}[n])}{I_{0-max}[1] - I_{0-max}[n]} \tag{4.24}$$

The boundary constraints are set as follow:

$$a_0 \cdot 0.05 \leq a \leq a_0 \cdot 5 \tag{4.25}$$

$$\frac{1}{2 \cdot \lambda_{peak}[n]} \leq b \leq \frac{1}{0.9 \cdot \lambda_{peak}[n]} \tag{4.26}$$

As already explained in Section 4.6.1, the parameter a is the inverse of the slope of the initial part of the excitation curve. The boundary constrain for this parameter are reported in Eq. (4.25) where a_0 is the initial value of the parameter. The range of variation guarantee a search path in the first $\lambda - i$ quadrant.

Parameter b is linked to the saturation level of the magnetization curve, thus the variation of λ is quite limited. Since available data might not include the saturated values of linked flux, the upper interval is set to the double of the last point[11] of the $\lambda - i$ curve. For the same reason b will be less than $1/\lambda_{peak}[n]$, but a careful value for the high bound of b has not to be too close to unity.

The exciting current waveforms are synthesized and used for the true rms calculation, since the waveforms are not sinusoidal. In order to obtain an accurate result, the waveforms consist at least of 80 points per complete cycle. With a discreet number of points, the formula used for estimate the true rms value is:

$$I_{rms} = \sqrt{\frac{1}{N-1} \cdot \sum_{n=1}^{N} i^2(n)} \tag{4.27}$$

with N number of points per complete cycle.

Five-leg transformer

The calculation of linked flux and current is based on the core equivalent representation obtained using the duality transformation. Only the inductive components are considered here; the resistive elements are taken in consideration for the core

[11] nameded here $\lambda_{peak}[n]$, typically above 100% excitation voltage.

losses calculation. The working circuit is the one shown in Fig. 4.18. The node ⓪ is grounded to avoid singularity problem.

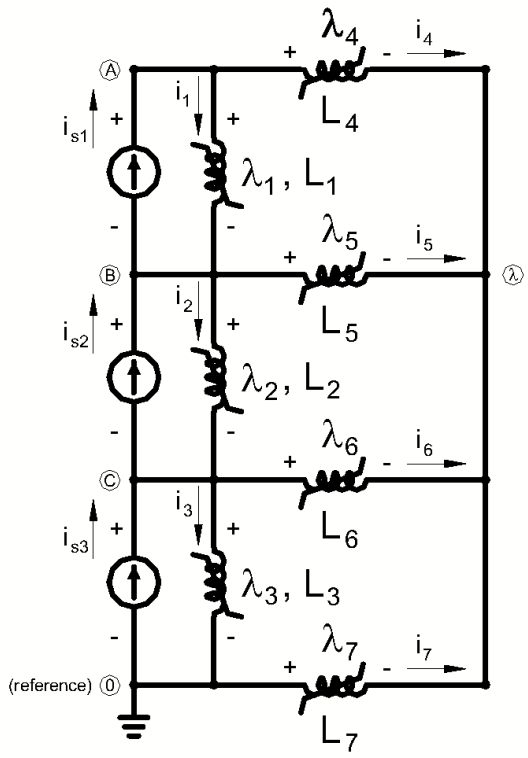

Figure 4.18: Five-leg core transformer. Electrical dual - Core equivalent [9].

It is preferred to work directly with linked flux rather then with voltage. This allow to consider only linear equations as $\big(\lambda(t) = L(i) \cdot i(t)\big)$ instead of differential equations $\big(v = \frac{dL(i)}{dt} \cdot i(t) = \frac{dL(i)}{di} \cdot \frac{di(t)}{dt} \cdot i(t)\big)$. Linked flux of the three sources are obtained from the excitation voltage of the open circuit as:

$$\lambda_{peak} = \sqrt{2} \cdot \frac{V_{ex}}{2\pi \cdot f} = \sqrt{2} \cdot \frac{V_{ex}}{\omega} \tag{4.28}$$

For open-circuit test a sinusoidal-symmetric source in normally used, thus the linked flux waveforms are:

$$\begin{cases} \lambda_{s1} = \lambda_{peak} \cdot \sin(\alpha) \\ \lambda_{s2} = \lambda_{peak} \cdot \sin(\alpha - \frac{2\pi}{3}) \\ \lambda_{s3} = \lambda_{peak} \cdot \sin(\alpha + \frac{2\pi}{3}) \end{cases} \tag{4.29}$$

From Fig. 4.18, remember that ⓪ is grounded, and that in steady-state

Section	Area ratio	Length ratio
Legs $_{(1,2,3)}$	1	1
Yokes $_{(5,6)}$	1	1.725
Outer legs $_{(4,7)}$	1	2.21

Table 4.2: Five-leg transformer. Typical normalized ratios.

$\lambda_{s1} + \lambda_{s2} + \lambda_{s3} = 0$, linked flux for each node are:

$$\begin{cases} \lambda_1 = 0 \\ \lambda_2 = -\lambda_{s1} = \lambda_{s2} + \lambda_{s3} \\ \lambda_3 = \lambda_{s3} \\ (\lambda_0 = 0) \end{cases} \tag{4.30}$$

Current through each branch are calculated using the Frolich equation referred to $\lambda - i$. The $\lambda - i$ characteristics for yokes and legs are scaled according to the normalized core dimensions reported in Tab. 4.2 (referred to Fig. 4.19).

$$i_1 = L_1 \cdot \frac{a \cdot (\lambda_1 - \lambda_2)/A_1}{1 - b \cdot |(\lambda_1 - \lambda_2)/A_1|} \tag{4.31}$$

$$i_2 = L_2 \cdot \frac{a \cdot (\lambda_2 - \lambda_3)/A_2}{1 - b \cdot |(\lambda_2 - \lambda_3)/A_2|} \tag{4.32}$$

$$i_3 = L_3 \cdot \frac{a \cdot (\lambda_3 - \lambda_0)/A_3}{1 - b \cdot |(\lambda_3 - \lambda_0)/A_3|} \tag{4.33}$$

$$i_4 = L_4 \cdot \frac{a \cdot (\lambda_1 - \lambda_\lambda)/A_4}{1 - b \cdot |(\lambda_1 - \lambda_\lambda)/A_4|} \tag{4.34}$$

$$i_5 = L_5 \cdot \frac{a \cdot (\lambda_2 - \lambda_\lambda)/A_5}{1 - b \cdot |(\lambda_2 - \lambda_\lambda)/A_5|} \tag{4.35}$$

$$i_6 = L_6 \cdot \frac{a \cdot (\lambda_3 - \lambda_\lambda)/A_6}{1 - b \cdot |(\lambda_3 - \lambda_\lambda)/A_6|} \tag{4.36}$$

$$i_7 = L_7 \cdot \frac{a \cdot (\lambda_0 - \lambda_\lambda)/A_7}{1 - b \cdot |(\lambda_0 - \lambda_\lambda)/A_7|} \tag{4.37}$$

An iterative method is implemented to find λ_λ, the linked flux value of the point Ⓛ, and the currents i_1, i_2, i_3, and i_4. The procedure is based on the condition $i_1 + i_2 + i_3 + i_4 = 0$ at node Ⓛ.[12]

[12] a more detailed description of the iterative method can be founded in Chapter 5

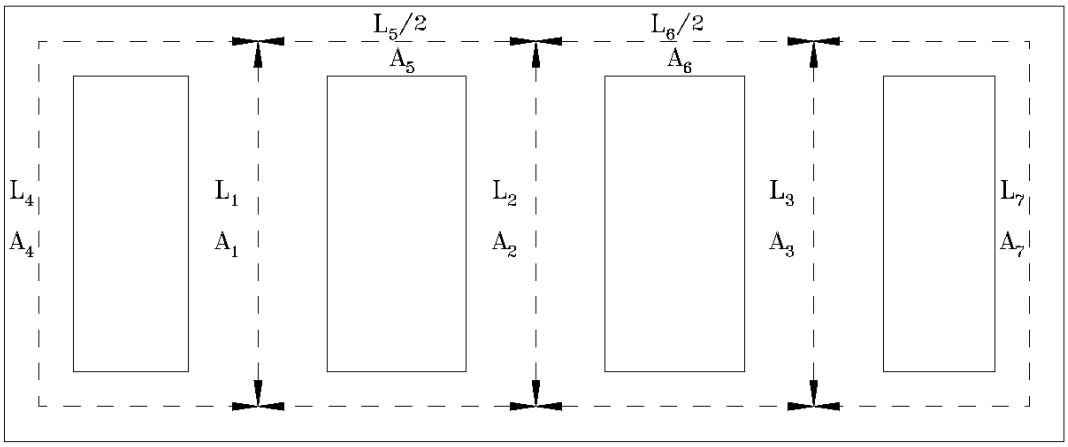

Figure 4.19: Relative dimension of a five-leg transformer.

The total phase-to-phase and line currents from each source are founded as:

$$\begin{cases} i_{s1} = i_1 + i_4 \\ i_{s2} = i_{s1} + i_2 + i_5 - i_1 \\ i_{s3} = i_3 - i_7 \end{cases} \tag{4.38}$$

for wye connection:

$$i_{L1} = i_{s1} \quad ; \quad i_{L2} = i_{s2} \quad ; \quad i_{L3} = i_{s3} \tag{4.39}$$

for delta connection:

$$i_{L1} = i_{s1} - i_{s3} \quad ; \quad i_{L2} = i_{s2} - i_{s1} \quad ; \quad i_{L3} = i_{s3} - i_{s2} \tag{4.40}$$

Equations from (4.30) to (4.40) are used iteratively in Eq. (4.22) to obtain the optimum a and b values. With the two optimum coefficients, magnetizing curves can be found for each limb of the transformer:

LEG: $$\lambda_1 = \frac{A_1 \cdot i_n}{a \cdot l_1 + b \cdot i_n} \tag{4.41}$$

OUTER LEG: $$\lambda_4 = \frac{A_4 \cdot i_n}{a \cdot l_4 + b \cdot i_n} \tag{4.42}$$

YOKE: $$\lambda_5 = \frac{A_5 \cdot i_n}{a \cdot l_5 + b \cdot i_n} \tag{4.43}$$

This process consider the basic version of the Frolich equation, but can be easily

extended to the other case with the parameter L_∞. It also can be used in the cases with three-parameter Frolich equation, if more then two excitation levels are available. These cases will be discussed in the Section 4.6.4.

Three-leg transformer

The optimization performed here is the same as that one used for the five-leg transformer. The difference is that now there are no outer legs providing closed ferromagnetic paths for the zero sequence fluxes. On the contrary, in a three-leg transformer those paths are through the air. Therefore, here the outer legs are modelled with a nearly zero linear inductance, which corresponds to an ideal case of near-infinite reluctance in the zero sequence flux path. Section 4.9 explain how to estimate these two inductances, for the moment they are supposed known and constant. Fig. 4.20 shows the duality transformation for this case.

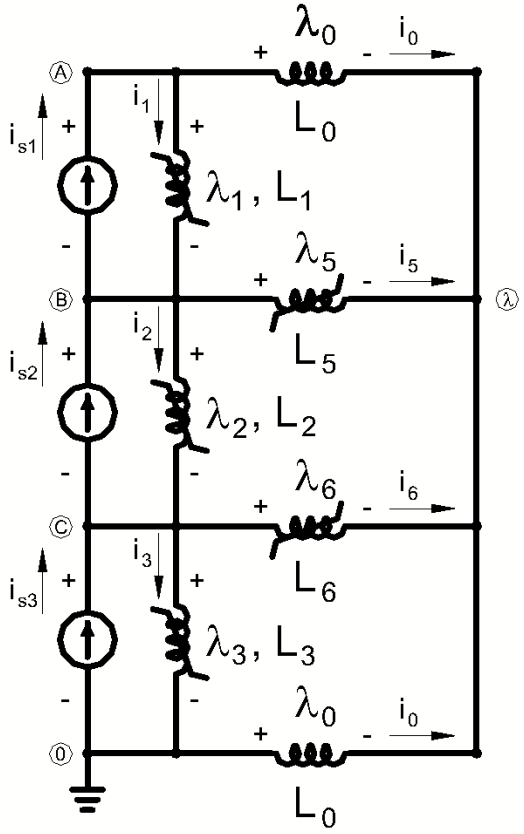

Figure 4.20: Three-leg core transformer. Electrical dual - Core equivalent [9].

The only two modified equations are (4.34) and (4.37). These become:

$$i_4 = \frac{\lambda_1 - \lambda_\lambda}{L_0} \tag{4.44}$$

$$i_7 = \frac{\lambda_0 - \lambda_\lambda}{L_0} \tag{4.45}$$

Tab. 4.3 report the typical normalized ratios for this kind of transformer, referring to Fig. 4.21.

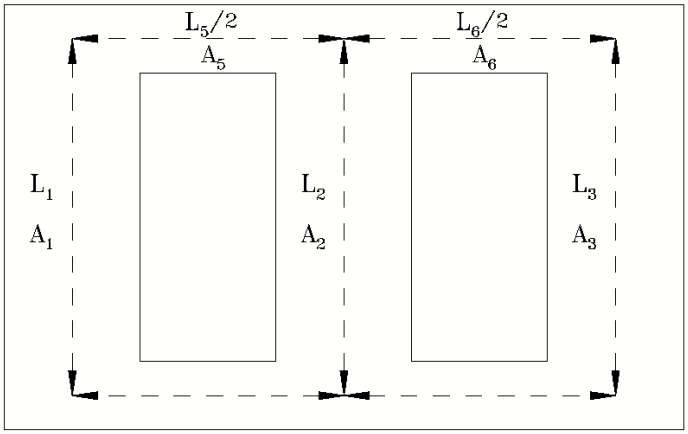

Figure 4.21: Relative dimension of a three-leg transformer.

Section	Area ratio	Length ratio
Legs $_{(1,2,3)}$	1	1
Yokes $_{(5,6)}$	1	1.725

Table 4.3: Three-leg transformer. Typical normalized ratios.

4.6.3 Two Level of Excitation Excitation Current for All Three Phases

When the excitation current is given for each phase, better fitting of the Frolich equation is obtainable.

The same approach explained before is applied here. The only change is that now the cost function $F(a, b)$ takes into account the excitation current for each phase when optimizing the parameter a and b. The cost function used in this case

is:

$$
\begin{aligned}
MinimizeF(a,b) = &\left(\frac{I_{rms,meas(phA)}@100\%V - I_{rms,calc(phA)}@100\%V}{I_{rms,meas(phA)}@100\%V}\right)^2 + \\
&+\left(\frac{I_{rms,meas(phB)}@100\%V - I_{rms,calc(phB)}@100\%V}{I_{rms,meas(phB)}@100\%V}\right)^2 + \\
&+\left(\frac{I_{rms,meas(phC)}@100\%V - I_{rms,calc(phC)}@100\%V}{I_{rms,meas(phC)}@100\%V}\right)^2 + \\
&+\left(\frac{I_{rms,meas(phA)}@110\%V - I_{rms,calc(phA)}@110\%V}{I_{rms,meas(phA)}@110\%V}\right)^2 + \\
&+\left(\frac{I_{rms,meas(phB)}@110\%V - I_{rms,calc(phB)}@110\%V}{I_{rms,meas(phB)}@110\%V}\right)^2 + \\
&+\left(\frac{I_{rms,meas(phC)}@110\%V - I_{rms,calc(phC)}@110\%V}{I_{rms,meas(phC)}@110\%V}\right)^2
\end{aligned} \tag{4.46}
$$

4.6.4 More than Two Level of Excitation

Sometimes factory or laboratory tests provide information for more than two excitation levels. Either average current or currents for all three phases can be specified in the factory test report. Then the method for estimating the magnetization curves for different transformer limbs has to be slightly modified to give the possibility to obtain the $\lambda - i$ curves based on any number of (V_{rms}, I_{rms}) points.

To obtain magnetization curves for the proposed core model considering different core types, rms voltages and currents of the test report have to be converted to the corresponding $\lambda_{peak} - i_{peak}$ curve by using *rms2peak* routine. Then the initial parameter a_0 and b_0 for the Frolich equation can be obtained. This is done by using Eq. (4.23) and (4.24), this time evaluated for the lower and higher know points.

The parameters then can be passed into the optimization routine, which has similar structure as in the case of two excitation levels. The cost function used for the optimization is an extension of Eq. (4.22) and (4.46). The function is defined as follows:

$$
\sum_{j=1}^{m}\sum_{i=1}^{n}\left(\frac{I_{rms,meas}[i,j] - I_{rms,calc}[i,j]}{I_{rms,meas}[i,j]}\right)^2 \tag{4.47}
$$

where j is the index of the excitation level, and m is the number of excitation levels; i is the index of the phases, and n is equal to 1 if average current is used, or to 3 if currents for all three phases is specified[13].

[13]In the case of average current, the average current level is: $I_{rms}[1,j] = I_{rms,avg}[j]$

With more than two level of excitation the tree-parameter Frolich equation can be used to obtain a more accurate result. The procedure has similar structure as in the case of two-parameter Frolich equation, but has to be reviewed based on what is discussed in Section 4.6.1. Initial condition for parameter c is $c_0 = 0$, and the variation bound is set to $-0.1 \leq c \leq 0.5$.

4.6.5 One Level of Excitation

It is quite likely that only one level of the excitation is provided by the factory test report. In such case, optimization methods based on the Frolich equation are not possible, since it is not possible to fit the Frolich equation to a single point, and therefore some assumptions have to be made in order to estimate the magnetization curves for each transformer limb.

The user must in this case provide an assumed design level of B_{max}. This can depend on the material, the transformer age, and the type of core. Typically, B_{max} values lie in a certain interval, which is much narrower than the range for the rated voltages (and linked flux). After assuming maximum flux density at 100% voltage, tabulated library of the $B-H$ curves will be used to find an appropriate B-H curve for a given B_{max}.

The selected B-H curve can then be fitted to the Frolich equation using the best fitting method.

The B-H curve obtained in this manner is later scaled to the normalized areas and lengths to match open circuit tests at 100% voltage to obtain $\lambda - i$ curves.

The process for estimating of the magnetization curves for one levels of excitation is summarized as a flowchart in Fig. 4.22. It will explained more in detail in Chapter 5.

4.6.6 Producing Curves for ATP

The saturation curves must be implemented as a set of piecewise-linear (λ, i) points used as an input for the ATP pseudo-nonlinear type-98 or true-nonlinear type-93 inductors. This is a common requirement for any continuous $\lambda - i$ curve, whether described by the Frolich equation or other fitting function.

It is necessary to automatically process the analytical expression of the Frolich equation to provide a piecewise-linear approximation, preserving the shape of the curve and avoiding clipping of the curve way below the saturated level or, on the contrary, climbing too high into saturation. In order to intelligently solve this

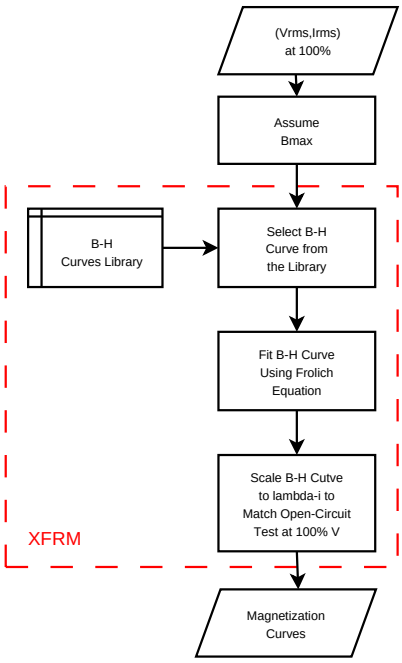

Figure 4.22: Estimating $\lambda - i$ curves for the case of only one known level of excitation.

problem, some analysis of the curves has to be made. Since magnetization curves are presented in this work as Frolich equations, its derivative can be analytically defined as:

$$\frac{d\lambda}{di} = \frac{A}{a \cdot l + b \cdot i} - \frac{A \cdot b \cdot i}{(a \cdot l + b \cdot i)^2} \quad (+L_\infty) \tag{4.48}$$

$$\frac{d\lambda}{di} = \frac{A}{a \cdot l + b \cdot i + c \cdot \sqrt{l \cdot i}} - \frac{A \cdot i \cdot (b + \frac{c\sqrt{l}}{2\sqrt{i}})}{(a \cdot l + b \cdot i + c \cdot \sqrt{l \cdot i})^2} \quad (+L_\infty) \tag{4.49}$$

(4.48) for two-parameter and (4.49) for three-parameter Frolich equation, in case with the addition of L_∞.

As elaborated earlier, when the areas and lengths of the limbs are not known, this equation still can be used with the normalized values for A and l, since the parameters a and b of the Frolich equation will provide the correct scaling.

The derivatives (4.48) and (4.49) can be analysed to obtain three specific points:

- the point of the maximum slope, derivative has its maximum value;
- the knee point, the derivative is equal to unity;
- the point where saturation is reached, and the derivative slope becomes constant.

These points define the general behaviour of the curve.

Extra points can be defined between the knee point and the saturation point, and between the maximum slope point and the knee point. Extra points increase the accuracy of the piecewise linearisation. Otherwise, a high number of points slow the simulation because a new $[A]$-matrix has to be inverted for any segment of the piecewise-linear curve.

Three extra points are defined in the range of the knee point to the saturation point. These points are found using the golden ratio[14] working backward from the saturation point covering 62% of the remaining distance to the knee. Since in this part the slope of the curve is lower then one, the current is used as reference for the splitting operation.

No extra points are defined in the range from the maximum slope point to the knee point.

As the Frolich function is defined, the maximum slope point correspond to the origin of the axis $\lambda - i$. Thus, the resulting saturation curve used as an input to the ATP nonlinear inductors consists of five total points, including (0,0). Fig. 4.23 show the piecewise linear approximation of the saturation curve; it refers to transformer data of Fig. A.2.

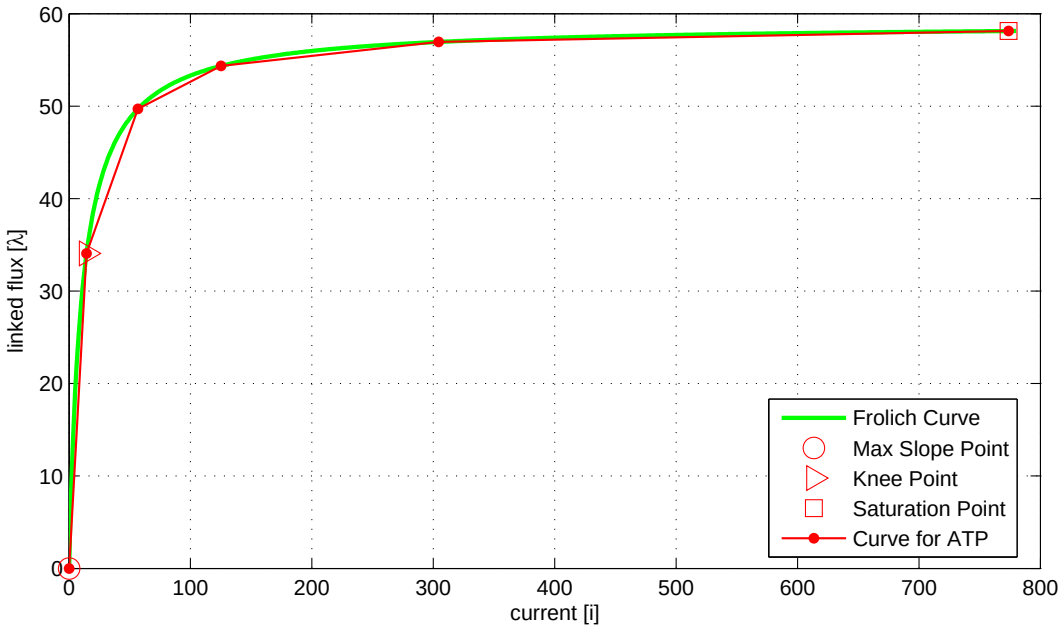

Figure 4.23: Piecewise linear approximation of the saturation curve.

[14] the range is divided as 62:38.

4.7 Design Information

When complete design information is available, estimation of the magnetization curves is rather straightforward, since the material type is known, as well as the core dimensions[15] and the number of turns of the windings. The material type defines the B-H curve, which is naturally the same for all the limbs of the transformer and can be approximated by the Frolich equation.

The B-H characteristic curves of material properties are available from the steel manufacturers' catalogs. It is difficult to work mathematically with the values appearing in the catalogs, however, it can be solved by fitting the Frolich equation.

The $\lambda - i$ curves of the transformer depend on the core configuration, thus can be estimated. First it is necessary to scale the $B - H$ curve according to the actual areas A and lengths l of the corresponding limbs. Then the number of turns of the winding the induction is referred to are taken into consideration. Finally the relationship between flux density and linked flux

$$\lambda = B \cdot A \cdot N \tag{4.50}$$

and the relation between magnetizing force and current

$$i = H \cdot l/N \tag{4.51}$$

give the $\lambda - i$ curve. Obviously, to obtain the correct curve for each section, the corresponding area and length have to be used.

4.8 Complete Approximation

This option is used when the only available data are the ratings of the transformer, voltage and power, and the BIL[16].

If BIL is unknown then it can be estimated as shown in Fig. 4.24 and 4.25, see [9], [25]. These figures plot the BIL and the BIL normalized versus voltage rating, respectively, for power oil-immersed transformers, for systems 765 kV and below. These figure has been extracted from an IEEE Standard document [25]. Standard nominal system voltages and maximum system voltages are included in ANSI C84.1-1989. Values listed as nominal system voltage in some cases (particularly voltages

[15] net cross-sectional areas and lengths.

[16] Basic Lightning Impulse Insulation Level

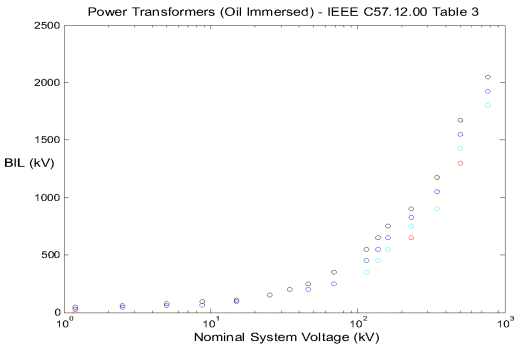

Figure 4.24: BIL vs voltage rating [9].

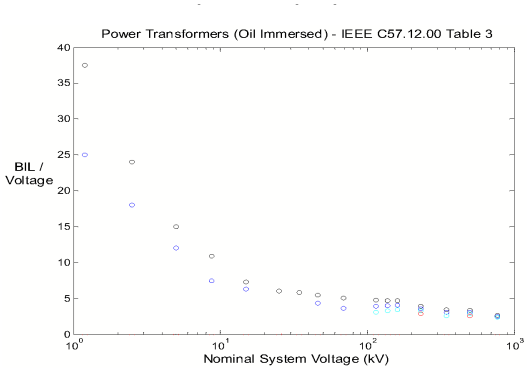

Figure 4.25: Normalized BIL vs voltage rating [9].

Transformer	Magnetizing current (%)			
(MVA)	BIL: 350	BIL: 650	BIL: 900	BIL: 1300
20	0.80	0.90	1.00	1.20
40	0.65	0.74	0.82	0.94
60	0.58	0.65	0.73	0.84
80	0.54	0.61	0.68	0.77
100	0.51	0.59	0.65	0.73
150	0.47	0.53	0.61	0.67
200	—	0.51	0.58	0.64
300	—	0.49	0.55	0.61
500	—	0.47	0.53	0.59

Table 4.4: Typical Value of Magnetising Current [9].

34.5 kV and below) are applicable to other lesser voltages of approximately the same value.

The estimation of the magnetizing current (I_m) is based on Tab. 4.4. Some fitting of the data is performed which results in:

$$I_m\% = 0.73 \cdot \left(\frac{BIL}{350}\right)^{0.2933} \cdot \left(\frac{s}{20}\right)^{-0.2154} \tag{4.52}$$

$$I_m\% = 0.855 \cdot \left(\frac{u}{150}\right)^{0.2283} \cdot \left(\frac{s}{20}\right)^{-0.2134} \tag{4.53}$$

where BIL is in kV, u is the rated voltage in kV, and s is the rated power in MVA. Eq. (4.52) is used when the basic insulation level (BIL) is known and Eq. (4.53) when BIL must be estimated.

For typical core model the user has to specify the maximum B-field (normally

1.5-1.7 Tesla) and the maximum core loss density (p_{max}). First a core material has to be guessed and this gives the a and b values in the Frolich equation. Here we refer to a and b as the parameter for the $B-H$ Frolich equation, and to a' and b' as the parameter for the $\lambda - i$ Frolich equation.

The following equation are then assumed:

$$\lambda_{max} = \frac{\sqrt{2} \cdot U_{rms}}{\omega} = B_{max} \cdot A \cdot N \tag{4.54}$$

$$H_{max} = \frac{a \cdot B_{max}}{1 - b \cdot B_{max}} = \sqrt{2} \cdot i_{rms} \cdot \frac{N}{l} \tag{4.55}$$

that give:

$$A \cdot N = \frac{\sqrt{2} \cdot U_{rms}}{\omega \cdot B_{max}} \tag{4.56}$$

$$\frac{N}{l} = \frac{a \cdot B_{max}}{(1 - b \cdot B_{max}) \cdot \sqrt{2} \cdot i_{rms}} \tag{4.57}$$

These give the parameters of the flux linkage-current characteristic:

$$a' = a \cdot \frac{l}{A \cdot N^2} \approx \omega \cdot (1 - b \cdot B_{max}) \cdot \frac{i_{rms}}{v_{rms}} \tag{4.58}$$

$$b' = b \cdot \frac{1}{A \cdot N} \approx b \cdot \frac{\omega \cdot B_{max}}{\sqrt{2} \cdot u_{rms}} \tag{4.59}$$

We see that the a' expression is independent on the magnetic material property a.

The core losses is estimated to

$$P_{loss} = p \cdot \rho \cdot A \cdot l = p \cdot \rho \cdot \frac{(1 - b \cdot B_{max}) \cdot 2 \cdot u_{rms} \cdot i_{rms}}{\omega \cdot a \cdot B_{max}^2} \tag{4.60}$$

where p $[W/kg]$ and ρ $[kg/m^3]$ are given, and the volume $A \cdot l$ is estimated from Eq. (4.56) and (4.57).

4.9 Zero Sequence Study

In the proposed hybrid model, zero sequence excitation effects are included as part of the core. The model of a three-leg transformer was tested in [9] in order to analyse the zero sequence behaviour, and confirm that the proposed representation is reasonable.

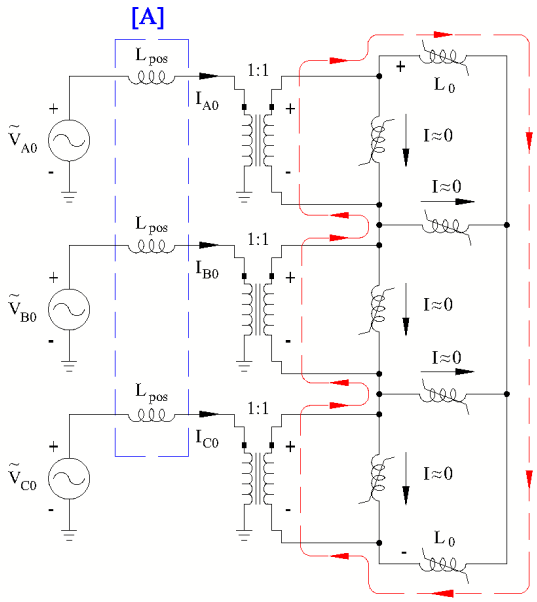

Figure 4.26: Zero sequence excitation [9].

Analysis of the core topology and the curves obtained from ATP simulations demonstrates the following:

- There are non-zero currents flowing through Lo even for a balanced three-phase excitation. Follow up laboratory testing and sensitivity analysis are recommended to obtain a thorough understanding of the possible range of values that Lo can take on and its effect on model performance;
- However, for balanced excitation, the currents flowing through small linear inductances representing zero sequence are equal;
- For zero sequence excitation the currents through legs and yokes are negligible as compared to the zero sequence currents, and the transformer behaviour is determined by the combination of positive sequence impedance of the [A]-matrix, and zero sequence impedance, which is implemented in the hybrid model as a part of the core.

Then, the overall zero sequence excitation performance of the hybrid model can be explained as shown in Fig. 4.26.

The zero sequence inductances L0 for the hybrid model can be calculated using the following relationships:

$$V_{AO} = V_{BO} = V_{CO} = V \tag{4.61}$$

$$I_{zero} = \sqrt{I_0^2 - \left(\frac{P}{V}\right)^2} \tag{4.62}$$

$$2 \cdot \omega \cdot L_0 = 3 \cdot X_{zero} \tag{4.63}$$

so that:

$$L_0 = \frac{3}{2}\frac{X_{zero}}{\omega} = \frac{3}{2 \cdot \omega}\frac{V}{I_{zero}} \tag{4.64}$$

4.10 Core Losses

Core losses are modelled as resistance and are used to add area to the anhysteretic excitation curve. For a proper representation of the core losses their dependence on frequency and excitation level should be considered.

Core losses can be modelled initially as a separate linear resistance, calculated at 100% rated voltage, in parallel with the nonlinear magnetizing inductance, see Fig. 4.2 in Section 4.3. Since core losses are nonlinear, the use of a linear resistance can result in errors for some type of simulation. This simple resistance can be replaced with a more sophisticated frequency-dependent version if needed.

The method for the practical implementation of the core loss resistance is based on the assumption that the resistive and the inductive parts of the core equivalent circuit can be separated and solved for independently. In the reality, this might not be exactly correct, since some nonlinear voltages can appear across the resistances in the combined circuit, thus changing the value of the total core loss. However, a series of studies have demonstrated that this approach provides quite reasonable accuracy (with errors of no more than 1%) [9]. This is also somewhat considered in the optimization routine for the core resistances estimation, where the resistance ratios were empirically found so as to provide the correct core losses.

The core loss calculation is done for the five-legged transformer as follows (using

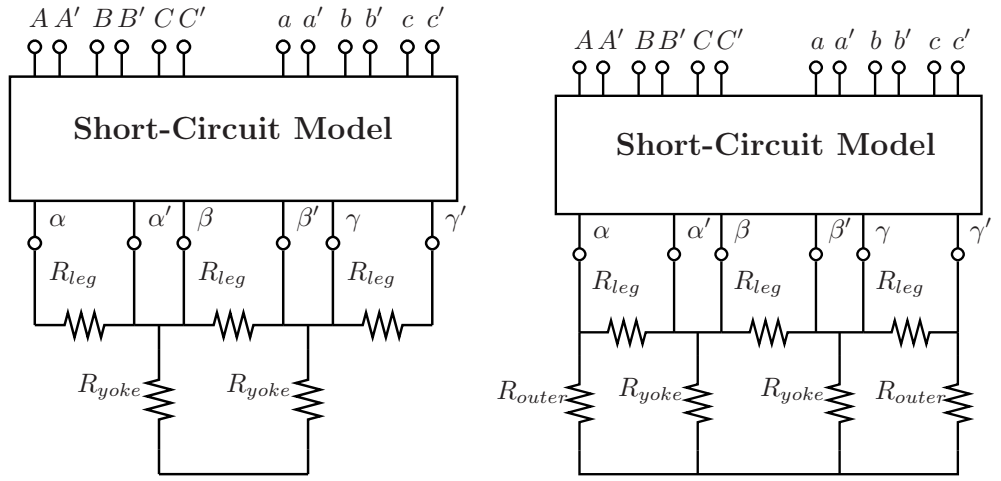

(a) Three-leg stacked core transformer. (b) Five-leg stacked core transformer.

Figure 4.27: Pure resistive circuits.

the constant resistances for each limb of the transformer):

$$P_{ex_calc} = 3 \cdot P_{leg} + 3 \cdot P_{yoke} + 2 \cdot P_{outer} \tag{4.65}$$

where P_{leg}, P_{yoke}, P_{outer} are power losses for an individual leg, yoke and outer leg, respectively.

Separating the resistive part of the core from the inductive, Fig. 4.13 is redrawn as shown in Fig. 4.27(b) and Fig. 4.27(a).

The voltages applied from the N+1th winding are the balanced three-phase line-to-line voltages. It is possible to solve the circuits analytically and calculate active power losses as a function of the applied excitation voltage (which is a known value) and the three resistances for legs, yokes and outer legs (which are unknown and need to be estimated).

After simplifying[17], Eq. (4.65) can be reformulated as:

$$P_{loss,calc} = \frac{3 \cdot V^2}{R_l} + \frac{3 \cdot V^2 \cdot R_o}{2 \cdot (R_o + R_y)^2} + \frac{V^2 \cdot (4 \cdot R_y^2 + 2 \cdot R_o \cdot R_y + R_o^2)}{2 \cdot R_y \cdot (R_o + R_y)^2} \tag{4.66}$$

where V is the excitation voltage; R_l, R_y, and R_o are the resistances of the legs, yokes and outer legs respectively; $P_{loss,calc}$ is the core losses from the factory test report.

This equation has been derived for the resistive circuit (i.e. linear voltages).

[17] the complete procedure can be found in Appendix C

In reality the combined circuit has some nonlinearity. Namely, the voltages of the yokes and outer legs are slightly nonlinear. However, this assumption does not seem to produce any significant error (less than 1%) [9].

The simplest well-known representation for the core losses is to have three equal resistances attached to each phase of the transformer. The value for this "equivalent" resistance can be calculated as follows:

$$R_{eq} = \frac{3 \cdot V^2}{P_{loss,meas}} \tag{4.67}$$

Comparing Eq. (4.66) and (4.67), it can bee easily seen that the leg resistance R_l cannot be less or equal than R_{eq}.

For three-leg transformer the resistance of the outer legs R_o is absent, so the last term of Eq. (4.65). Eq. (4.66) become:

$$P_{loss,calc} = \frac{3 \cdot V^2}{R_l} + \frac{V^2}{2 \cdot R_y} \tag{4.68}$$

If more than one level of excitation is available, a set of points for the $v - i$ characteristic of the core resistances can be found.

From simulations result that fitting three parameters (R_l, R_y and R_o) when only one value of P_{loss} is known give uncertain and inaccurate results.

The core losses depend to the weight of the iron, and all the iron uses in a transformer has the same specific losses. The suggested solution uses the relative volume to relate the value of the three core-resistances, reads:

$$p = \frac{P}{\delta \cdot A \cdot l} = \frac{V^2}{R \cdot (\delta \cdot A \cdot l)} \tag{4.69}$$

$$R_l = \frac{R_y}{\mathcal{V}_{yoke}} = \frac{R_l}{\mathcal{V}_{outer}} \tag{4.70}$$

where δ is the density of the iron $[kg/m^3]$, p is the specific losses $[W/kg]$, $\mathcal{V}_y$ and $\mathcal{V}_o$ are the relative volume of yokes and outer leg. These volumes are relative to the volume of the leg.

Eq. (4.66) and (4.68) can then be simplified gather V and R_l. Numerical optimization methods are not necessary and the core losses resistance can be found

as:

$$R_l = \frac{V^2}{P_{loss,calc}} \cdot \left(3 + \frac{3 \cdot \mathcal{V}_o}{2 \cdot (\mathcal{V}_o + \mathcal{V}_y)^2} + \frac{4 \cdot \mathcal{V}_y^2 + 2 \cdot \mathcal{V}_o \cdot \mathcal{V}_y + \mathcal{V}_o^2}{2 \cdot \mathcal{V}_y \cdot (\mathcal{V}_o + \mathcal{V}_y)^2}\right) \tag{4.71}$$

$$R_l = \frac{V^2}{P_{loss,calc}} \cdot \left(3 + \frac{1}{2 \cdot \mathcal{V}_y}\right) \tag{4.72}$$

for five and three-leg transformers respectively. Finally, R_y and R_o are obtained from Eq. (4.70).

Chapter 5

Model Implementation

This chapter describes how the core model presented in Chapter 4 is implemented in ATPDraw. The main routine is called "*BuildCore*". The general structure of the program is quite straightforward. Exception is the case when test report data are available. In this case the computational effort is quite high due to the presence of iterative cycles.

5.1 *BuildCore* Routine

The routine has been implemented using *Borland Delphi 6* [26], a development framework based on pascal programming language. *Numerical Recipes in Fortran77* [27] was used as reference for the implementation of minimization, interpolation and root finding procedures.

Fig. 5.1 shows the routine's flow chart. The program is divided in two main parts: core magnetization and core losses. Based on the type of input data available, different strategies are followed. Input data is inserted from the graphical user interface. Fig. 5.2 shows the different interfaces for the cases: design parameters, test report, and typical values. For all the types of input data, the relative length and area dimension are also specified. The complete input data interface is shown in Fig. 3.6, page 23. The data acquisition is handled externally to the *BuildCore* routine. Part of the data is also preprocessed.

In design parameters the coefficients a and b are referred to the $B - H$ curve. Parameter a, b, d, e, and density can be specified manually or chosen from a material database[1]. In case of test report the zero sequence data can be specified, in the

[1] under construction.

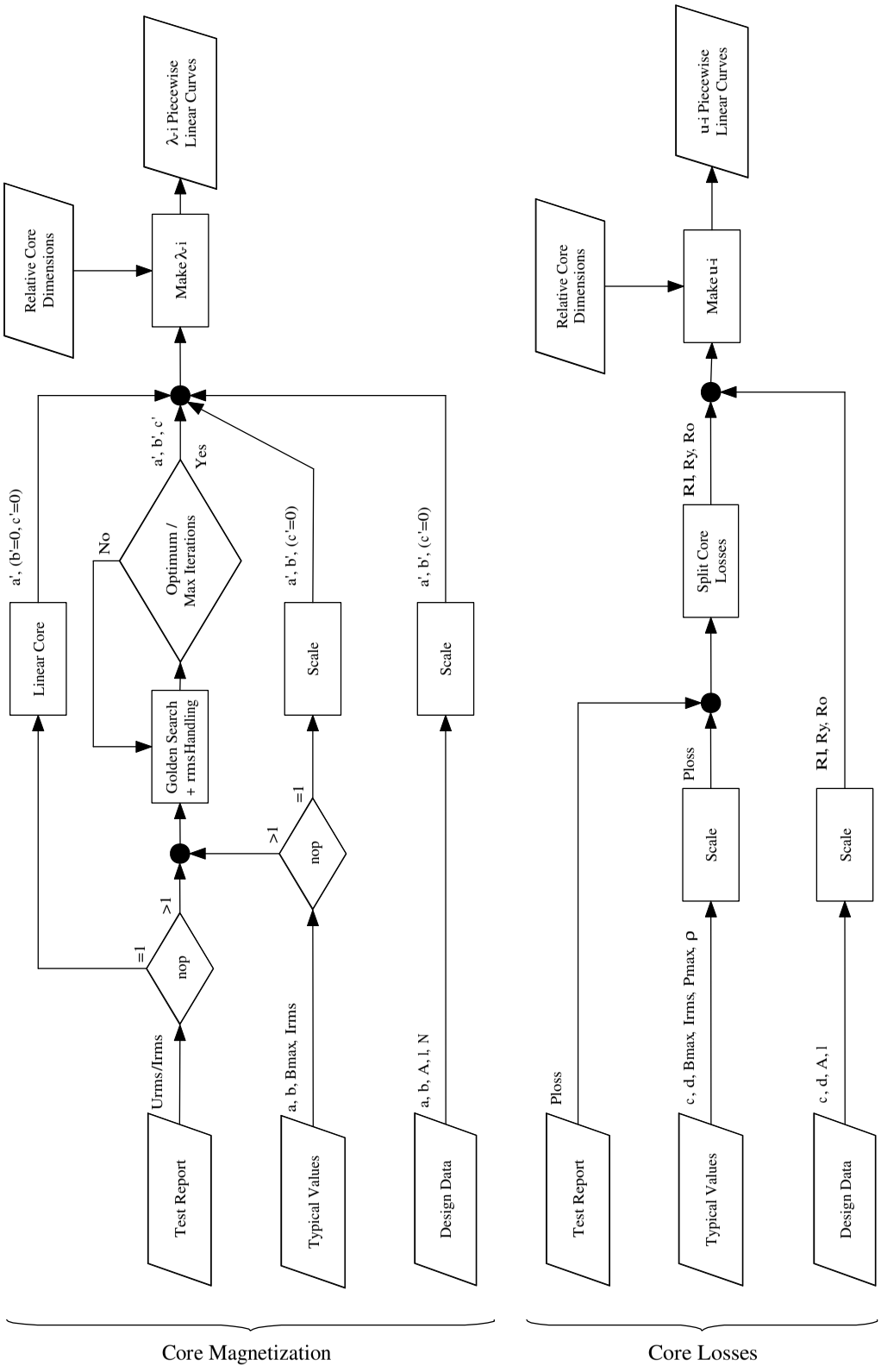

Figure 5.1: *BuildCore* routine. Flow chart

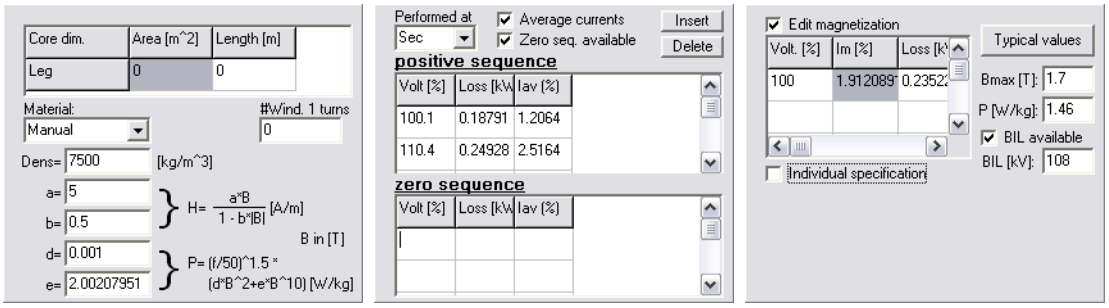

(a) Design parameters. (b) Test report. (c) Typical values.

Figure 5.2: Graphical user interface of XFMR.

same manner of the positive sequence data. Typical-value tab can be used when no experimental data are available. B_{max} and specific losses per kilo have to be specified.

The routine does not give any visible output to the user. The output consists in piecewise linear curves of nonlinear core inductances and resistances. The curves are then handled by other routines that create the EMTP files.

In most of the cases the input data follows a plain path. They are just rescaled to obtain the proper final values. The most complex part of the work is the section related to the core magnetization in case of test report data.

Fig. 5.3 gives a schematic representation of the subroutines dependences. The grey blocks are parts not yet implemented. They show future features and capability. The structure of the routine allow an easy extension to the triplex and shell core-type transformers. For the moment only three- and five-leg core-type transformers are supported. The two and three parameter Frolich equation can be also improved introducing new routines that can deal with the empty-space effect L_∞.

The whole *BuildCore* routine is composed of almost 1400 lines of code, where more then 1000 have been written only for the *CoreTestReport* procedure and its subroutines. Due to its sophistication, it is interesting to analyse more in detail this section of the program.

5.2 *CoreTestReport* Subroutine

The iterative process presented in Section 4.6 is implemented in the *CoreTestReport* subroutine. In two cases the process is complex: when more then two point are specified in test report data or in typical values, with edit magnetization box checked.

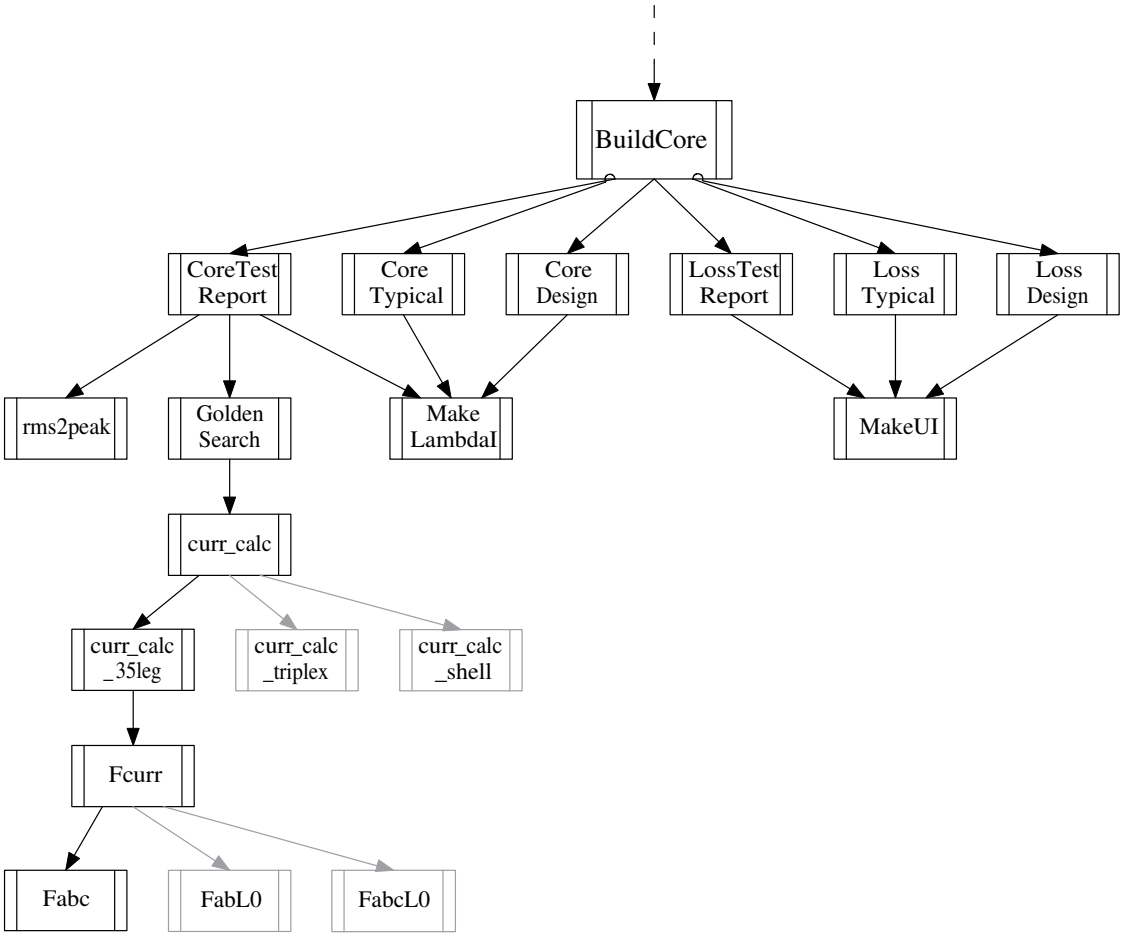

Figure 5.3: Program routines dependence

When only one point in the test report is known, the core is modelled linearly. In future version of the routine suppositions will be introduce to obtain a nonlinear core model also for this case.

When enough data is available, an iterative process starts to fit the a, b, and c parameters with the test report data. The searching of the three parameters is a nonlinear and multidimensional problem. The more robust and straightforward search method is the "*Golden Section Search in One Dimension*"[27]. This method can be applied to multi-dimensional problems performing successive cycles of optimizations for each variable. The main steps of this part of the program are shown in Fig. 5.4. They are:

- Preprocessing of the open circuit currents, the resistive component is subtracted to isolate the magnetization currents.
- Estimating the phase linkage flux and currents peak from the rms voltage and

magnetization currents. This part is handled by the *rms2peak* routine. The routine takes into account the coupling type of the transformer.

- Calculating the initial values and the boundary conditions for parameters c, a, b.
- Searching the optimum parameter of Frolich equation. *GoldenSearch* routine is called in sequence for parameters c, a, b. The sequence allows to obtain the most accurate value for the last parameter. In this case b is the most important parameter. The routine is repeated until an optimum value is found. In case of number of points higher than two it is difficult to reach an optimum. Testing the program results that hundred iterations give accurate results.
- Building the output curves: a_{opti}, b_{opti}, and c_{opti} are passed to the *MakeLambdaI* routine that built the piecewise linear curve.

5.3 Conclusion

The routine has been implemented. Some significative results are reported in the next chapter.

The *CoreTestReport* procedure requires many iterations and sub-cycles. This part of the program execution requires about 20-30 seconds on a 1500 MHz Pentium M personal computer. The speed of the routine can be improved implementing more advanced methods for nonlinear multi-variable fitting problem. These methods are more complex end usually requires the calculation of derivatives. At this stage the main focus was to obtain a robust and simple routine necessary for testing the model. Therefore these advanced method are not implemented.

In order to make the program as robust as possible, each of the expected errors are handled by the program.

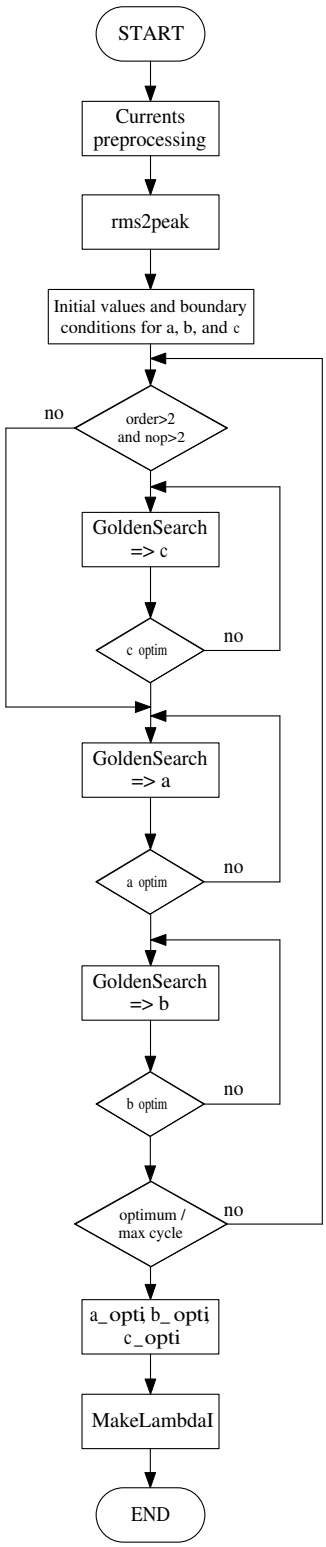

Figure 5.4: *CoreTestReport* routine.

Chapter 6

Laboratory Tests

This chapter presents a series of tests performed on a small distribution transformer. The tests intend to analyse the effects of the core magnetization. Open-circuit and zero-sequence tests have been performed. The tests were useful to improve the understanding of the physical behaviour of a transformer. In the next chapter the waveform measured during the tests will be compared with the simulated waveform to validate the model presented in the previous chapters.

6.1 Aim of the laboratory test

The tests on the transformer have been performed for two main intents:

- Examine the behaviour of a transformer under real working condition. This enhance the comprehension of the theoretical studies.
- Evaluate the proposed model through a comparison between simulated and measured data.

The aim of this thesis is to investigate the core representation. Tests are performed on a small power unit transformer in order to characterize the no-load losses and magnetizing currents of the transformer. Overexcitation is observed with particular attention. The more relevant tests to perform are open-circuit and zero sequence tests. A lot of works presenting guideline and direction for testing transformers can be found in the literature, see [25], [28], [29], [30], [31], and [32]. The standard procedure of open-circuit test is to acquire only one point at rated voltage. In this work the transformer is tested on a wide range of excitation, from 10% to

130% of rated voltage. A high number of points is recorded in order to have a good description of the non-linear behaviour.

Many tests are performed in order to understand the behaviour of the transformer in details:

- wattmeter-voltmeter-ammeter open-circuit test, delta and wye couplings;
- open-circuit test, wye coupling;
- open-circuit test, delta coupling, phase current;
- open-circuit zero-sequence, parallel of the LV windings;
- open-circuit zero-sequence, series of the LV windings.

The first test is performed using analog instrument. For all the other tests voltage and current waveforms are measured with a digital scope. The main results are described in the following sections.

6.2 Test Cell Set Up

Fig. 6.1 shows a schematic sketch of the test-cell. The main devices used in the experiments are also shown in Fig. 6.1. The components and their characteristics are now explained.

The tested transformer is shown in Fig. 6.2. It is a 100 kVA distribution transformer fabricated by EB National Transformer, now ABB Transformer, in 1990. No official documentation has been found about this transformer. The only set of known data is the rating plate, see Fig. 6.3 and Tab. 6.1. The unit is a three-phase three-leg transformer. The low-voltage-side has accessible terminal, so both delta and wye connection can be configured. The high voltage side is wye coupled and the neutral terminal is available.

Power	100 kVA	
f	50 Hz	
HV Y	36 kV	1.60 A
LV y	400 V	144 A
LV d	231 V	250 A
Coupling	YNyn0 - YNd11	

Table 6.1: Transformer Data.

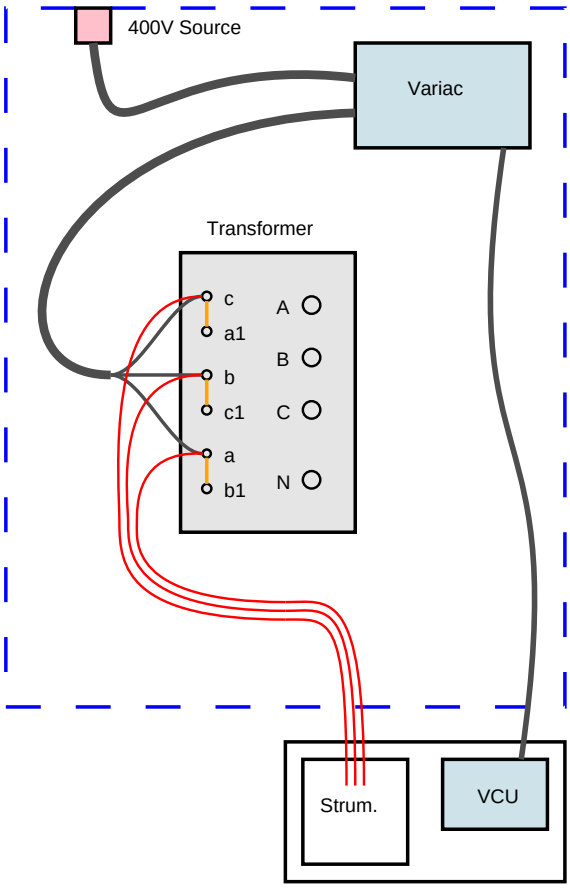

Figure 6.1: Schematization of the test cell setup.

The transformer is energized by a motorized variac. The variac control unit (VCU) is placed outside the test cell. The supply voltage can be regulated between zero and 400 volts. The maximum current is limited by a fuse of 63 amps. No data is known about the impedance of the variac and of the primary source.

In the low-right corner of Fig. 6.1, the operator-working-table where the measuring instruments and the VCU are placed is shown. This setup allows the operator to control the excitation level with the VCU and to use the measuring instruments from a location outside the test cell. Therefore, any risk for the operator to enter in contact with high voltage is avoided. Moreover, the door of the cell is equipped with a safety switch connected to the VCU. If the door is open while the transformer is energized, the power source is automatically turned off.

Test are performed with analog and digital devices. Analog devices are used for standard wattmeter-voltmeter-ammeter (power, voltage and current) tests. The instruments use for the test are rms voltmeter, rms amperometer and active power wattmeter, all in class β=0.5. The waveforms of voltage and currents are obtained

Figure 6.2: Tested transformer.

Figure 6.3: Transformer plate data.

with a digital scope. The unit, a Yokogawa DL708 digital scope, is equipped with six high voltage input modules. Active-probe current transformers are used to measure the current waveforms. No real-time measure is required and only periodic waveforms are measured. The waveforms are acquire at $4kS/period$ in order to obtain accurate waveforms.

6.3 Open-Circuit Test

6.3.1 Method for No-load Losses and Excitation Currents Measurements (Wattmeter-Voltmeter-Ammeter)

The first tests performed on the transformer follow the standard procedure for transformer testing, see [25], [28] and [29].

No-load losses (also referred to as excitation losses, core losses, and iron losses) are the losses in a transformer when it is energized without supplying load. The losses are a very small part of the power rating of the transformer, usually less than 1%. No-load losses include:

- core loss,

Quantity	Device	Description
1	Transformer	see Fig. 6.3 and Tab. 6.1
1	Variac	380V motorized variac with control unit
3	Analog voltmeter	120/240/480V, 120div, β=0.5
3	Analog ammeter	1.2/6A, 120div, β=0.5
3	Analog wattmeter	1.25/2.5/5A, 50/100/200/400V, 120div, β=0.5
1	Digital scope	Yokogawa DL708
3	Active current probe	Max current=50A p-p, ratio 1/1000
1	Active current probe	Max current=250A rms, ratio 1/1000
3	Resistances	100Ω, to use with the CT
3	Voltage splitter	Hand-build, $15M\Omega/15k\Omega$, ratio≈1/1000

Table 6.2: List of equipments.

- dielectric loss,
- conductor loss in the windings due to the excitation current.

These losses increase with the excitation voltage. The no-load losses consist primarily of the core loss in the transformer core. Core loss is a function of the magnitude, frequency, and waveform of the impressed voltage.

Excitation current (or no-load current) is the current that maintains the rated magnetic flux excitation in the core of the transformer. The excitation current is generally expressed in percent of the rated current of the winding in which it is measured. The measurement of excitation current is usually carried out together with the test for no-load losses. The excitation current has two main components: an inductive component and a resistive component. The inductive component is due to the magnetization of the core. Thus, it is non-linearly proportional to the excitation voltage. The capacitive component is due to the charging current and dielectric losses for both the capacitance of the internal winding and the capacitance to the ground. This capacitive current is linearly proportional to the excitation voltage. Between these two current component, the inductive component of the exciting current is usually the dominant component.

IEEE Standard [29] suggests to use three-wattmeter method. The basic configurations for three-phase circuit is shown in Fig. 6.4. The three main case for the different connection of a three-phase transformer are reported: delta connection, Fig. 6.4(a); wye connection with neutral unavailable, Fig. 6.4(b); and wye connection with neutral available, Fig. 6.4(c). The ammeters measure the three line excitation currents, and the voltmeter the three phase voltages. The no-load loss is the

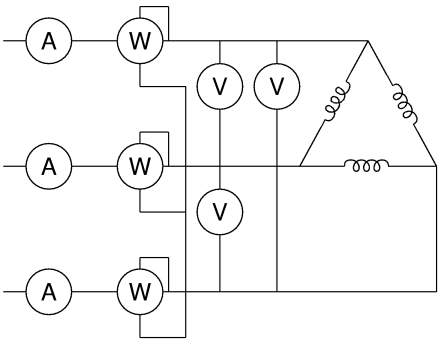

(a) Delta coupling.

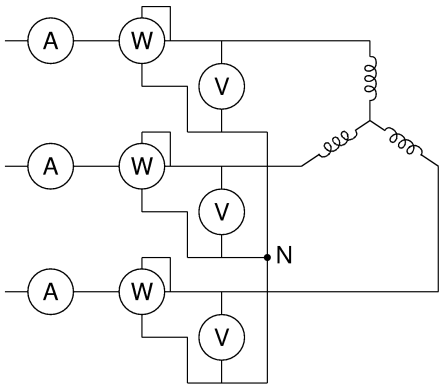

(b) Wye coupling, neutral unavailable.

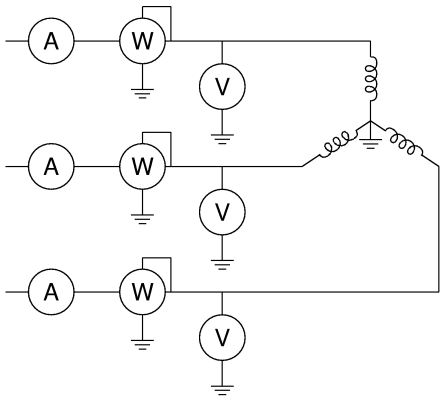

(c) Wye coupling, neutral available.

Figure 6.4: Three-wattmeter method.

sum of the three wattmeter indications: $P_0 = P_{W1} + P_{W2} + P_{W3}$.

Also a two-wattmeter method can be applied. However, it should not to be used in transformer loss tests because of the following reasons:

- an unbalanced distribution of no-load losses and excitation currents exists between phases;
- the applied voltage and the excitation current waveforms of the no-load loss test are intrinsically distorted;
- transformers have a low power factor when connected for measuring losses, and small errors can result in large measurement error.

6.3.2 Test for No-load Losses and Excitation Currents Measurements (Wattmeter-Voltmeter-Ammeter)

The tests with analog instruments are performed to obtain a set of indicative values and to reproduce the standard test usually performed on transformers.

Three-wattmeter tests are performed following the procedure presented in the previous section. Instead of performing the tests only at the rated voltage, more levels of excitation are applied to the experiment. The voltage level is varied from a minimum to a maximum. The limited sensibility of the instruments set the minimum. The maximum value is represented by the first reached limit between the maximum current and the maximum voltage. This allows to describe the magnetization curve of the transformer.

The three different setup of Fig. 6.4 are tested and the results are compared. Tables with the data obtained from the experiment are reported in Appendix D.

Fig. 6.5 is obtained from the data of the open-circuit tests when transformer is delta coupled. I_{0-avg} is the average between the values of the three line current measured by the ammeter. I_{cl} represents the resistive current due to the core-loss. It is obtained from:

$$I_{cl} = \frac{P_0}{\sqrt{3} \cdot V} \tag{6.1}$$

The magnetizing current (I_m) is an inductive current, and reads:

$$I_m = \sqrt{I_{0-avg}^2 - I_{cl}^2} \tag{6.2}$$

These three current are represented in percent of the rated current as function of the percent supplied voltage.

Fig. 6.6 and Fig. 6.7 are obtained following the same procedure. Here the transformer is wye-connected. The two possible setup with and without star-point connected to the neutral are compared in Fig. 6.6. The curves with index "N" are referred to the case of star-point connected to the neutral. Fig. 6.6 shows that the two cases are comparable. The case with the star-point connected to the neutral seems to be preferable because with the same instruments it was possible to get a higher range of values. Fig. 6.7 shows the complete set of current for this latter case.

All the previous figure report percent current. Fig. 6.8 compares the results of delta and wye connections. It is observable that the curves are overlapped.

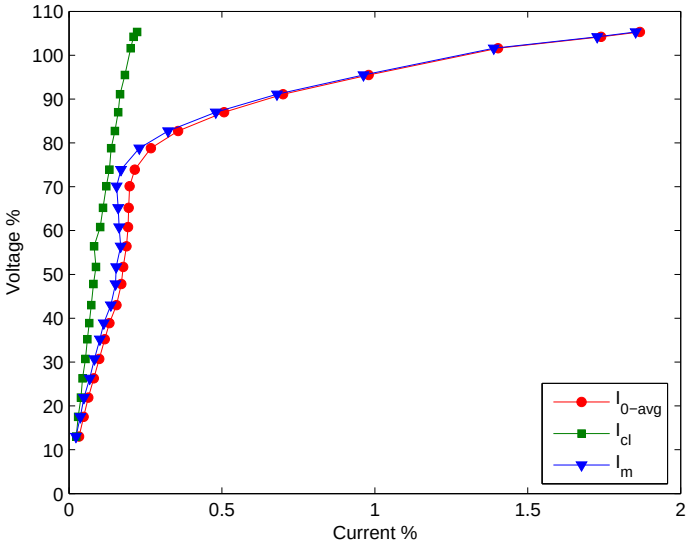

Figure 6.5: Currents in delta-connected transformer.

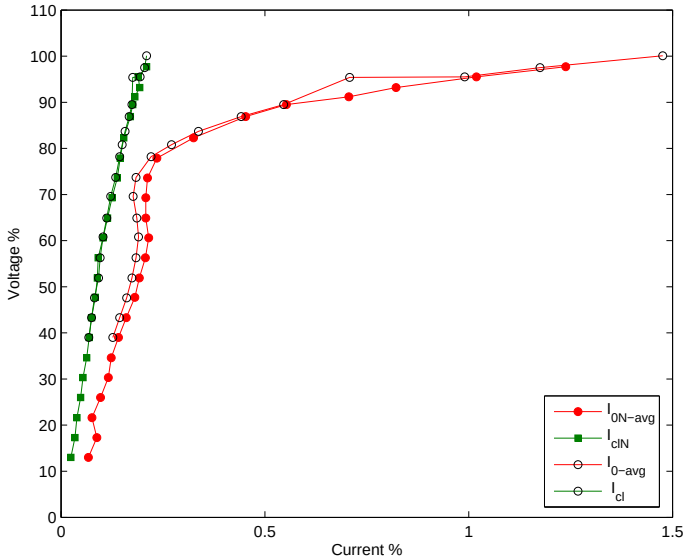

Figure 6.6: Currents in wye-connected transformer. Comparison.

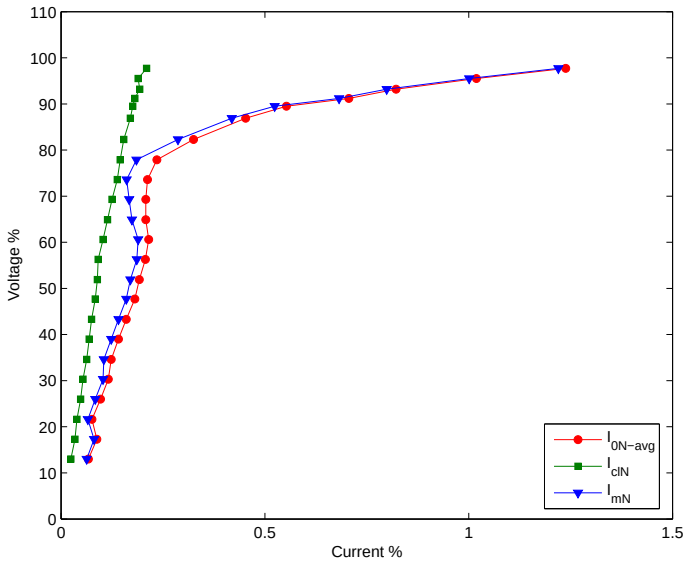

Figure 6.7: Currents in wye-connected transformer. Star-point attached to neutral.

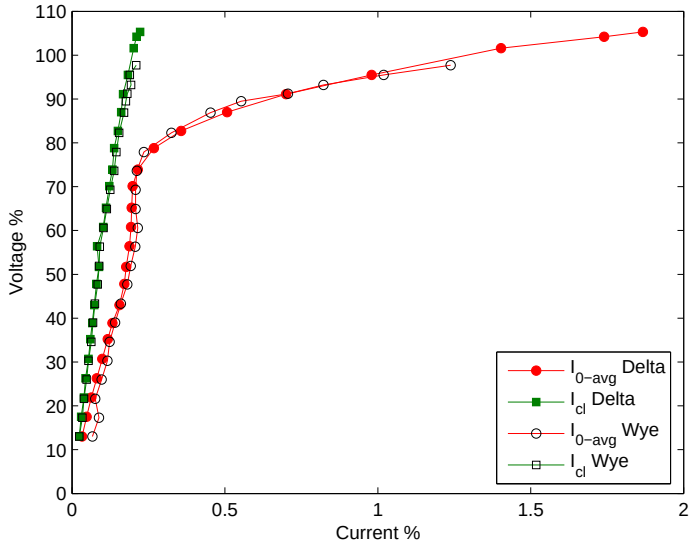

Figure 6.8: Comparison between delta and wye coupling.

6.4 Digitized Measurements

In this section the open circuit tests (with delta and wye coupling) are repeated, but using a digital scope instead analog instruments. To be able to investigate on the real waveform shape it is important to work with instruments that allow to check the waveforms of the measured signal. The measure of only rms values lack of information and can result inaccurate.

6.4.1 Open-Circuit Test, Wye Coupling

The neutral is available, so a configuration with star-point connected to the neutral is used for this set of tests.

The maximum available level of voltage match the rated voltage. For this reasons no overexcitation test can be performed with wye connected transformer.

Some of the curves acquired with the digital scope are reported for different level of excitation voltage. Elaborating the data it is possible to calculate the real rms value of phase-voltage, current and core-losses. Tab. D.4 in Appendix D reports this data.

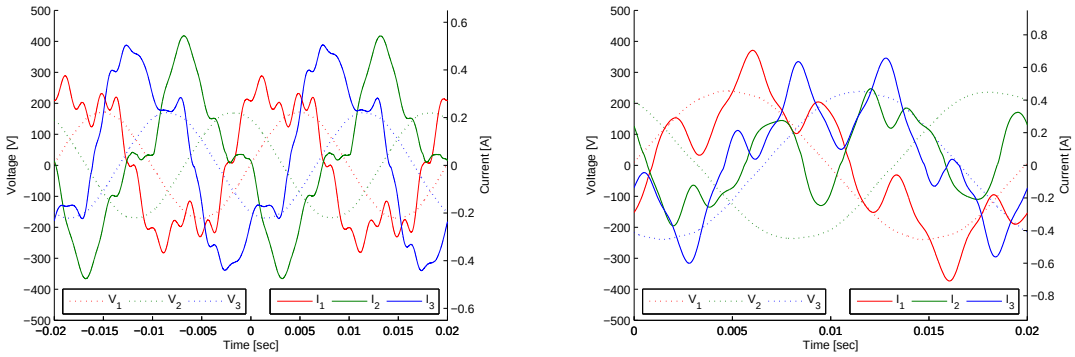

(a) 50% rated voltage

(b) 75% rated voltage

Figure 6.9: Voltage and current waveform. Points 10 and 14 of Tab. D.4.

Fig. 6.10 is particularly indicative. It is possible to observe the sinusoidal waveform of the phase-voltage and the distorted waveform of the current. Examining more in detail the current waveforms, it is possible to observe the different shape of I_2 (middle phase) compared with I_1 and I_3 (these two are quite similar). This difference is due to the non-symmetrical construction of the transformer core. The current is mainly composed by a resistive and an inductive components. The inductive component is dominant, in fact the current is 90 degree shifted respect to

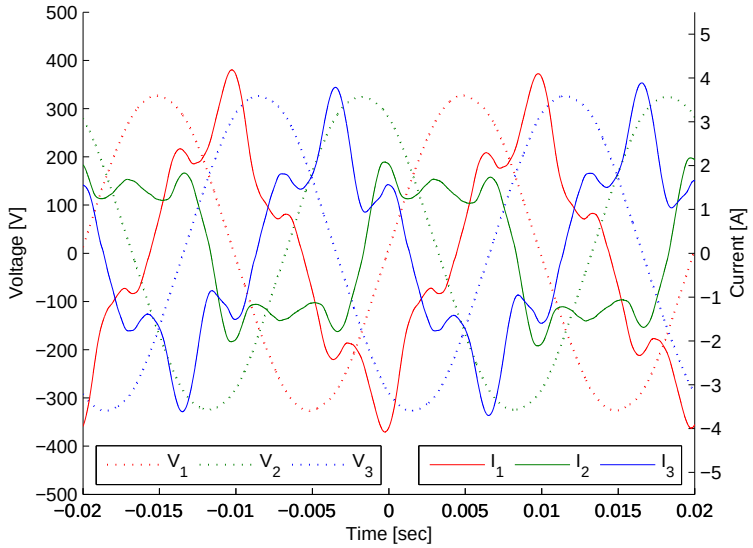

Figure 6.10: Voltage and current waveform at rated voltage (point 23 of Tab. D.4).

the corresponding voltage. The resistive current is in phase with the voltage. For this reason, its presence do not influence the peaks of the current waveforms.

The data of the previous tests (where analog instruments have been used) and the data of this test are recorded simultaneously. It is interesting to compare the two sets of data. Fig. 6.11 shows the comparison. Each set of two points (blue and red marks) is directly comparable because it refers to the same voltage level. Due to the distorted current, analog ammeter and wattmeter seem to overestimate the rms current and the active power. Consider now the points for the highest excitation level. For the current there is a difference of $0.2A$ between the two curves. The ammeter used is in class $\beta = 0.5$ and has an upper range of $6A$ and its absolute error is $0.03A$. For the active power the difference is $44W$. The wattmeter used is in class $\beta = 0.5$ and has an upper range of $1000W$ and its absolute error is $5W$. The absolute error of both the instruments are much lower then the difference between measured and computed values. Therefore, this difference cannot be caused by the inaccuracy of the instruments alone.

6.4.2 Open-Circuit Test, Delta Coupling

The limit of the wye connection is that it is not possible to test the overexcitation of the transformer. This is due to the low excitation voltage obtainable with the available devices. For this reason testing the transformer with the delta connection

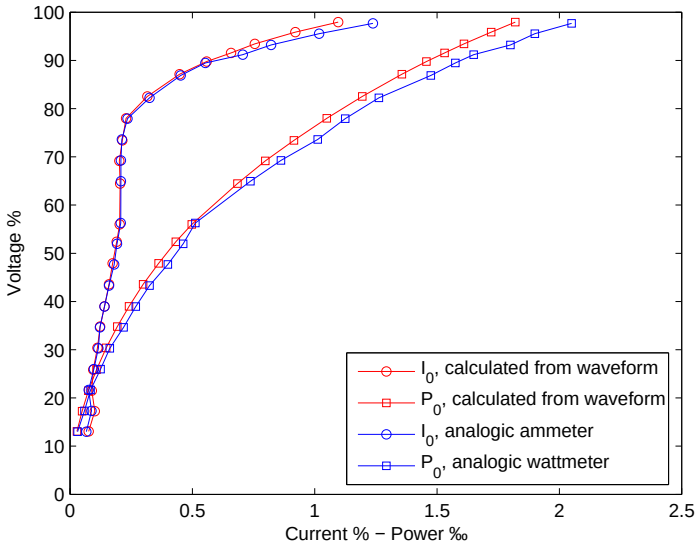

Figure 6.11: Comparison between different set of data. Wye coupling.

provides more interesting results.

The availability of the low voltage terminal give the possibility of measure directly the phase current of the transformer. From the phase current it is always possible to obtain the line current, but the opposite is not feasible. For this reason phase currents have been measured.

Fig. 6.12 show voltage and phase current waveforms for different level of excitation (around 50%, 75%, 100% 115% and 130%). Tab. D.5 in Appendix D reports the rms value of line current and excitation voltage, and the no-load loss for more tested points. The data of the table is obtained elaborating the waveform. 130% is the maximum excitation level, because the peak of the phase current reaches the upper range limit of the current transformers.

With delta coupling the voltage waveforms result distorted already at low level of excitation. Such high distortion, also for small currents, cannot be caused by a high source impedance. Likely the problem is an asymmetric voltage source resulting in a zero-sequence component. The intrinsically relation of $\sum V = 0$ (because of the delta coupling) have to be satisfied. If the voltage source is symmetric the relation is always satisfied. On the other side, a small deviation of the voltage causes problems. In order to satisfy the relation between the phase voltage a homopolar current is created inside the delta coupled windings:

$$i_1 + i_2 + i_3 = i_0 \neq 0 \tag{6.3}$$

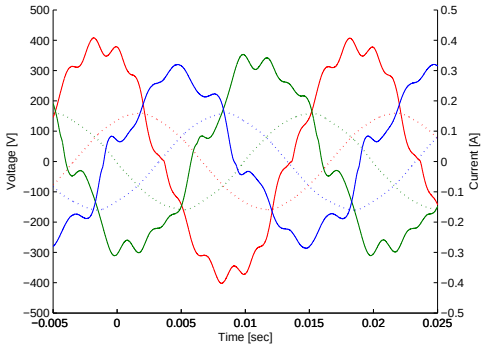

(a) 50% rated voltage.

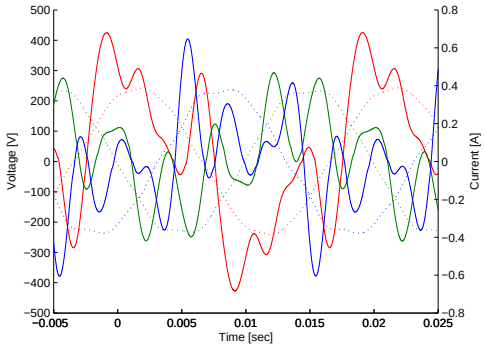

(b) 75% rated voltage.

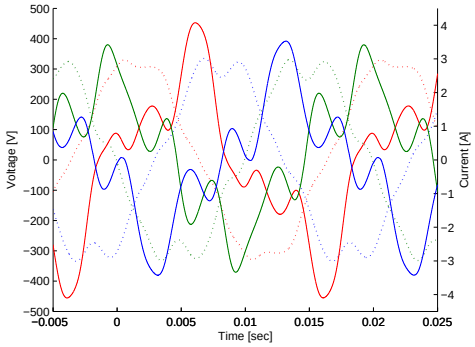

(c) 100% rated voltage.

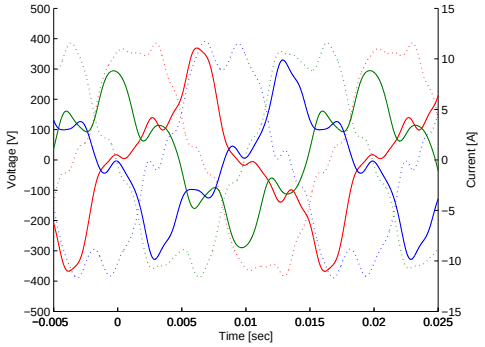

(d) 115% rated voltage.

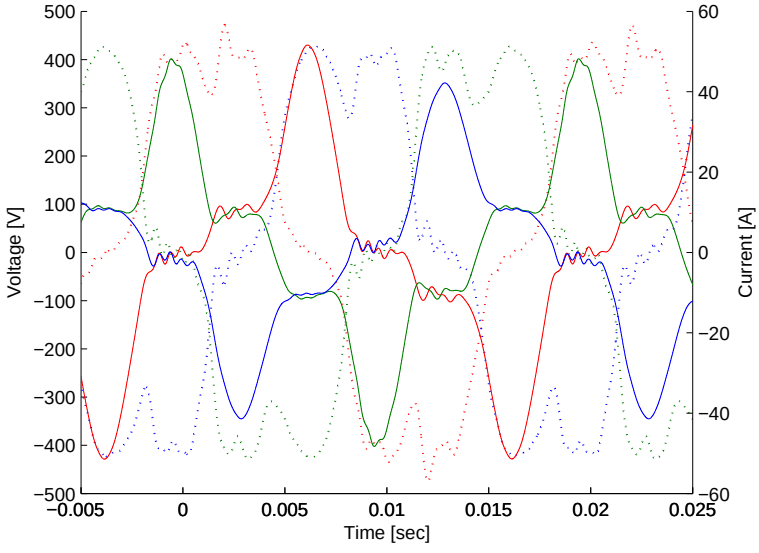

(e) 130% rated voltage.

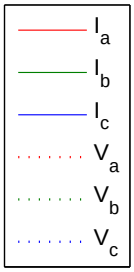

(f) Legend.

Figure 6.12: Voltage and phase current waveform. Point 9, 15, 25, 32 and 44 of Tab. D.5.

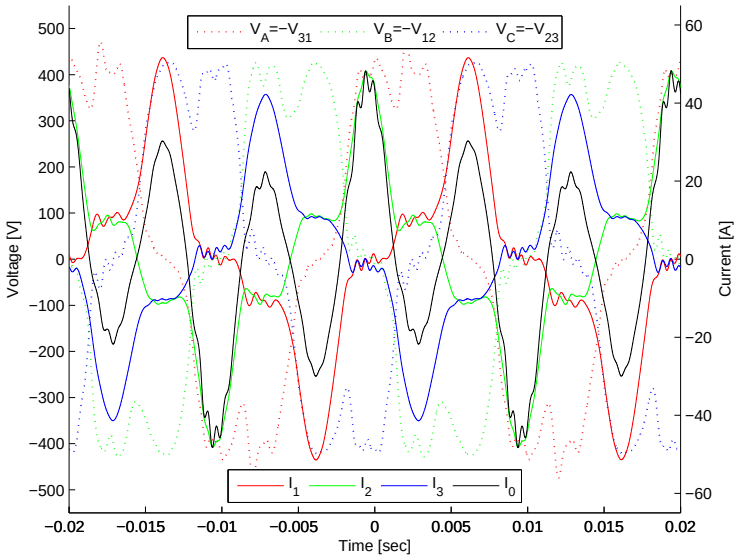

Figure 6.13: Homopolar current for delta coupling.

This current can be observed in Fig. 6.13. It has a base frequency three times greater than of the rate frequency of the transformer. The homopolar current flows through the winding causes a voltage-drop. The voltage relation is modified as:

$$\sum v = (v_1 - Z \cdot i_0) + (v_2 - Z \cdot i_0) + (v_3 - Z \cdot i_0) = 0 \tag{6.4}$$

where Z is the impedance of the windings, which is quite low in the transformer. The low value of impedance is not favourable in this case because this causes a high homopolar current, comparable to the value of the exciting current. For the wye coupling the voltage is not distorted the same way.

Fig. 6.14 shows the comparison of $V_{ex}\% - I_0\%$ and $V_{ex}\% - P_0‰$ when measured with analog instruments or calculated from the waveforms. With delta coupling the error of the analog instruments seems to be lower than what shown in Fig. 6.11. The voltage waveform is distorted, therefore an overestimation of the voltage level is expected. A direct comparison of the measured points it is not possible because the data is not registered from the same experiment.

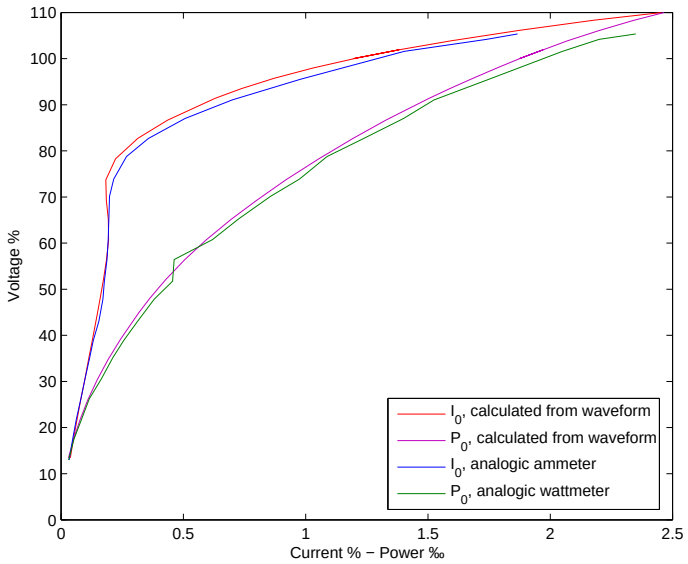

Figure 6.14: Comparison between different set of data. Delta coupling.

6.5 Zero Sequence

During normal operation, the three-phase voltages are symmetric. Also the fluxes on the three-transformer limbs are symmetric. Therefore, the sum of the three limb fluxes is always zero and these fluxes only go through the iron core. When voltage source is asymmetric, then the sum of the three fluxes is not necessary zero. A homopolar flux is created.

In the five-leg transformers the zero-sequence flux pass through the outer-legs. Therefore, the zero-sequence inductance for five-leg transformer is known once the $B - H$ magnetizing curve is known.

Three-leg transformers do not have a low-reluctance zero-sequence path in the iron core. The flux goes through the air gap and in the transformer-tank. Therefore, the zero-sequence inductance for three-leg transformers has to be measured.

To measure the zero-sequence inductance the phases of the transformer have to be energized with a single-phase source. At this point there are two different approaches:

- The three phases connected in series, same I gives same H-field. The method is proposed by Fuchs [31].
- The three phases connected in parallel, same U gives same B-field.

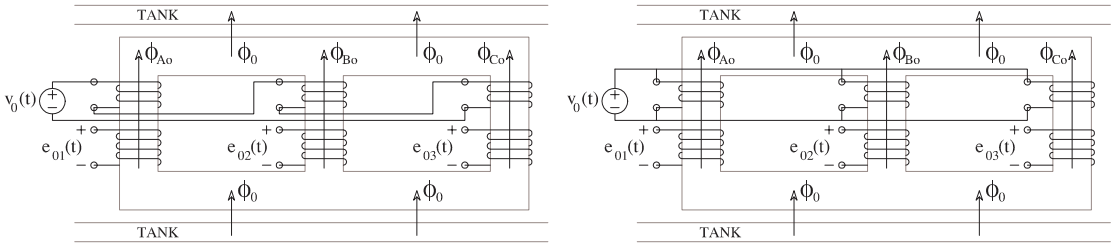

(a) Series connection. (b) Parallel connection.

Figure 6.15: Zero-sequence test setup.

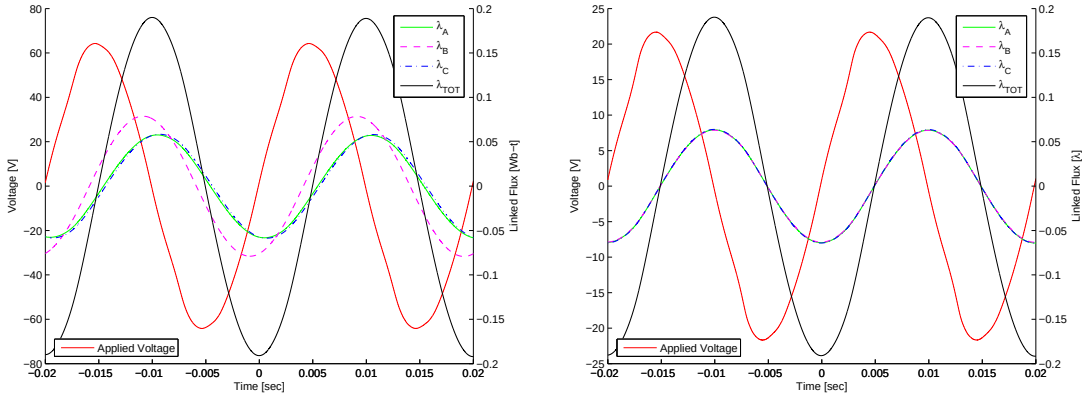

(a) Series connection. (b) Parallel connection.

Figure 6.16: Zero-sequence voltage and linked-flux waveform.

Experiments prove that the parallel connection is more appropriate.

Fig. 6.16 shows the two cases with single-phase excitation with respectively series and parallel connection. When series connection is used (Fig. 6.16(a)) the fluxes of the three phases do not result exactly in phase. This fact leads to that not the whole flux goes outside the core of the transformer. When parallel connection is used (Fig. 6.16(b)) the three fluxes are overlapped. This means that the only possible return path is outside the transformer core. For this reason a parallel connection is chosen for zero-sequence measurements.

The linked flux waveforms are obtained as integral of the induced voltage. The induced voltage is measured on the high-voltage side and then converted to the low-voltage side with the turn-ratio. The current on the high-voltage side is zero[1]. Therefore the no leakage-flux or voltage-drop effects occur. For this reason, to calculate the flux it is preferable to measure the induced voltage on high-voltage

[1] very low because the resistive voltage partitioner.

than the applied voltage on low voltage side. The high voltage is measured using a resistive voltage partitioner. Fig. 6.17 shows the equipment. Each phase uses three $5M\Omega$ high-voltage resistances and one $15k\Omega$ resistance.

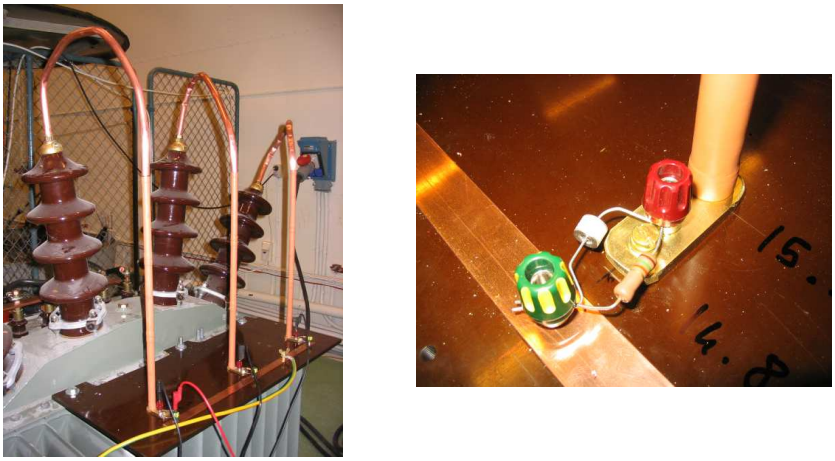

Figure 6.17: Resistive voltage partitioner.

The leakage flux λ_0 versus the input current i_0 is the zero sequence characteristic. However this characteristic has an hysteretic behaviour due to the magnetizing losses of the iron-core. The curve can be corrected. Since this loss is an active power, it can be calculated from the voltage and current waveforms as average value of the instantaneous power. In case of discrete points it is:

$$p(n) = v(n) \cdot i(n) \tag{6.5}$$

$$P = \frac{1}{N-1} \sum_{n=1}^{N} p(n) \tag{6.6}$$

Then the equivalent parallel resistance representing the magnetization losses reads:

$$R_m = \frac{V_{rms}^2}{P_m} \tag{6.7}$$

And finally the magnetizing current is calculated as follow, see Fig. 6.18:

$$i_m = i_0 - i_{los} \tag{6.8}$$

$$i_{los} = \frac{v}{R_m} \tag{6.9}$$

where i_0 is the total measured current. This two equations are the extension of Eq. (6.1) and (6.2) for instantaneous or discrete values.

In this way the current due to the losses results in phase with the voltage and the magnetizing current results 90 degree forward shifted from the voltage. Fig. 6.18 shows the correction on the current waveform.

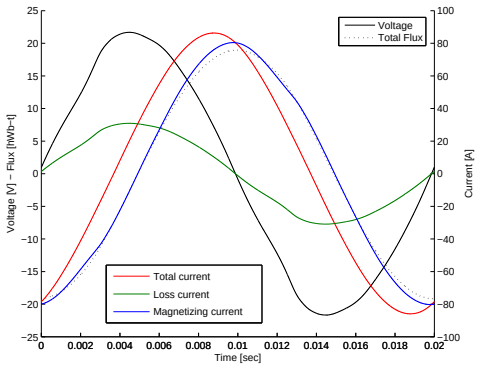

Figure 6.18: Current waveforms. Separation of effect.

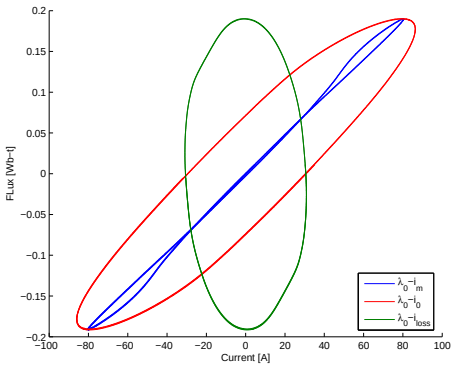

Figure 6.19: $\lambda_0 - i_0$ characteristics.

The $\lambda - i$ characteristics for the three currents are shown in Fig. 6.19. It is interesting to notice how the hysteretic characteristic which represents the relation between the flux linkage and the total current (i_0) is an oval with an oblique principal axis. The area of the oval represent the losses. The $\lambda_0 - i_0$ can be split in two part. The part due to the losses ($\lambda_0 - i_{loss}$) is an oval with a vertical principal axis. The oblique line ($\lambda_0 - i_m$) represents the pure zero-sequence inductive effect. Considering this last curve, it is acceptable to assume the zero sequence characteristic to be linear and L_{zero} to be constant.

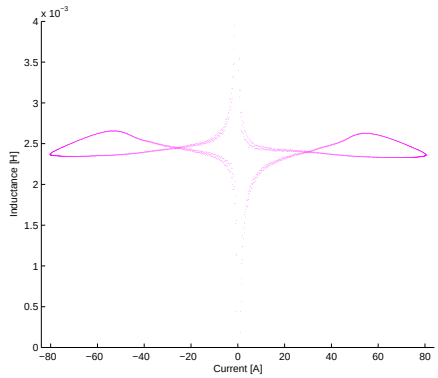

Figure 6.20: Zero-sequence inductance. Variation over one period.

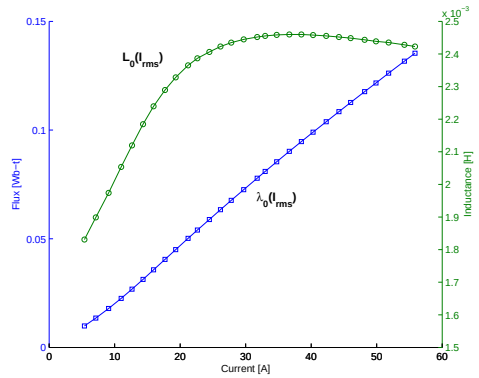

Figure 6.21: Zero-sequence inductance. Variation of excitation level.

Fig. 6.20 shows the zero-sequence inductance L_{zero} as a function of the exciting

current for one cycle of sinusoidal voltage. It can be observed that for this transformer the zero-sequence inductance results about $2.4mH$. The vertical asymptote is due to the loss of accuracy in the computation of $L_{zero} = \lambda/i$ while current and flux approach together the zero. Fig. 6.21 shows the average zero-sequence inductance for different level of excitation. The variation of L_{zero} results bounded between 1.8 and $2.5mH$. For low level of excitation the value of L_{zero} is lower. This is due to capacitive effects. However, analysing the capacitive behaviour is beyond the scope of this work.

L_0 is not the value of the inductance in the equivalent circuit of Fig. 4.26 at pag. 62. According to Eq. (4.64) at pag. 63 is:

$$L_0 = \frac{3}{2} \cdot L_{zero} \tag{6.10}$$

6.6 Conclusions

The tests on the transformer highlight the importance of a correct setup of the test equipment. It is shown how an asymmetry of the supply voltage can cause problem. Moreover, the presence of distorted current is inevitable while working with non-linear components.

To ensure repeatability of the tests and reliability of the results it is important that the transformer follows the virgin magnetization curve at any energization. This can be ensured if the unit is correctly demagnetized. Before and after each test it is important to follow a specific de-energized procedure. The demagnetizing procedure consist in a slow de-energization of the transformer. This process ensure that a minimum residual induction remain in the core of the transformer. If no de-energization is carried out the transformer is energized with unknown initial condition.

I was faced with two main problem during the test section: low voltage level for wye coupling and distorted voltage waveform for delta coupling. The source voltage level correspond to the transformer rated voltage with wye coupling. This does not permit to test the transformer in overexcitation if it is wye connected. The lack of tests in overexcitation do not allow a correct representation of the magnetizing curve. The rated voltage of delta coupling is $\sqrt{3}$ times smaller than the supply voltage level. Thus, in this case there are no problem to overexcite the transformer.

During the tests I obtain distorted waveforms. This is a problem for the rms instruments that do not operate in the typical condition. For high level of distortion

rms instruments do not report accurate measures. A high source impedance can cause distortion on the voltage. If the voltage is not sinusoidal, also the flux is distorted and a distorted flux do not agree with the hypothesis of the model.

It is necessary to be aware of any of the addressed problems before starting any experiment. To be able to see unexpected behaviour it is important to work with instruments that allow to check the waveforms of the measured signal. The measure of only rms values lack of information and can result inaccurate.

A suggestion is to measure the phase currents, if possible. This is true especially for the delta coupling. If only line currents are measured, the homopolar current cannot be observed.

In the next chapter value from Appendix D will be inserted in to the transformer model. It will be possible to compare the validity of the model comparing simulated and measured current waveforms.

Chapter 7

Results, Model Validation

This chapter validates the model presented previously. First the current waveforms measured in the laboratory are compared with current waveforms obtained from the simulation. Then the results obtained from test report and design information for the transformer of Fig. A.1 are compared. The match of the results for the two cases will show the robustness of the model. Finally, the result from an ATP simulation is shown to demonstrate how the XFMR general transformer component can be used.

7.1 Waveforms Comparison

The performance of the two and three parameters Frolich equation

$$\lambda = \frac{i}{a + b \cdot i + c \cdot \sqrt{i}} \tag{7.1}$$

where the parameters a, b, and c are calculated from test data is tested by comparing the waveforms. These parameters are inserted in a Matlab routine that provides current waveforms.

Frolich parameters provide the relation between linkage flux and current. Thus, flux waveforms are needed as input for the Matlab program. The voltage waveforms measured in the laboratory are distorted, so sinusoidal flux cannot be used to build the current waveforms. The actual leakage flux waveforms are thus calculated as integral of the measured voltage waveforms. Initial integration constants are computed setting the average flux waveform to zero. Fig. 7.1 shows an example of the leakage flux waveform of phase 1 and its relative voltage. It refers to point 44 of

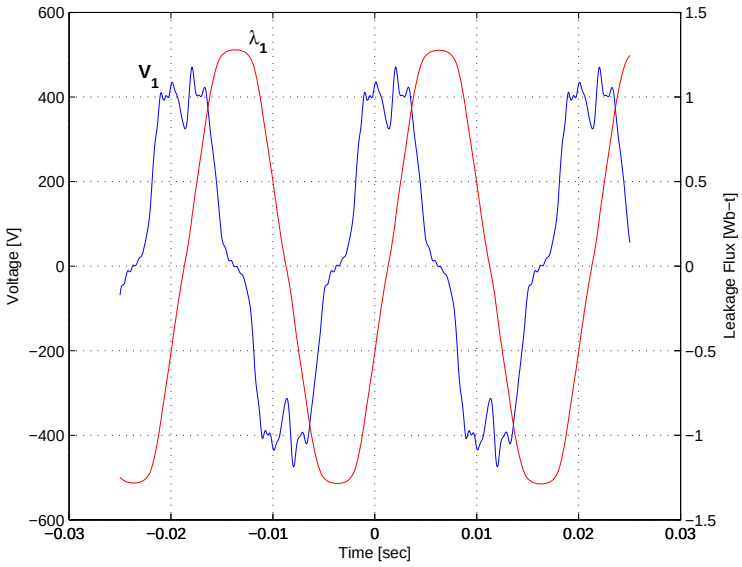

Figure 7.1: Voltage and flux waveforms. Phase 1.

Tab. D.5. Similar curves are obtained for the other phases.

Flux waveforms and Frolich parameter (referred to the $\lambda - i$ curve) are then used in a routine similar to *curr_ calc*-routine of Fig. 5.3. Fig. 7.2 to 7.5 reports the results of the simulations compared with the laboratory data. Tab. 7.1 report the Frolich equation parameters for each of the examined cases.

Fig.	Coupl.	Frolich eq.	a	b	c	Data points	Tab.
7.2	Wye	ord.3	0.12477	0.92302	-0.01	18,21,23	D.4
7.3	Wye	ord.2	0.11978	0.91855	—	18,21,23	D.4
7.4	Delta	ord.3	0.27203	0.69981	0.33921	23,30,35,44	D.5
7.5	Delta	ord.2	0.77797	0.73007	—	23,30,35,44	D.5

Table 7.1: Simulation results. Frolich parameters. Wye and delta coupling.

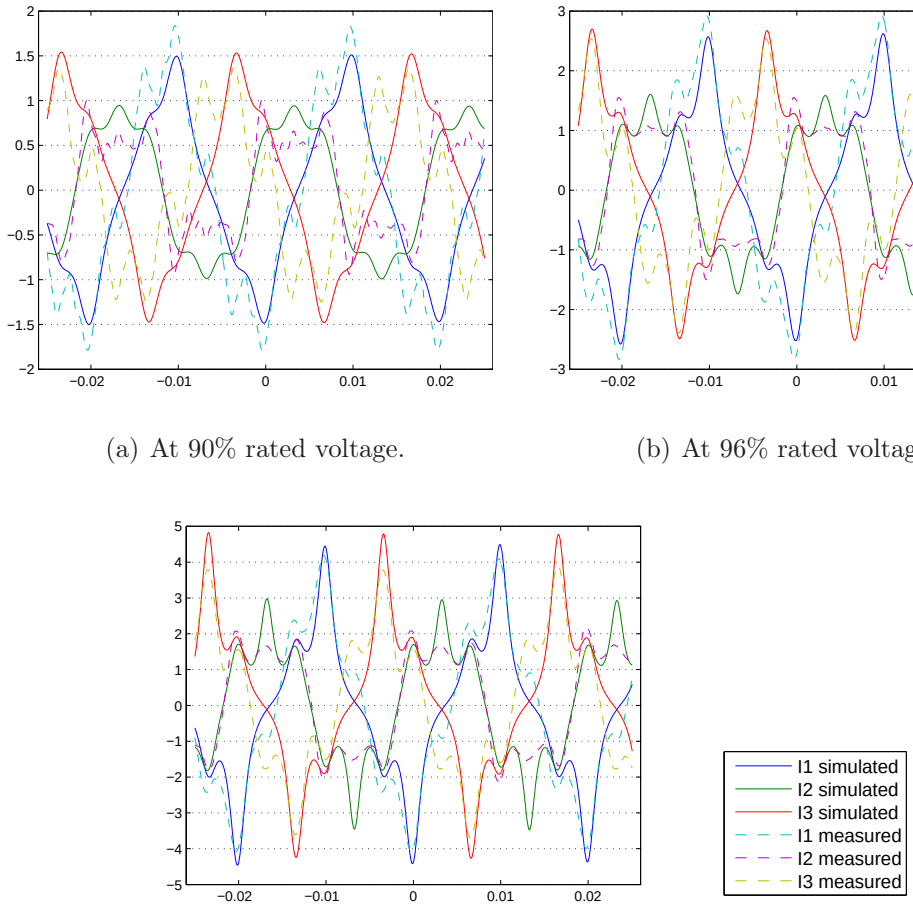

(a) At 90% rated voltage.

(b) At 96% rated voltage.

(c) At 100% rated voltage.

(d) Legend.

Figure 7.2: Comparison between simulated and measured current waveforms. Wye coupling. Frolich order three.

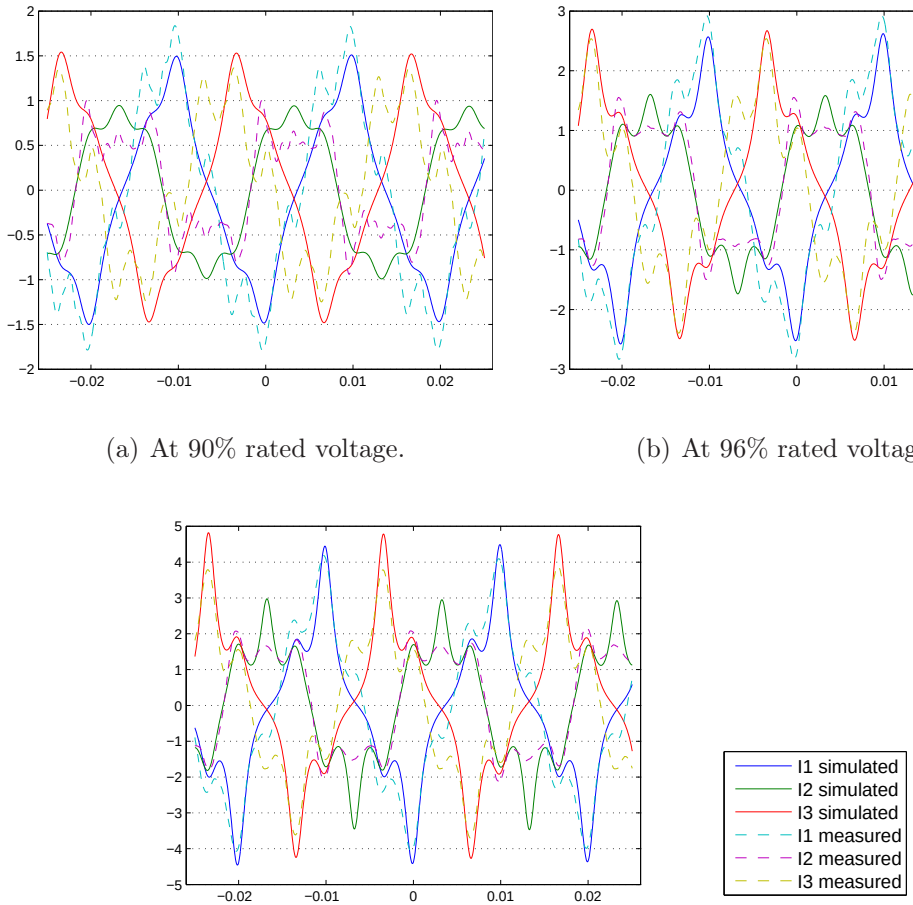

(a) At 90% rated voltage.

(b) At 96% rated voltage.

(c) At 100% rated voltage.

(d) Legend.

Figure 7.3: Comparison between simulated and measured current waveforms. Wye coupling. Frolich order two.

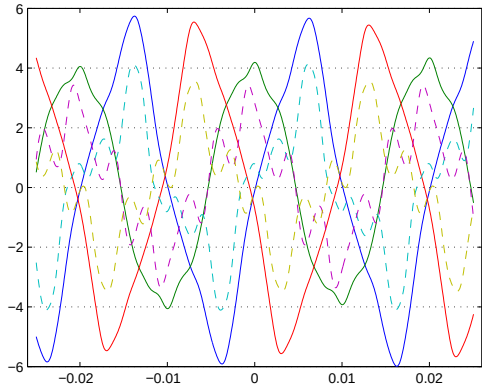

(a) At 100% rated voltage.

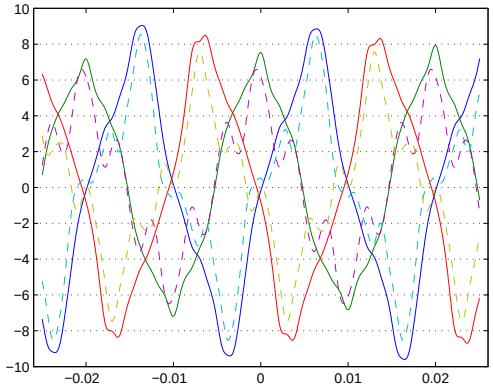

(b) At 110% rated voltage.

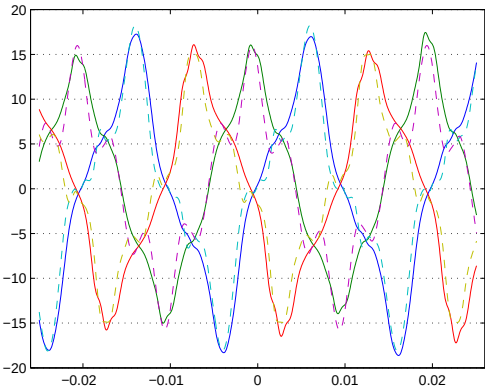

(c) At 120% rated voltage.

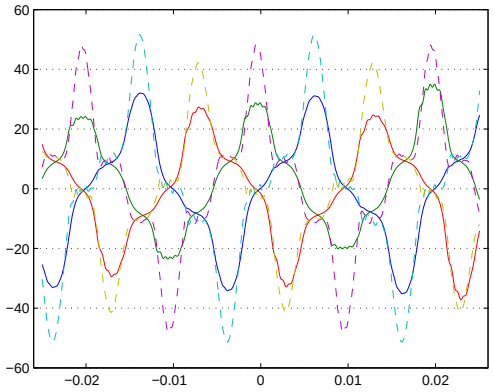

(d) At 130% rated voltage.

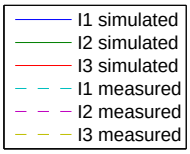

(e) Legend.

Figure 7.4: Comparison between simulated and measured current waveforms. Delta coupling. Frolich order three.

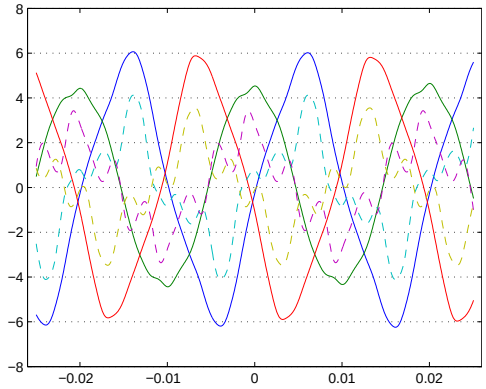

(a) At 100% rated voltage.

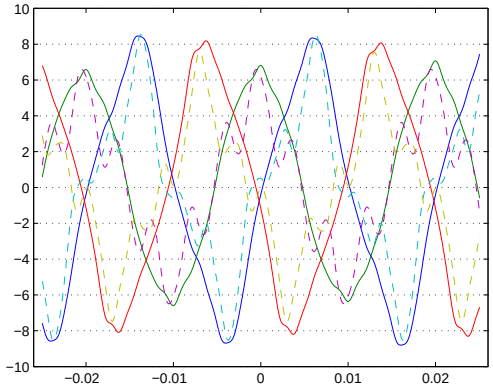

(b) At 110% rated voltage.

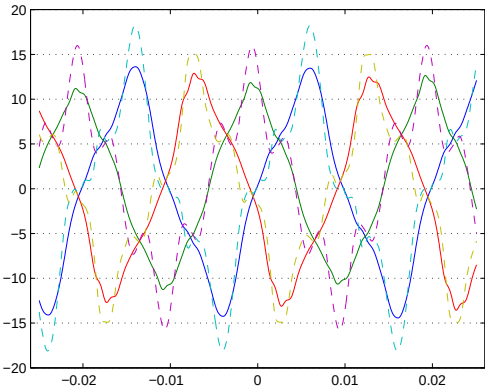

(c) At 120% rated voltage.

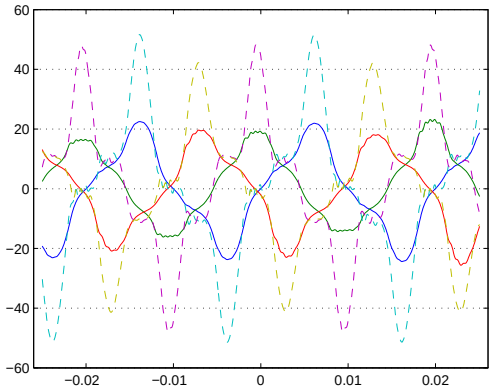

(d) At 130% rated voltage.

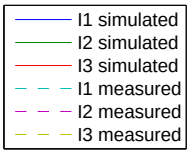

(e) Legend.

Figure 7.5: Comparison between simulated and measured current waveforms. Delta coupling. Frolich order two.

Observations:

- In the case of wye coupling, the simulated waveforms fit well with the measured curves.
- At 100% rated voltage (Fig. 7.2(c)) there is a good match of the two curves for all the three phases. Also most of the secondary peak are detected by the simulation.
- No difference can be noticed between three and two parameters Frolich equation for the wye coupling (respectively Fig. 7.2 and 7.3). The effect of the three parameter Frolich equation cannot be appreciated when there are no input data relative to the saturation area.
- Comparison between Fig. 7.4 and 7.5 shows a general improved behaviour in the case of three parameters Frolich equation.
- The fitting for the delta coupling cases (Fig. 7.4 and 7.5) is not so good as for the wye coupling. This is probably due to the high distorted voltage waveforms. The model assumes that open-circuit test has been carried out with a sinusoidal voltage source. In this case the voltage peak can be estimated with the simple relation: $\lambda_{peak} = \sqrt{2} \cdot V_{rms}/\omega$. For distorted voltage the assumption is no longer valid and cause some problems. Fig. 7.6 explains in detail the poor accuracy of the model for the case of Fig. 7.4(d). Fig. 7.6(a) compares the measured voltage waveform for one phase with the sinusoidal waveform taken into account in the computations. The two curves have the same rms value. Fig. 7.6(b) shows the flux waveforms calculated from the relative voltages. We refer to "measured flux" as the integral of the measured voltage, and to "equivalent flux" as the integral of the sinusoidal voltage. The peak of the measured flux is lower than the peak of the equivalent flux. Fig. 7.6(c) shows the $\lambda - i$ magnetization curve obtained from the fitting of the Frolich parameters. The fitting procedure is based on the equivalent flux, because the assumption of a sinusoidal voltage. The red crosses in the same figure are the maximum points of the measured current and flux. They represent the magnetic steel property. For high flux, the $\lambda - i$ curve is higher than the red crosses. Therefore, for the same excitation level the modelled curve give a lower current peak value. Finally, Fig. 7.6(d) compare the modelled $V_{rms} - I_{rms}$ curve with the measured rms values.

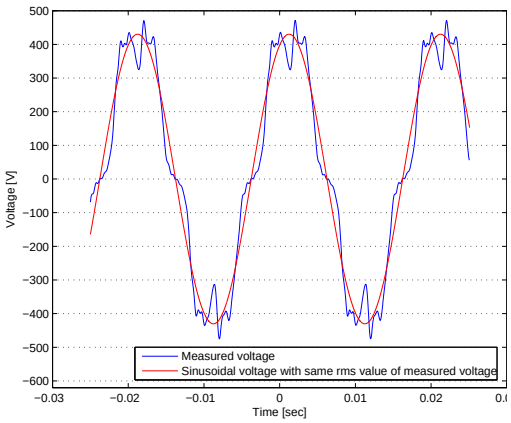

(a) Voltage waveform.

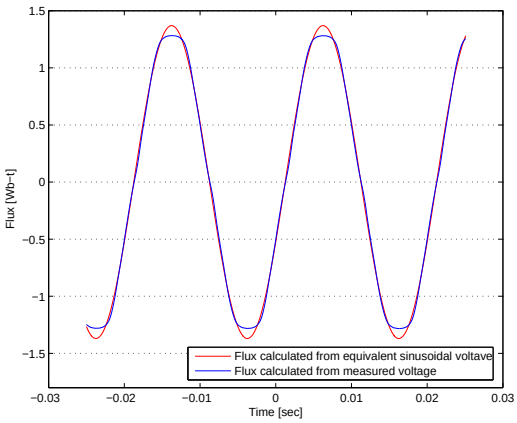

(b) Flux waveform.

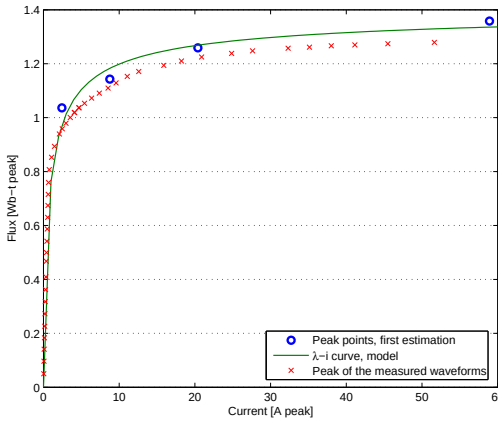

(c) $\lambda - i$ magnetization curve.

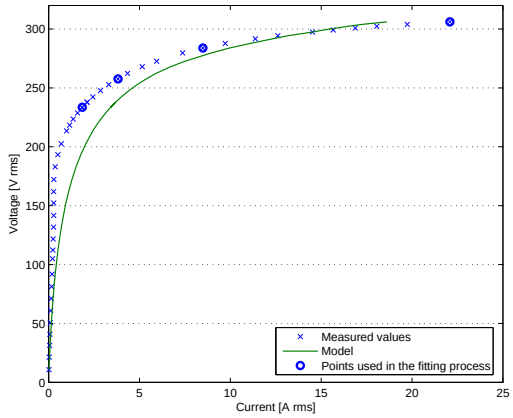

(d) $V_{rms} - I_{rms}$ magnetization curve.

Figure 7.6: Problems due to the distorted voltage waveforms.

- The simulated current waveforms represent only the pure magnetization currents. They do not consider any loss and capacitive effect components. The measured current waveforms are preprocessed to remove the current component due to the losses. It is not possible to remove the current component due to the capacitive effect because the lack of data. The capacitive currents are comparable to the magnetising currents at low excitation level. A capacitive current is 180 degree shifted to the inductive current, so its presence decreases the total current. As already said, the study of the capacitive effects is beyond the scope of this project, but in this case can explain unexpected behaviours in the initial part of the magnetizing curve.

- The Frolich equation parameters refer to the iron core characteristic. Therefore, similar values are expected for the same transformer, independently on the transformer configuration. The values in Tab. 7.1 are slightly different. This is mainly due to different excitation level of the input data. Simulations for delta and wye coupling are repeated using the same excitation levels as a basic for the fitting process. Tab. 7.2 reports the results, and we see that the a and b now are quite similar.

Coupl.	Frolich eq.	a	b	Data points	Tab.
Wye	ord.2	0.11978	0.91855	18,21,23	D.4
Delta	ord.2	0.13541	0.92879	18,21,23	D.5

Table 7.2: Simulation results for matching voltage ratio data.

The main problem of these comparisons are that the set of data are referred to distorted voltage waveform. Better behaviour of the model and better fitting of the measured curves is expected when the tests do not involve distorted voltage waveforms. As already mention in Chapter 6, the results of the laboratory tests improve if the three-phase voltage source is symmetric.

7.2 Test Report v.s. Design Information

The program is now tested in a different way. No waveform comparison is addressed here. The main purpose is to compare simulation results obtained from design parameters data with results obtained from test report data. The transformer uses as tests object is a 20 MVA 66/6.7 kV YNyn0 three-leg transformer produced in 1969. The test report data is reported in Fig. A.1. Tab. 7.3 summarizes the design information data needed in the simulation. More detailed constitutional information is restricted by the manufactures.

Material	M6 (guess)	
Number of windings	69	
Density	7650 Kg/m^3	
Leg absolute dimensions	$A = 0.1406\ m^3$	$L = 2.23\ m$
Yoke relative dimension	$A = 1.13$	$L = 1.411$

Table 7.3: Design parameters.

Data source	a	b	c
Design parameters	0.033315	0.051538	—
Test report, Fr.2	0.030444	0.052751	—
Test report, Fr.3	0.013085	0.050424	0.016315

Table 7.4: Frolich parameters. Comparison between design parameters and test report.

The results of the simulations are the Frolich parameters reported in Tab. 7.4 and the ATP listing in Appendix E. Fig. 7.7 summarizes the results. The magnetization curves are obtained from the Frolich parameters. The piecewise linear curves are obtained from the ATP listing and they refer to "`COREA COREB`" values. These represent the non linear inductance for the leg A of the transformer.

It is important to highlight that the design parameters and the test report results are obtained with two totally different procedures. For this reason a complete match of the results cannot be expected, but a similarity will strengthen the validity of the model. Fig. 7.7 shows that the equivalence of the curves is quite good.

The design information on the magnetic steel propriety is missing. The transformer is produced in 1969, thus the core material proprieties differ from more modern one. The guess of the material is probably an explanation of the difference between the curves in Fig. 7.7.

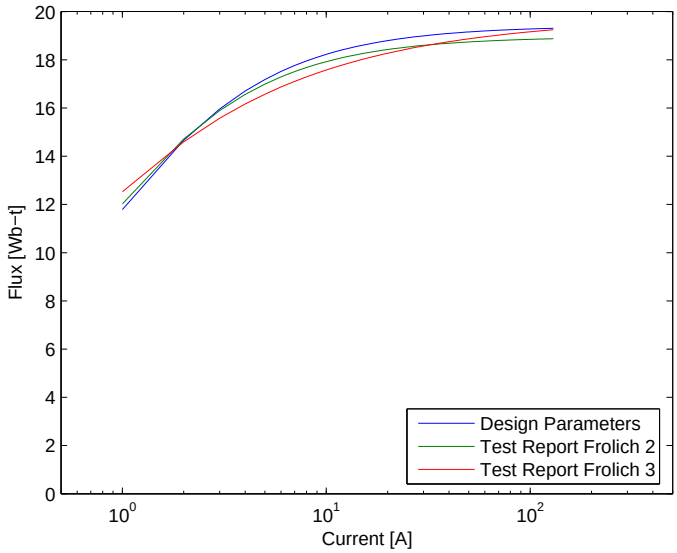

(a) Logarithmic scale.

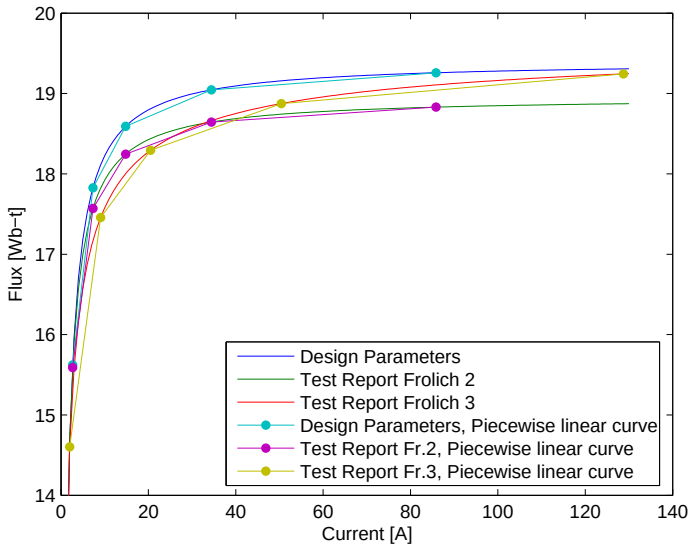

(b) Detail.

Figure 7.7: Leg magnetization curves. Comparison between design parameters and test report.

7.3 ATPDraw Electrical Network

In this section the results of three ATP simulations are shown. The simulations have to be considered more an example of the capability of the transformer model then a real case study. The model used for the simulation includes inductive, resistive, and nonlinear core effects, but not capacitive effects. The transformer data used in the simulation refers to transformer of Fig. A.1.

The first simulation is an open-circuit test. The circuit is shown in Fig. 7.8(a). It examines the steady-sate behaviour of a transformer energized at 100% and 130% rated voltage. The relative current waveforms are shown in Fig. 7.8.

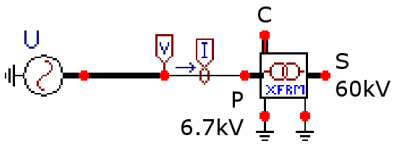

(a) Circuit.

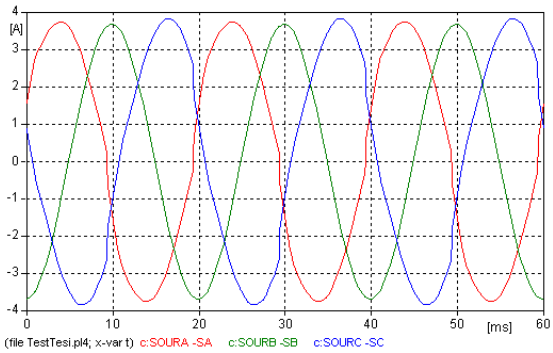

(b) Current waveforms at 100% rated voltage.

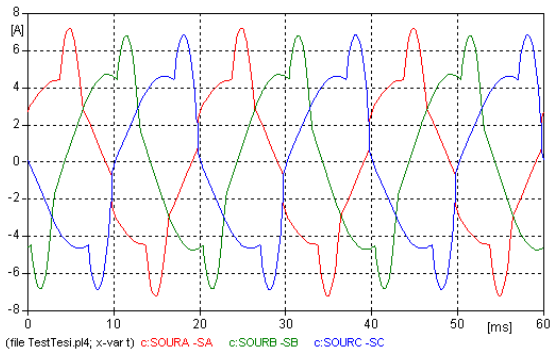

(c) Current waveforms at 130% rated voltage.

Figure 7.8: Open-circuit simulation.

The second simulation shows a transient simulation of the energization of a transformer. It focuses on inrush currents and the only attenuation is due to the transformer.

The switch shown in Fig. 7.9(a) is needed to obtain a transient behaviour. The transformer is first energized at the rated voltage [0-10 ms close-switch]. Then, the switch is open [10-20 ms]. Finally, the transformer is energized again at the rated voltage. In this situation the transformer has residual flux that contributes to the inrush currents. Fig. 7.9(d) shows the behaviour in the first instants during the

switching operation. Fig. 7.9(c) shows the first two peaks of the inrush currents. Fig. 7.9(b) shown the trend for the first five seconds. The rated current of the transformer is $In = 1724\ A$; can be observed that the first peak is lower than this value.

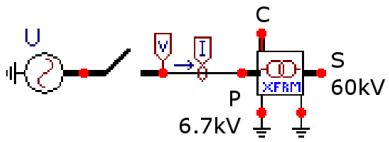

(a) Circuit.

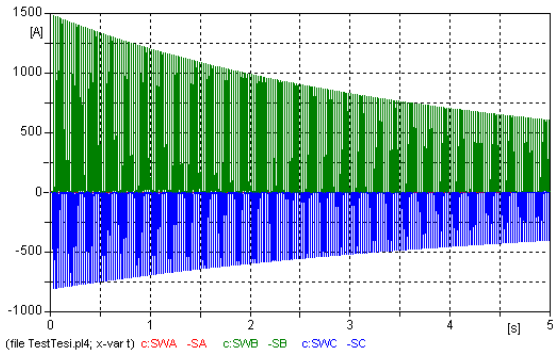

(b) Inruch current. 5 seconds.

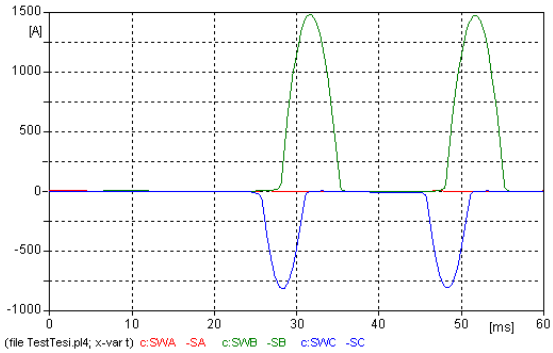

(c) Inrush currents. First two peaks.

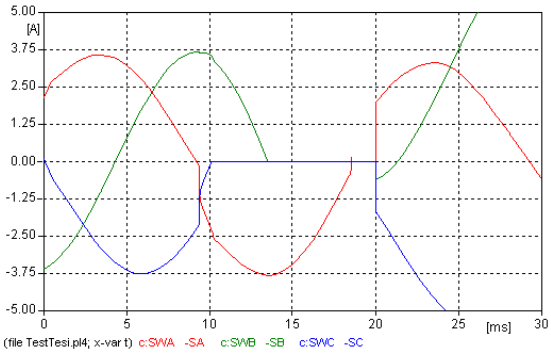

(d) Inrush currents. Switching operation.

Figure 7.9: Inrush currents simulation.

The third simulation repeats the previous case, but an electrical-line is inserted between the source and the transformer. The associated circuit is shown in Fig. 7.10(a). The presence of the line mitigate the inrush currents and accelerate their attenuation. On the other side, the line impedance causes a voltage distortion due to the nonlinear current waveforms. The relative current and voltage waveforms are shown in Fig. 7.10.

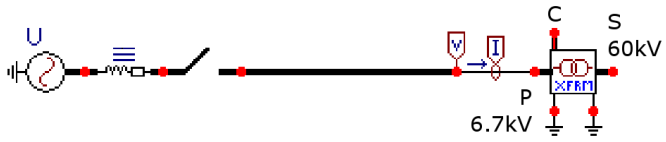

(a) Circuit.

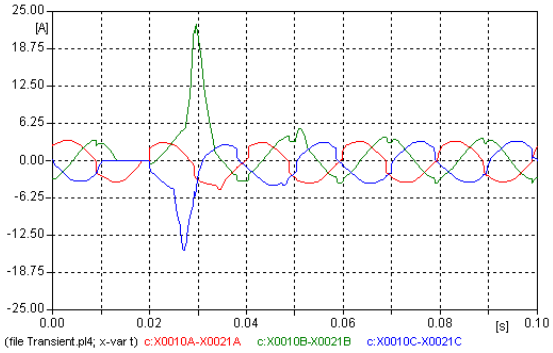

(b) Inrush currents.

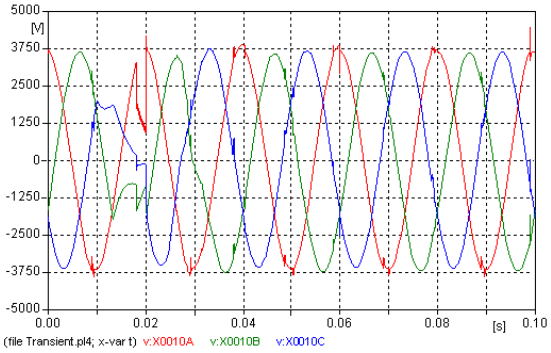

(c) Distortion in the voltage waveforms.

Figure 7.10: Inrush currents. Line.

Chapter 8

Conclusions

The main purpose of the work presented in this thesis is to suggest and test a topologically correct transformer core model. The model implemented is innovative for multiple data set that can be specified and for its validity and applicability to a large number of transformer type.

The work is based on [9]. Extensively work has been carried out on the core modelling. In addition to the implementation of the core model, the most important changes and improvements concern this Frolich equation, parameter estimation technique in case of factory test report and complete approximation, model of the core losses. For the first time the model has been validated using experimental data.

The main conclusions of this work are outlined below:

- A general transformer (XFMR) component has been developed for ATPDraw. The component is "self-contained"[1] and intuitive to use. The advanced features and the simple interface make XFMR a valuable supplement to electric network simulation.

- The most innovative part of XFMR is the core model. The model is based on a topologically correct core model that gives a proper and accurate representation of the nonlinear behaviour of the transformer. Such kind of model is indispensable if one wants to investigate switching transients or take into account the saturable characteristic of the transformer.

- Novel aspect of this work is the establishment of the modified Frolich equation, with and without the empty-space effect (L_∞). This new version of the Frol-

[1] do not require any external circuit to model nonlinear behaviour.

ich equation allows a more accurate fitting of the transformer magnetization curve.

- ATP *SATURA*-routine has been revisited in order to take into account the difference between delta and wye coupling. The new routine has been called *rms2peak*. It is believed that this routine alone can describe the magnetization curve without any equation fitting, when a good set of data is provided. Analysing this aspect is beyond the scope of this work. It will be investigated and the results will be presented to the *EEUG Meeting 2005*, the European EMTP-ATP Conference, held at the Warsaw University of Technology, Poland on September 12-14, 2005 [33].

- The laboratory test session is a real case study. It helps in a better understanding of the problem and warns of possible problem related to experimental tests. More work has to be carried out to completely validate the model. More accurate tests and comparisons with real behaviour are needed.

- The implementation of the transformer model in a computational program provide an accurate understanding of the problems. This intensive study of the model, in both physical and mathematical ways, helps to discover lack of accuracy and possible improvement points of the model. The most important aspects of future development and improvement are briefly discussed in the next section.

8.1 Future Development

The model is still in a early stage of development. New types of core have to be addressed (shell and triplex), and more accurate test has to be performed.

The main lack in the routine implementation concerns the finding of the optimal parameters of the Frolich equation. Actually a multi dimension golden section search method is used. Firstly, this method do not converge fast enough. Secondly, it only ensures that the given results is in a boundary of the optimum. Furthermore, the results depend on initial points and boundary constraints. An alternative routine or an improved golden-search routine should be implemented. The main difficulty is due to the nonlinear and multi-variable character of the problem.

While coding the model it is important not to forget the physical meaning of the work. Up to now, the three parameter Frolich equation seems to work well in

the model. It is then important to verify if the c-parameter of the Frolich equation has also a physical meaning. For example, this can be done creating a database of fitting parameters based on commercial transformer-steel and analysing the acquire improvement.

Future improvement of the model concerns the empty-space effect. This effect has not been implemented in the model. Due to the fact that it characterizes the slope of the magnetization curve for high saturation level, it is believed that more accurate results can be obtain if this effect is taken into accounts.

The zero sequence induction requires a more detailed study. An accurate value of L_0 is important in the case of three-leg transformer. The main difficulty is the absence of a standard form of zero-sequence test-report.

At the moment, the core losses are modelled linearly. It is interesting to study more in detail the nonlinear behaviour of the core losses due to their dependence on the voltage rate and the frequency. Also the hysteretic effect in the magnetization should be taken into account.

A capacitive effect on the magnetization current has been observed for low excitation voltage. The capacitive effect should be included in the model in order to obtain a good representation also for low level of excitation. At higher excitation level this effect is negligible.

The main purpose of modelling is to represent a physical behaviour in the simplest way. Study the sensitivity of the model allows to investigate the dependence between parameters and the accuracy of the model. When the most important parameters are detected, they can be handled with more accuracy. On the other side, the accuracy of the secondary parameter can be reduced in order to simplify the computational cost.

This model has been created to be applicable up to the first resonance peak. The high frequency behaviour is a subject for future investigations.

Appendix A

Transformer Test Reports

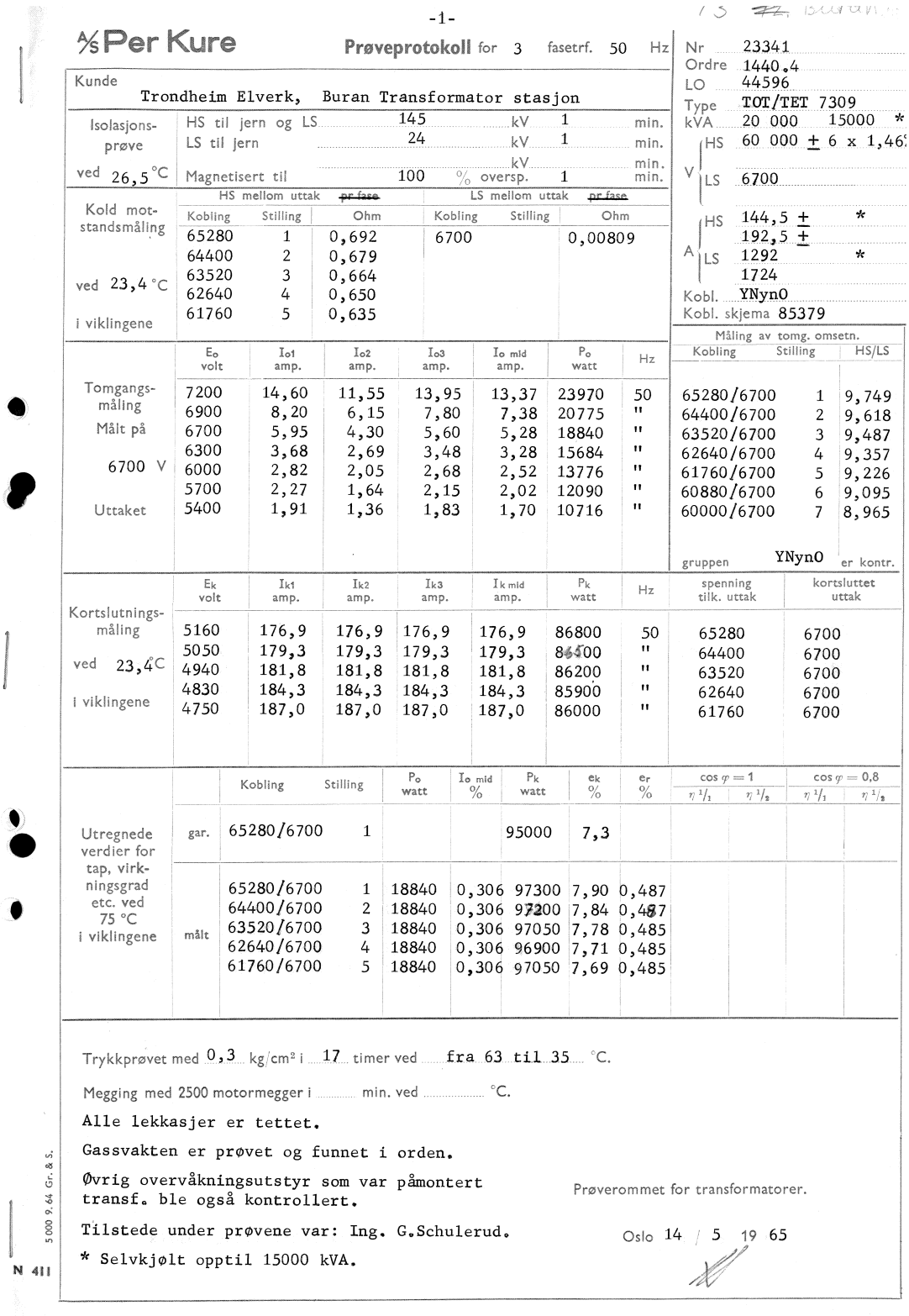

-1-

A/S Per Kure — **Prøveprotokoll** for 3 fasetrf. 50 Hz

Nr 23341
Ordre 1440.4
LO 44596
Type TOT/TET 7309
kVA 20 000 15000 *
V HS 60 000 ± 6 x 1,46
V LS 6700
A HS 144,5 ± *
A HS 192,5 ±
A LS 1292 *
A LS 1724
Kobl. YNyn0
Kobl. skjema 85379

Kunde: Trondheim Elverk, Buran Transformator stasjon

Isolasjonsprøve ved 26,5 °C:
- HS til jern og LS: 145 kV 1 min.
- LS til jern: 24 kV 1 min.
- Magnetisert til: 100 % oversp. 1 min.

Kold motstandsmåling ved 23,4 °C i viklingene

HS mellom uttak pr fase			LS mellom uttak pr fase		
Kobling	Stilling	Ohm	Kobling	Stilling	Ohm
65280	1	0,692	6700		0,00809
64400	2	0,679			
63520	3	0,664			
62640	4	0,650			
61760	5	0,635			

Tomgangsmåling målt på 6700 V Uttaket

E_o volt	I_{o1} amp.	I_{o2} amp.	I_{o3} amp.	$I_{o\ mid}$ amp.	P_o watt	Hz
7200	14,60	11,55	13,95	13,37	23970	50
6900	8,20	6,15	7,80	7,38	20775	"
6700	5,95	4,30	5,60	5,28	18840	"
6300	3,68	2,69	3,48	3,28	15684	"
6000	2,82	2,05	2,68	2,52	13776	"
5700	2,27	1,64	2,15	2,02	12090	"
5400	1,91	1,36	1,83	1,70	10716	"

Måling av tomg. omsetn.

Kobling	Stilling	HS/LS
65280/6700	1	9,749
64400/6700	2	9,618
63520/6700	3	9,487
62640/6700	4	9,357
61760/6700	5	9,226
60880/6700	6	9,095
60000/6700	7	8,965

gruppen YNyn0 er kontr.

Kortslutningsmåling ved 23,4°C i viklingene

E_k volt	I_{k1} amp.	I_{k2} amp.	I_{k3} amp.	$I_{k\ mid}$ amp.	P_k watt	Hz	spenning tilk. uttak	kortsluttet uttak
5160	176,9	176,9	176,9	176,9	86800	50	65280	6700
5050	179,3	179,3	179,3	179,3	86500	"	64400	6700
4940	181,8	181,8	181,8	181,8	86200	"	63520	6700
4830	184,3	184,3	184,3	184,3	85900	"	62640	6700
4750	187,0	187,0	187,0	187,0	86000	"	61760	6700

Utregnede verdier for tap, virkningsgrad etc. ved 75 °C i viklingene

	Kobling	Stilling	P_o watt	$I_{o\ mid}$ %	P_k watt	e_k %	e_r %	cos φ = 1 $\eta\ 1/1$	cos φ = 1 $\eta\ 1/2$	cos φ = 0,8 $\eta\ 1/1$	cos φ = 0,8 $\eta\ 1/2$
gar.	65280/6700	1			95000	7,3					
målt	65280/6700	1	18840	0,306	97300	7,90	0,487				
	64400/6700	2	18840	0,306	97200	7,84	0,487				
	63520/6700	3	18840	0,306	97050	7,78	0,485				
	62640/6700	4	18840	0,306	96900	7,71	0,485				
	61760/6700	5	18840	0,306	97050	7,69	0,485				

Trykkprøvet med 0,3 kg/cm² i 17 timer ved fra 63 til 35 °C.

Megging med 2500 motormegger i ..... min. ved ..... °C.

Alle lekkasjer er tettet.

Gassvakten er prøvet og funnet i orden.

Øvrig overvåkningsutstyr som var påmontert transf. ble også kontrollert.

Tilstede under prøvene var: Ing. G.Schulerud.

* Selvkjølt opptil 15000 kVA.

Prøverommet for transformatorer.

Oslo 14 / 5 19 65

5000 9.64 Gr. & S.

N 411

Figure A.1: A/S PerKure Transformer.

TRANSFORMER TEST REPORT

Date of Test 6/3/71 Customer's Order C-67899 Our Order C-04070-5

Type OA/FOA/FOA Phase 3 Cycles 60 Rise 55°/65°C Taps See N.P. Dwg. #307256 Spec. 13018

H. V. Volts 345000 Grd.Y/199200 L. V. Volts 118000 Grd.Y/68200 T.V. Volts 13800Δ

KVA 296000/394000/490000 * KVA 296000/294000/490000 * KVA 77000/102667/128333 *

Serial Number				C-04070-5-1			Guarantees
Polarity See N.P. Dwg. #307256		Transf. Conn.: 345000-118000		Volts @ 296 MVA			
W.M. Copper Loss @ Full Load 75°C				375940			
Core Loss @ 100% Voltage				✓ 297600			310000
Total Loss @ Full Load 100% Voltage				676540			695000
Core Loss @ 110% Voltage			**	402240			390000
% Exciting Current @ 100% Voltage				✓ 0.7			1.00
% Exciting Current @ 110% Voltage				1.4			2.00
% Impedance @ 75°C			Z_{pt}	6.21			6.30
% Resistance @ 75°C				0.128			
% Reactance @ 75°C				6.20			
% Regulation @ 100% P.F. Full Load				0.32			0.33
% Regulation @ 80% P.F. Full Load				3.94			4.05
% Efficiency @ Full Load 100% P.F.				99.77			99.76
% Efficiency @ ¾ Load 100% P.F.				99.77			99.75
% Efficiency @ ½ Load 100% P.F.				99.73			99.71
% Efficiency @ ¼ Load 100% P.F.				99.56			99.55
Total H.V. Resistance in Ohms @ 75°C (Series Wdg. - Tap "A")				0.6756			
Total T.V. Resistance in Ohms @ 75°C (Common Wdg.)				0.1635			
Total T.V. Resistance in Ohms @ 75°C				0.01748			
% Impedance @ 75°C (345000-13800 Volts) [illegible] MVA			Z_{pt}	55.9			55.0
% Impedance @ 75°C (118000-13800 Volts) [illegible] MVA			Z_{st}	42.1			40.0
INSULATION TESTS							
H.V. and L.V. and Core to T.V. Volts for 1 Min.				50000			50000
T.V. to Core Volts for 1 Min.				34000			34000
Induced Voltage in H.V. Winding Line to Ground				460000			460000
Induced Voltage in H.V. Winding Line to Line				575000			575000
TEMPERATURE RISE		MVA	296	394	490		
Connected: 362000-118000 Volts		Series Wdg.	42.4	43.5	47.9		
Copper Rise Corrected to Shutdown °C		Common Wdg.	43.3	43.3	47.5		55
Oil Rise °C			51.4	33.7	33.2		

Unless otherwise specified the above Tests are in accordance with the latest A. S. A. and N. E. M. A. Standards.

Remarks:	@ 77000 KVA	@ 102667 KVA	@ 128333 KVA
T.V. Gradient °C:	10.9	15.5	19.0

* KVA @ 65°C Rise: H.V. and L.V. 330000/440000/550000: T.V. - 86240/114987/143733.

** The Core Loss Value Exceeding Guarantee was submitted to and accepted by the customer.

This transformer satisfactorily withstood Impulse Tests. See Impulse Test Report.

This transformer satisfactorily withstood Switching Surge Tests. See Switching Surge Test Report

See Page #2 for additional test performance data.

Figure A.2: Transformer Test Report Two.

Appendix B

Inversion of Frolich Equations

B.1 2 Parameter Frolich Equation

$$\lambda = \frac{i}{a + b \cdot i} \tag{B.1}$$

$$\frac{\lambda}{i} = \frac{1}{a + b \cdot i} \tag{B.2}$$

$$i = \frac{a \cdot \lambda}{1 - b \cdot \lambda} \tag{B.3}$$

B.2 3 Parameter Frolich Equation

$$\lambda = \frac{i}{a + b \cdot i + c \cdot \sqrt{i}} \tag{B.4}$$

$$\frac{a}{i} + \frac{c}{i^{\frac{1}{2}}} + b - \frac{1}{\lambda} = 0 \tag{B.5}$$

This is a second grade equation: Substituting

$$\frac{1}{i} = x^2 \tag{B.6}$$

become:

$$a \cdot x^2 + c \cdot x + b - \frac{1}{\lambda} = 0 \tag{B.7}$$

Solutions for x are:

$$x = \frac{-c \pm \sqrt{c^2 + \frac{4 \cdot a}{\lambda} - 4 \cdot a \cdot b}}{2 \cdot a} \tag{B.8}$$

then replacing back the Eq. (B.6):

$$i = \left(\frac{2 \cdot a}{-c \pm \sqrt{c^2 + \frac{4 \cdot a}{\lambda} - 4 \cdot a \cdot b}} \right)^2 \tag{B.9}$$

Results that only the solution with minus is solution of Eq. (B.4). To avoid singularity problem when $\lambda = 0$, Eq. (B.9) is reformulated as:

$$i = \frac{4 \cdot a^2 \cdot \lambda}{\left(-c \cdot \sqrt{\lambda} - \sqrt{(c^2 - 4 \cdot a \cdot b) \cdot \lambda + 4 \cdot a} \right)^2} \tag{B.10}$$

Inserting the coefficients A and l become:

$$i = l \cdot \frac{4 \cdot a^2 \cdot \frac{\lambda}{A}}{\left(-c \cdot \sqrt{\frac{\lambda}{A}} - \sqrt{(c^2 - 4 \cdot a \cdot b) \cdot \frac{\lambda}{A} + 4 \cdot a} \right)^2} \tag{B.11}$$

B.3 2 Parameter and L_∞ Frolich Equation

$$\lambda = \frac{i}{a + b \cdot i} + L_\infty \cdot i \tag{B.12}$$

Substituting

$$\begin{aligned} a + b \cdot i &= x \\ \rightarrow b \cdot &= x - a \\ \rightarrow i &= \frac{x - a}{b} \end{aligned} \tag{B.13}$$

become:

$$\begin{aligned} \lambda &= \frac{\frac{x-a}{b}}{x} + L_\infty \cdot \frac{x - a}{b} = \\ &= \frac{L_\infty \cdot x^2 + (1 - L_\infty \cdot a) \cdot x - a}{b \cdot x} \end{aligned} \tag{B.14}$$

$$L_\infty \cdot x^2 + (1 - \lambda \cdot b - L_\infty \cdot a) \cdot x - a = 0 \tag{B.15}$$

Replacing back the Eq. (B.13),solving and collecting:

$$L_\infty \cdot b^2 \cdot i^2 + (L_\infty \cdot a \cdot b + b - b^2 \cdot \lambda) \cdot i - a \cdot b \cdot \lambda = 0 \tag{B.16}$$

that can be written in a simpler way as:

$$A \cdot i^2 + B \cdot i + C = 0$$

with

$$\begin{aligned} A &= L_\infty \cdot b^2 \\ B &= L_\infty \cdot a \cdot b + b - b^2 \cdot \lambda \\ C &= -a \cdot b \cdot \lambda \end{aligned}$$

The solution of Eq. (B.12) is the one with the plus sign.

B.4 3 Parameter and L_∞ Frolich Equation

$$\lambda = \frac{i}{a + b \cdot i + c \cdot \sqrt{i}} + L_\infty \cdot i \tag{B.17}$$

Substituting

$$i = I^2 \tag{B.18}$$

become:

$$\lambda - L_\infty \cdot I^2 = \frac{I^2}{a + b \cdot I^2 + c \cdot I} \tag{B.19}$$

that inverted is:

$$\frac{1}{\lambda - L_\infty \cdot I^2} = \frac{a}{I^2} + b + \frac{c}{I} \tag{B.20}$$

Can be written as

$$1 = \left(\frac{a}{I^2} + b + \frac{c}{I}\right) \cdot \left(\lambda - L_\infty \cdot I^2\right) \tag{B.21}$$

that solved is:

$$\underbrace{L_\infty \cdot b}_{A} \cdot I^4 + \underbrace{L_\infty \cdot c}_{B} \cdot I^3 + \underbrace{(L_\infty \cdot a - \lambda \cdot b + 1)}_{C} \cdot I^2 \underbrace{-\lambda \cdot c}_{D} \cdot I \underbrace{-\lambda \cdot a}_{E} = 0 \tag{B.22}$$

that is a quartic equation in I.

Quartic Equation

Quartic equation can be solved analytically. Find the solution of a quartic equation is not very simple, therefore the process is reported here.

The general quartic equation

$$A \cdot I^2 + b \cdot I^3 + C \cdot I^2 + D \cdot I + E = 0 \tag{B.23}$$

is considered. Substituting

$$I = y - \frac{B}{4 \cdot A} \tag{B.24}$$

become:

$$A \cdot \left[y - \frac{B}{4 \cdot A}\right]^4 + B \cdot \left[y - \frac{B}{4 \cdot A}\right]^3 + C \cdot \left[y - \frac{B}{4 \cdot A}\right]^2 + D \cdot \left[y - \frac{B}{4 \cdot A}\right] + E = 0$$

that after performing all the simplifications become a depressed quartic equation because the absence of the third grade term:

$$y^4 + 2 \cdot \alpha \cdot y - \beta \cdot y - \gamma = 0 \tag{B.25}$$

with

$$\begin{aligned}
\alpha &= \frac{C}{2 \cdot A} - \frac{3 \cdot B^2}{16 \cdot A^2} \\
\beta &= \frac{B \cdot C}{2 \cdot A^2} - \frac{D}{A} - \frac{B^3}{8 \cdot A^3} \\
\gamma &= \frac{3 \cdot B^4}{256 \cdot A^4} - \frac{B^2 \cdot C}{16 \cdot A^3} + \frac{B \cdot D}{4 \cdot A^2} - \frac{E}{A}
\end{aligned}$$

Adding and subtracting α^2:

$$y^4 + 2 \cdot \alpha \cdot y^2 + \alpha^2 = \alpha^2 + \beta \cdot y + \gamma \tag{B.26}$$

$$(y^2 + \alpha)^2 = \alpha^2 + \beta \cdot y + \gamma \tag{B.27}$$

$$(y^2 + \alpha + w)^2 = 2 \cdot w \cdot y^2 + \beta \cdot y + (w^2 + 2 \cdot \alpha \cdot w + \alpha^2 + \gamma) \tag{B.28}$$

It is possible to find w such as also the term at the right side become a square

equation. This can be obtain for:

$$\Delta = \beta^2 - 8 \cdot w \cdot (w^2 + 2 \cdot \alpha \cdot w + \alpha^2 + \gamma) = 0 \tag{B.29}$$

that is a cubic equation in w:

$$w^3 + \underbrace{2 \cdot \alpha}_{r} \cdot w^2 + \underbrace{(\alpha^2 + \gamma)}_{s} \cdot w \underbrace{- \frac{\beta^2}{8}}_{t} = 0 \tag{B.30}$$

This equation can be solved as follow:

$$w^3 + r \cdot w^2 + s \cdot w + t = 0 \tag{B.31}$$

Defining

$$Q = \frac{r^2 - 3 \cdot s}{9} \tag{B.32}$$

$$R = \frac{2 \cdot r - 9 \cdot r \cdot s + 27 \cdot t}{54} \tag{B.33}$$

- if $R^2 < Q^3$ with

$$\vartheta = \arccos\left(\frac{R}{\sqrt{q^3}}\right) \tag{B.34}$$

  the real solution is:

$$w = -2 \cdot \sqrt{Q} \cdot \cos\left(\frac{\vartheta}{3}\right) - \frac{r}{3} \tag{B.35}$$

- if $R^2 \geq Q^3$ with

$$S = -\text{sign}(R) \cdot \left[\text{abs}(R) + \sqrt{R^2 - Q^3}\right]^{\frac{1}{3}} \tag{B.36}$$

$$T = \begin{cases} \frac{Q}{S} & \text{if } S \neq 0 \\ 0 & \text{if } S = 0 \end{cases} \tag{B.37}$$

  the real solution is:

$$w = (S + T) - \frac{r}{3} \tag{B.38}$$

Once the real value of w is known, the quartic equation become:

$$y^2 + \alpha + w = \pm\left[H\left(y + \frac{B}{4 \cdot w}\right)\right] \tag{B.39}$$

with

$$H = \sqrt{2 \cdot w} \tag{B.40}$$

The Eq. (B.39) can be devided in two quadric equation that give the four different solution:

$$y_{1,2,3,4} = \mp\frac{H}{2} \pm \sqrt{\frac{H^2}{4} - \left(\alpha + w + \frac{H \cdot \beta}{4 \cdot w}\right)} \tag{B.41}$$

Between these solutions one is real. Replacing back

$$i = \left(y - \frac{B}{4 \cdot A}\right)^2 \tag{B.42}$$

the real solution is the solution of the Eq. (B.17)

Appendix C

Solution of Core Losses Calculation

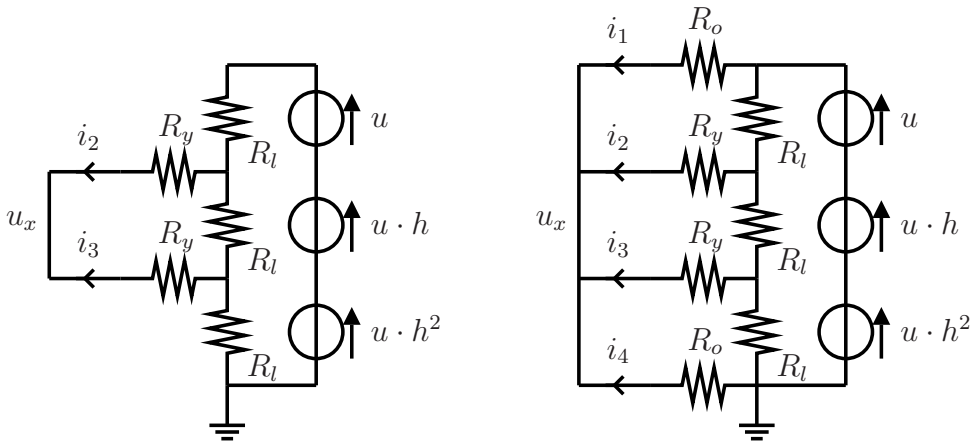

(a) Three-leg stacked core transformer.

(b) Five-leg stacked core transformer.

Figure C.1: Core losses, resistive circuits.

The resistive circuit of the five-leg transformer is shown in Fig. C.1(b). Based on this circuit it results:

$$i_1 = i_4 = -\frac{u_x}{R_0} \tag{C.1}$$

$$i_2 = \frac{u \cdot (h^2 + h) - u_x}{R_y} \tag{C.2}$$

$$i_3 = \frac{u \cdot h^2 - u_x}{R_y} \tag{C.3}$$

Where $h = e^{-j\frac{2}{3}\pi}$ and $h^2 = e^{j\frac{2}{3}\pi}$.
For the Ampere's current low in the point u_x is:

$$i_1 + i_2 + i_3 + i_4 = 0 \;\Rightarrow\; -2 \cdot \frac{u_x}{R_0} + \frac{u \cdot (h^2 + h) - u_x}{R_y} + \frac{u \cdot h^2 - u_x}{R_y} = 0 \qquad \text{(C.4)}$$

from which it is possible to find u_x as:

$$\begin{aligned} ux &= \frac{u \cdot (2 \cdot h^2 + h)}{R_y \cdot (\frac{2}{R_0} + \frac{2}{R_y})} = \\ &= u \cdot \frac{R_o}{2 \cdot (R_o + R_y)} \cdot (2 \cdot h^2 + h) = \\ &= u \cdot \frac{R_o}{R_o + R_y} \cdot (1 + \frac{h}{2}) \end{aligned} \qquad \text{(C.5)}$$

The active power is defined as:

$$P = |i|^2 \cdot R \qquad \text{(C.6)}$$

so it is necessary to find $|i1|^2$, $|i2|^2$, and $|i3|^2$. Considering

$$1 + \frac{h}{2} = \frac{3}{4} - j\frac{\sqrt{3}}{4} \qquad \text{(C.7)}$$

will be:

$$i_2 = \frac{u \cdot (h^2 + h) + u \cdot (1 + h/2) \cdot \frac{R_o}{R_o + R_y}}{R_y} =$$
$$= \frac{u}{R_y} \cdot (-1 + (1 + \frac{h}{2}) \cdot \frac{R_o}{R_o + R_y}) \tag{C.8}$$
$$|i_2|^2 = \frac{u^2}{R_y^2}((-1 + \frac{3}{4}\frac{R_o}{R_0 + R_y})^2 + (\frac{\sqrt{3}}{4}\frac{R_o}{R_0 + R_y})^2) =$$
$$= \frac{u^2}{R_y^2}(1 - \frac{3}{2}\frac{R_o}{R_0 + R_y} + \frac{3}{4}\frac{R_o^2}{(R_0 + R_y)^2}) \tag{C.9}$$

$$i_3 = \frac{u}{R_y} \cdot (h^2 + (1 + \frac{h}{2})\frac{R_o}{R_o + R_y}) \tag{C.10}$$
$$|i_3|^2 = |i_2|^2 \tag{C.11}$$

$$i_1 = \frac{u}{R_o + R_y} \cdot (1 + \frac{h}{2}) \tag{C.12}$$
$$|i_1|^2 = \frac{u^2}{(R_o + R_y)^2} \cdot \frac{3}{4} \tag{C.13}$$

Finally the power losses of the core are:

$$P = 3\frac{u^2}{R_l} + 2 \cdot |i_2|^2 \cdot R_y + 2 \cdot |i_1|^2 \cdot R_o =$$
$$= 3\frac{u^2}{R_l} + \frac{u^2}{R_y} \cdot 2 \cdot (1 - \frac{3}{2}\frac{R_o}{R_o + R_y} + \frac{3}{4}\frac{R_o^2}{(R_o + R_y)^2}) + u^2 \cdot \frac{R_o}{(R_o + R_y)^2} \cdot \frac{3}{2} =$$
$$= 3\frac{u^2}{R_l} + \frac{u^2}{2 \cdot R_y \cdot (R_o + R_y)^2} \cdot (4 \cdot R_y^2 + 2 \cdot R_o \cdot R_y + R_o^2) + u^2 \cdot \frac{R_o}{(R_o + R_y)^2} \cdot \frac{3}{2} \tag{C.14}$$

For three-leg transformer is:

$$u_x = \frac{u \cdot h}{2} \tag{C.15}$$

so

$$i_2 = i_3 = \frac{u \cdot h - u_x}{R_y} = \\ = \frac{u \cdot h - \frac{u \cdot h}{2}}{R_y} = \\ = \frac{u \cdot h}{2 \cdot R_y} \tag{C.16}$$

$$|i_2|^2 = \frac{u^2}{4 \cdot R_y^2} \tag{C.17}$$

that gives the following simpler equation for the power losses:

$$P = 3\frac{u^2}{R_l} + 2 \cdot R_y \cdot |i_2|^2 = \\ = 3\frac{u^2}{R_l} + \frac{u^2}{2 \cdot R_y} \tag{C.18}$$

Appendix D

Lab Test Data

	V V_{rms}	V% %	P_0 W	I_{01} A_{rms}	I_{02} A_{rms}	I_{03} A_{rms}	I_{0-avg} A_{rms}	I_{cl} A_{rms}	I_m A_{rms}
1	30.0	13.0	3.1	0.100	0.070	0.080	0.083	0.060	0.058
2	40.5	17.5	5.3	0.130	0.110	0.120	0.120	0.076	0.093
3	50.5	21.9	8.4	0.180	0.140	0.150	0.157	0.096	0.123
4	60.7	26.3	11.6	0.230	0.180	0.200	0.203	0.110	0.171
5	70.8	30.7	16.6	0.275	0.225	0.240	0.247	0.135	0.206
6	81.3	35.2	21.3	0.325	0.270	0.285	0.293	0.151	0.252
7	89.8	38.9	25.6	0.360	0.310	0.320	0.330	0.165	0.286
8	99.3	43.0	31.3	0.450	0.350	0.360	0.387	0.182	0.341
9	110.5	47.8	38.1	0.455	0.380	0.450	0.428	0.199	0.379
10	119.5	51.7	45.6	0.480	0.410	0.440	0.443	0.220	0.385
11	130.3	56.4	46.3	0.510	0.430	0.470	0.470	0.205	0.423
12	140.3	60.8	61.9	0.520	0.425	0.500	0.482	0.255	0.409
13	150.7	65.2	72.5	0.540	0.410	0.515	0.488	0.278	0.402
14	162.0	70.1	85.6	0.540	0.430	0.515	0.495	0.305	0.390
15	170.7	73.9	97.5	0.565	0.510	0.540	0.538	0.330	0.425
16	182.0	78.8	108.8	0.670	0.665	0.675	0.670	0.345	0.574
17	191.0	82.7	123.8	0.870	0.870	0.940	0.893	0.374	0.811
18	201.0	87.0	140.0	1.150	1.225	1.425	1.267	0.402	1.201
19	210.3	91.1	152.5	1.600	1.700	1.950	1.750	0.419	1.699
20	220.7	95.5	175.0	2.300	2.350	2.700	2.450	0.458	2.407
21	234.7	101.6	205.0	3.325	3.300	3.900	3.508	0.504	3.472
22	240.7	104.2	220.0	4.250	4.050	4.750	4.350	0.528	4.318
23	243.3	105.3	235.0	4.575	4.325	5.100	4.667	0.558	4.633

Table D.1: Open-circuit test. Delta coupling. Lab report.

	V V_{rms}	V% %	P_0 W	I_{01} A_{rms}	I_{02} A_{rms}	I_{03} A_{rms}	I_{0-avg} A_{rms}	I_{cl} A_{rms}	I_m A_{rms}
1	90	39.0	26.3	0.200	0.200	0.150	0.183	0.097	0.155
2	100	43.3	32.5	0.220	0.220	0.180	0.207	0.108	0.176
3	110	47.6	38.8	0.250	0.240	0.205	0.232	0.117	0.200
4	120	51.9	47.5	0.270	0.260	0.220	0.250	0.132	0.212
5	130	56.3	53.8	0.290	0.270	0.235	0.265	0.138	0.226
6	140	60.8	62.5	0.300	0.280	0.240	0.273	0.148	0.230
7	150	64.9	72.5	0.310	0.270	0.225	0.268	0.161	0.215
8	161	69.6	85.0	0.305	0.260	0.200	0.255	0.176	0.184
9	170	73.7	98.8	0.310	0.255	0.230	0.265	0.193	0.181
10	181	78.2	112.5	0.360	0.270	0.325	0.318	0.208	0.241
11	187	80.8	121.3	0.425	0.335	0.410	0.390	0.217	0.324
12	193	83.7	131.3	0.530	0.410	0.515	0.485	0.226	0.429
13	201	86.9	145.0	0.695	0.535	0.680	0.637	0.241	0.589
14	207	89.5	155.0	0.855	0.660	0.845	0.787	0.250	0.746
15	220	95.4	167.5	1.110	0.860	1.090	1.020	0.253	0.988
16	221	95.5	185.0	1.475	1.225	1.575	1.425	0.279	1.397
17	225	97.5	200.0	1.775	1.450	1.850	1.692	0.296	1.666
18	231	100.1	210.0	2.250	1.800	2.325	2.125	0.303	2.103

Table D.2: Open-circuit test. Wye coupling, floating star-point. Lab report.

	V V_{rms}	V% %	P_0 W	I_{01} A_{rms}	I_{02} A_{rms}	I_{03} A_{rms}	I_{0-avg} A_{rms}	I_{cl} A_{rms}	I_m A_{rms}
1	10	4.5	0.3	0.110	0.150	0.150	0.137	0.010	0.136
2	20	8.7	1.6	0.090	0.160	0.160	0.137	0.026	0.134
3	30	13.0	3.1	0.000	0.150	0.140	0.097	0.035	0.090
4	40	17.3	5.9	0.000	0.210	0.170	0.127	0.049	0.117
5	50	21.6	8.4	0.000	0.200	0.130	0.110	0.056	0.095
6	60	26.0	12.5	0.090	0.200	0.130	0.140	0.069	0.122
7	70	30.3	16.3	0.100	0.230	0.170	0.167	0.077	0.148
8	80	34.6	21.9	0.120	0.220	0.190	0.177	0.091	0.151
9	90	39.0	26.9	0.150	0.240	0.220	0.203	0.100	0.177
10	100	43.3	32.5	0.180	0.250	0.260	0.230	0.108	0.203
11	110	47.7	40.0	0.200	0.280	0.300	0.260	0.121	0.230
12	120	51.9	46.3	0.240	0.280	0.310	0.277	0.128	0.245
13	130	56.3	51.3	0.250	0.300	0.345	0.298	0.131	0.268
14	140	60.6	62.5	0.260	0.300	0.370	0.310	0.149	0.272
15	150	64.9	73.8	0.260	0.300	0.340	0.300	0.164	0.251
16	160	69.3	86.3	0.300	0.260	0.340	0.300	0.180	0.240
17	170	73.6	101.3	0.335	0.230	0.350	0.305	0.199	0.232
18	180	77.9	112.5	0.410	0.230	0.375	0.338	0.208	0.267
19	190	82.3	126.3	0.630	0.310	0.465	0.468	0.221	0.413
20	201	86.9	147.5	0.820	0.460	0.675	0.652	0.245	0.604
21	207	89.5	157.5	1.020	0.570	0.800	0.797	0.254	0.755
22	211	91.2	165.0	1.300	0.700	1.050	1.017	0.261	0.983
23	215	93.2	180.0	1.500	0.900	1.150	1.183	0.279	1.150
24	221	95.5	180.0	1.750	1.150	1.500	1.467	0.272	1.441
25	226	97.7	205.0	2.200	1.400	1.750	1.783	0.303	1.757

Table D.3: Open-circuit test. Wye coupling, star-point connected to neutral. Lab report.

	V_{ex} V_{rms}	$V_{ex}\%$ %	I_{0-avg} A_{rms}	P_0 W
1	30.19	13.1	0.110	2.86
2	39.87	17.3	0.146	4.92
3	49.64	21.5	0.128	7.52
4	59.72	25.9	0.137	10.85
5	70.16	30.4	0.162	14.82
6	80.40	34.8	0.177	19.32
7	90.06	39.0	0.203	24.11
8	100.59	43.5	0.229	29.92
9	110.68	47.9	0.251	36.21
10	120.99	52.4	0.275	43.26
11	129.34	56.0	0.292	49.75
12	148.91	64.5	0.295	68.44
13	159.74	69.2	0.291	79.81
14	169.56	73.4	0.308	91.52
15	180.11	78.0	0.330	104.93
16	190.65	82.5	0.456	119.49
17	201.28	87.1	0.645	135.62
18	207.37	89.8	0.805	145.67
19	211.49	91.6	0.948	153.13
20	215.82	93.4	1.087	161.02
21	221.45	95.9	1.326	172.15
22	226.21	97.9	1.579	181.97
23	230.87	99.9	1.856	192.64

Table D.4: Open-circuit test. Wye coupling, star-point connected to neutral. Waveform elaboration.

	V_{ex} V_{rms}	$V_{ex}\%$ %	I_{0-avg} A_{rms}	P_0 W		V_{ex} V_{rms}	$V_{ex}\%$ %	I_{0-avg} A_{rms}	P_0 W
1	31.05	13.4	0.095	3.07	23	231.19	100.1	3.016	187.91
2	40.34	17.5	0.127	5.07	24	235.44	101.9	3.454	197.04
3	50.02	21.7	0.163	7.71	25	231.05	100.0	2.994	187.56
4	60.14	26.0	0.202	10.98	26	235.46	101.9	3.455	197.19
5	70.27	30.4	0.243	14.86	27	239.83	103.8	3.978	206.89
6	80.26	34.7	0.281	19.25	28	245.17	106.1	4.682	220.22
7	90.70	39.3	0.323	24.44	29	250.22	108.3	5.444	234.30
8	103.66	44.9	0.373	31.74	30	254.98	110.4	6.291	249.28
9	110.90	48.0	0.400	36.28	31	259.60	112.4	7.156	265.98
10	120.26	52.1	0.433	42.75	32	265.30	114.8	8.494	290.50
11	130.20	56.4	0.465	50.50	33	269.89	116.8	9.828	312.43
12	139.99	60.6	0.486	59.12	34	276.91	119.9	12.178	351.18
13	150.49	65.1	0.484	69.54	35	280.90	121.6	13.989	377.24
14	159.98	69.3	0.463	79.89	36	284.84	123.3	15.988	405.70
15	170.24	73.7	0.458	91.90	37	288.85	125.0	18.655	438.98
16	180.85	78.3	0.557	105.40	38	291.45	126.2	20.656	463.21
17	191.10	82.7	0.786	119.45	39	294.58	127.5	23.669	494.69
18	200.24	86.7	1.091	132.83	40	296.32	128.3	25.464	513.80
19	211.12	91.4	1.574	150.48	41	298.01	129.0	27.367	532.86
20	215.97	93.5	1.845	158.97	42	299.26	129.5	29.183	548.09
21	221.14	95.7	2.178	168.41	43	300.84	130.2	31.747	568.51
22	226.40	98.0	2.582	178.35	44	303.08	131.2	35.395	602.84

Table D.5: Open-circuit test. Delta coupling. Waveform elaboration.

Appendix E

Files Generated by ATPDraw

This appendix reports the listing generated by ATPDraw. Only the part relative to the nonlinear representation is reported.

E.1 Data Based on Design Parameters

```
BEGIN NEW DATA CASE
C ------------------------------------------------------------
C Generated by ATPDRAW  juni, lørdag 11, 2005
C A Bonneville Power Administration program
C Programmed by H. K. Høidalen at SEfAS - NORWAY 1994-2003
C ------------------------------------------------------------
$DUMMY, XYZ000
C  dT  >< Tmax >< Xopt >< Copt >
   1.E-6    .001
     500       1       1       1       1       0       0
C        1         2         3         4         5
C 345678901234567890123456789012345678901234567890123456789
/BRANCH
C < n 1>< n 2><ref1><ref2>< R  >< L  >< C  >
C < n 1>< n 2><ref1><ref2>< R  >< A  >< B  ><Leng><><>0
C ------------------------------------------------------------
C Nonlinear core representation
C ------------------------------------------------------------
98COREA COREB             15.6232.6719
```

```
    15.623235751    2.6718681431
    17.825800087    7.3063947092
    18.591134824    14.805216255
    19.045326371       34.437386
    19.257780231    85.835073836
 9999.
  COREA COREB             3306.2
98COREB COREC             15.6232.6719
    15.623235751    2.6718681431
    17.825800087    7.3063947092
    18.591134824    14.805216255
    19.045326371       34.437386
    19.257780231    85.835073836
 9999.
  COREB COREC             3306.2
98COREC                   15.6232.6719
    15.623235751    2.6718681431
    17.825800087    7.3063947092
    18.591134824    14.805216255
    19.045326371       34.437386
    19.257780231    85.835073836
 9999.
  COREC                   3306.2
98COREB IX0001            16.3462.6719
    16.345615676    2.6718681431
    19.492026537    7.3063947092
     20.65289495    14.805216255
    21.359480782       34.437386
    21.694648247    85.835073836
 9999.
  COREB IX0001            2073.6
98COREC IX0001            16.3462.6719
    16.345615676    2.6718681431
    19.492026537    7.3063947092
     20.65289495    14.805216255
    21.359480782       34.437386
```

```
    21.694648247    85.835073836
 9999.
  COREC IX0001            2073.6
  COREA IX0001                    0.01
  COREA IX0001              1.E9
        IX0001                    0.01
        IX0001              1.E9
C ------------------------------------------------------
```

E.2 Data Based on Test Report

Three parameter Frolich equation

```
BEGIN NEW DATA CASE
C ------------------------------------------------------
C Generated by ATPDRAW  juni, lørdag 11, 2005
C A Bonneville Power Administration program
C Programmed by H. K. Høidalen at SEfAS - NORWAY 1994-2003
C ------------------------------------------------------
$DUMMY, XYZ000
C  dT  >< Tmax >< Xopt >< Copt >
   1.E-6    .001
     500       1       1       1       1       0       0
C        1         2         3         4         5
C 345678901234567890123456789012345678901234567890123456789
/BRANCH
C < n 1>< n 2><ref1><ref2>< R  >< L  >< C  >
C < n 1>< n 2><ref1><ref2>< R  >< A  >< B  ><Leng><><>0
C ------------------------------------------------------
C Nonlinear core representation
C ------------------------------------------------------
98COREA COREB             14.6032.0039
    14.602865485    2.0039011073
    17.456405631    9.0673645366
    18.292761995    20.496288504
    18.874503382    50.417600004
```

```
    19.244193539    128.75261075
 9999.
  COREA COREB             2631.8
98COREB COREC             14.6032.0039
    14.602865485    2.0039011073
    17.456405631    9.0673645366
    18.292761995    20.496288504
    18.874503382    50.417600004
    19.244193539    128.75261075
 9999.
  COREB COREC             2631.8
98COREC                   14.6032.0039
    14.602865485    2.0039011073
    17.456405631    9.0673645366
    18.292761995    20.496288504
    18.874503382    50.417600004
    19.244193539    128.75261075
 9999.
  COREC                   2631.8
98COREB IX0001            16.3322.6719
    16.331600199    2.6718681431
    19.643566118    12.089819382
    20.617769183    27.328384672
     21.29559396    67.223466672
    21.726202173    171.67014767
 9999.
  COREB IX0001            1650.6
98COREC IX0001            16.3322.6719
    16.331600199    2.6718681431
    19.643566118    12.089819382
    20.617769183    27.328384672
     21.29559396    67.223466672
    21.726202173    171.67014767
 9999.
  COREC IX0001            1650.6
  COREA IX0001                    0.01
```

```
  COREA IX0001              1.E9
        IX0001                    0.01
        IX0001              1.E9
C ------------------------------------------------------------
```

Two parameter Frolich equation

```
BEGIN NEW DATA CASE
C ------------------------------------------------------------
C Generated by ATPDRAW  juni, lørdag 11, 2005
C A Bonneville Power Administration program
C Programmed by H. K. Høidalen at SEfAS - NORWAY 1994-2003
C ------------------------------------------------------------
$DUMMY, XYZ000
C  dT  >< Tmax >< Xopt >< Copt >
   1.E-6    .001
     500       1       1       1       1       0       0
C        1         2         3         4         5
C 345678901234567890123456789012345678901234567890123456789
/BRANCH
C < n 1>< n 2><ref1><ref2>< R  >< L  >< C  >
C < n 1>< n 2><ref1><ref2>< R  >< A  >< B  ><Leng><><>0
C ------------------------------------------------------------
C Nonlinear core representation
C ------------------------------------------------------------
98COREA COREB             15.5892.6719
    15.589412769    2.6718681431
    17.568973343    7.3063947092
    18.245496447    14.805216255
    18.644273301       34.437386
    18.830119026    85.835073836
 9999.
  COREA COREB             2631.8
98COREB COREC             15.5892.6719
    15.589412769    2.6718681431
    17.568973343    7.3063947092
```

```
    18.245496447    14.805216255
    18.644273301       34.437386
    18.830119026    85.835073836
 9999.
  COREB COREC             2631.8
98COREC                   15.5892.6719
    15.589412769    2.6718681431
    17.568973343    7.3063947092
    18.245496447    14.805216255
    18.644273301       34.437386
    18.830119026    85.835073836
 9999.
  COREC                   2631.8
98COREB IX0001            16.4172.6719
    16.417454286    2.6718681431
    19.273055927    7.3063947092
    20.304315691    14.805216255
    20.926268626       34.437386
    21.219787098    85.835073836
 9999.
  COREB IX0001            1650.6
98COREC IX0001            16.4172.6719
    16.417454286    2.6718681431
    19.273055927    7.3063947092
    20.304315691    14.805216255
    20.926268626       34.437386
    21.219787098    85.835073836
 9999.
  COREC IX0001            1650.6
  COREA IX0001                    0.01
  COREA IX0001              1.E9
        IX0001                    0.01
        IX0001              1.E9
C ------------------------------------------------------
```

Bibliography

[1] EMTP. Online: `http://www.emtp.org`.

[2] ATPDraw. Online: `http://www.ece.mtu.edu/atp/ATPDraw/ATPDraw.html`.

[3] L. Prikler and H.K. Høidalen. *ATPDRAW version 3.5, User Manual*, 2002.

[4] Canadian-American EMTP User Group. *ATP-EMTP Rule Book*, 1996.

[5] H.K. Dommel. *Electromagnetic Transient Program. Reference Manual (EMTP Theory Book)*. Bonneville Power Administration, Portland, 1986.

[6] *EEUG Course 2004, Modelling Rotating Machine & Transformer in ATP-EMTP*, October, 6 2004. Organized by NTNU and EEUG.

[7] B.A. Mork, F. Gonzalez-Molina, and J. Mitra. Parameter estimation and advancement in transformer models for emtp simulations. task/activity mtu-4/ndsu-2: Library of models topologies. Technical report, submitted to Bonneville Power Administration, Portland USA, 2003.

[8] B.A. Mork, F. Gonzalez-Molina, and D. Ishchenko. Parameter estimation and advancement in transformer models for emtp simulations. task/activity mtu-6: Parameter estimation. Technical report, submitted to Bonneville Power Administration, Portland USA, 2003.

[9] B.A. Mork, F. Gonzalez-Molina, and D. Ishchenko. Parameter estimation and advancement in transformer models for emtp simulations. task/activity mtu-7: Model performance and sensitivity analysis. Technical report, submitted to Bonneville Power Administration, Portland USA, 2004.

[10] S. Leva and A.P Morando. Topological transition from magnetic networks to the electric equivalent ones when iron losses are present. *Proceedings of the 43rd IEEE Midwest Symposium on Circuits and Systems*, 2:642–645, 2000.

[11] C.M Arturi. Transient simulation and analysis of a three-phase five-limb step-up transformer following an out-of-phase syncronization. *IEEE Trans. Power Delivery*, 6(1):196–207, 1991.

[12] A.P. Morando and S. Leva. *Elettrotecnica, Reti e campi*. Esculapio, Bologna, 2001.

[13] A.P. Morando and S. Leva. *Note di teoria dei Campi Vettoriali*. Esculapio, Bologna, 2000.

[14] A.P. Morando and S. Leva. *Elettrotecnica, Mutuo induttore tempo invariante*. Esculapio, Bologna, 2001.

[15] J.A. Martinez-Velasco and B.A. Mork. Transformer modeling for low frequency transients - the state of the art. In *International Conferance on Power System Transients - IPST'03 in New Orleans, USA*, 2003.

[16] A. Tokic, I. Uglesic, and F. Jakl. An algorithm for calculation of low frequency transformer transients. In *International Conferance on Power System Transients - IPST'03 in New Orleans, USA*, 2003.

[17] W. Enright, N. Watson, and O. Nayak. Three-phase five-limb unified magnetic equivalent circuit transformer model for pscad v3. In *International Conferance on Power System Transients - IPST'99 in Budapest, Hungary*, 1999.

[18] W. Enright, O.B Nayak, G.D. Irwin, and J. Arrillaga. An electromagnetic transients model of multi-limb transformer using normalized core concept. In *International Conferance on Power System Transients - IPST'97 in Seattle, USA*, 1997.

[19] F. de León and A. Semlyen. Complete transformer model for electromagnetic transients. *IEEE Trans. Power Delivery*, 9(1):231–239, January 1994.

[20] S.V. Kulkarni and S.A. Khaparde. *Transformer Engineering, Design and Practice*. Marcel Dekker, Inc., NewYork-Basel, 2004.

[21] M.J. Heathcote and A.C. Franklin. *The J&P Transformer Book: a practical technology of the power transformer*. Oxford, 12th edition, 1998.

[22] J.H. Harlow, editor. *Electric Power Transformer Engineering*. CRC Press LLC, 2004.

[23] D.A. Tziouvaras, P. McLaren, and other. Mathematical model for current, voltage, and coupling capacitor voltage transformers. *IEEE Trans. Power Delivery*, 15(1):62–72, January 2000.

[24] W.L.A. Neves and H.W. Dommel. On modelling iron core nonlinearities. *IEEE Trans. Power Systems*, 8(2):417–425, May 1993.

[25] IEEE Standard General Requirements for Liquid-Immersed Distribution, Power, and Regulating Transformer. IEEE Std C57.12.00, June 2000.

[26] Borland Delphi. Online: `http://www.borland.com/us/products/delphi/index.html`.

[27] Numerical Recipes in Fortran 77. Online: `http://www.library.cornell.edu/nr/`.

[28] IEEE Standard Test Code for Liquid-Immersed Distribution, Power, and Regulating Transformers. IEEE Std C57.12.90, June 1999.

[29] IEEE Guide for Trnasformer Loss Measurement. IEEE Std C57.123, December 2002.

[30] A Gaudreau, P Pitcher, L. Boulduc, and A. Coutu. No-load losses in transformer under overexcitation/inrush-current conditions: Test and a new model. *IEEE Trans. Power Delivery*, 17(14):1009–1017, October 2002.

[31] E.F. Fuchs and Y. You. Measurement of $\lambda - i$ characteristics of asymmetric three-phase transformers and their applications. *IEEE Trans. Power Delivery*, 17(4):983–990, October 2002.

[32] A. Medina, A.M. Maldonado, L. Sanchez, and C.M. Sanchez. Experimental determination of magnetic saturation and hysteresis characteristics in power transformers with the wvav method. *IEEE Power Engineering Society Summer Meeting*, 4:2434–2438, July 2000.

[33] EEUG, European EMTP User Group. Online: `http://www.eeug.de`.